c. 3

LOS ALAMOS SCIENTIFIC LABORATORY

OF THE UNIVERSITY OF CALIFORNIA

LOS ALAMOS, NEW MEXICO

CONTRACT W-7405-ENG. 36 WITH THE
U.S. ATOMIC ENERGY COMMISSION

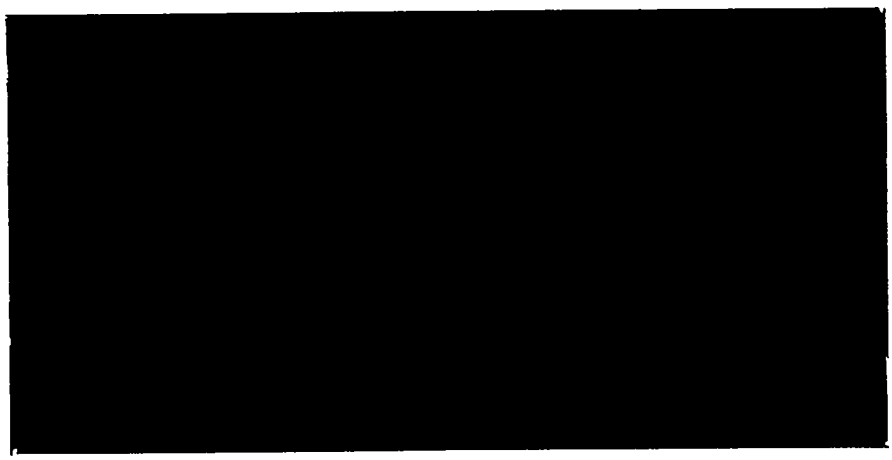

LOS ALAMOS SCIENTIFIC LABORATORY

of the

UNIVERSITY OF CALIFORNIA

Report written:
January 15, 1955

Report distributed: DEC 13 1955

LA-1429

INELASTIC CROSS SECTIONS FOR FISSION SPECTRUM NEUTRONS

by

H. A. Bethe
J. R. Beyster
R. E. Carter

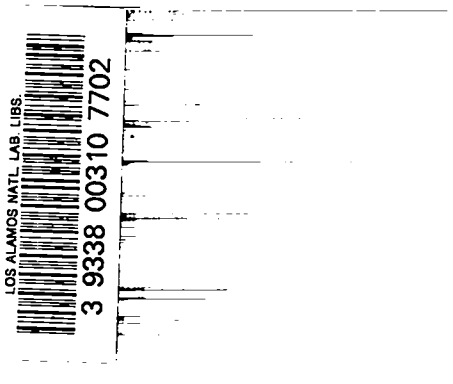

PHYSICS

ABSTRACT

The general problem of determining inelastic cross sections from sphere transmission measurements is considered. Experimental problems encountered in this type of investigation are discussed. Analytical methods of correcting for multiple scattering and other important effects in spherical shells are presented. These methods are applied to the determination of average inelastic cross sections of many materials for fission spectrum neutrons. Experimental work with U^{238}, Np^{237}, and $Al^{27}(n,p)Mg^{27}$ threshold detectors is evaluated.

ACKNOWLEDGMENTS

During the course of the measurements and calculations reported herein, the authors benefited from the contributions of many members of Los Alamos Scientific Laboratory. Those whose assistance was most essential are as follows:

(1) C. W. Johnstone with the electronic apparatus.

(2) B. G. Carlson, M. Goldstein, R. Von Holdt, Mrs. B. J. Masters, and P. E. Harper with the numerical computations.

(3) E. D. Cashwell, C. J. Everett, and J. M. Kister with setting up and performing the Monte Carlo calculations on the MANIAC.

Discussions with H. H. Barschall and J. M. B. Kellogg initiated the experimental program. Their support continued throughout the work.

John E. Evans assisted in planning and performing the first measurements, and W. George and E. Bennett joined us during two consecutive summers as participants in the summer graduate student program of LASL.

Many of the spheres were lent to us by E. R. Graves and R. W. Davis, and we take this opportunity to thank them. Spheres were supplied by Knolls Atomic Power Laboratory for the measurements of zirconium and titanium.

CONTENTS

TABLES

ILLUSTRATIONS

CHAPTER 3 THICK-SHELL THEORY AND ISOTROPIC SCATTERING

CHAPTER 5 DETERMINATION OF ESCAPE PROBABILITIES

CHAPTER 6 CORRECTIONS

CHAPTER 7 DETECTOR CHARACTERISTICS

DEFINITIONS*

Roman Alphabet

Symbol	Definition
A	Atomic weight
$a(\mu)$	Defined by Eq. 5.5
a_n	n + 1 coefficient in cosine series expansion of elastic scattering angular distribution function. Eq. 4.6
b	Distance between center of source and center of detector in a sphere transmission experiment
$b(\mu)$	Defined by Eq. 5.5
C_{tot}	Total number of second or higher order neutron collisions in the shell. Eq. 3.40
C_{In}	Total number of second or higher order inelastic collisions in the shell. Eq. 3.41
C_2	Total number of second collisions preceded by first elastic collisions. Eq. 4.2
C_{ji}	Effective cross section for transferring neutrons from group j to group i, considering all processes. Section 8.2 and Eq. 8.15
$c(\mu)$	Defined by Eq. 5.5
D	Distance from the surface of a spherical shell at which the normal mode flux may be considered zero (extrapolated end point). Eq. 3.24
E_1	Number of neutrons that have at least one elastic collision. Eq. 3.1
E_n	Number of neutrons that have n elastic collisions. Equation 3.11, for example
E'	Denotes the neutron energy after loss of energy on either elastic or inelastic collisions
$\overline{E}$	Average energy after an elastic collision. Eq. 6.43
$F(\theta)\, d\omega$	Probability of elastic scattering at angle θ into solid angle $d\omega$. Eq. 6.39
$f_n(r)\, dr$	The fraction of neutrons making n collisions which make their nth collision between r and r + dr. Eqs. 3.1, 3.9, 5.4, and 5.13
$f(r,\alpha)$	Neutron flux at point r. Eq. 4.7
$G(\theta,r,r_j,r_{j+1})$	Probability of a second collision in subshell r_j to r_{j+1} if a neutron scatters on its first collision at position r into angle θ. Section 5.2
g	Neutrons emitted per collision or 1 + f in neutron diffusion theory. Eq. 3.20

* To assist the reader, equation and section numbers have been added to definitions in some cases.

H	Distance between points (x_0,y_0) and (x,y,z) in Fig. 6.7
I_n	Number of events in which the collisions through $n-1$ are elastic and the nth collision is inelastic. Eqs. 2.4, 3.7, and 3.14
I'_n	Defined in the same way as I_n except that total cross section instead of transport cross section is used on the first collisions. Eq. 4.4
J_1	Correction for finite source-to-detector distance to be subtracted from observed transmission. Eqs. 6.9 and 6.10
J_2	Correction term for finite detector size inside the sphere to be added to observed transmission. Eqs. 6.27 and 6.28
K	Ratio of the inside radius of sphere to the outside radius, r_1/r_2
k	One of the unknowns in the normal mode flux expression (Eq. 3.19) which is fixed by the choice of sphere size and transport cross section
L	Defined by Eq. 2.16
l_{tr}	Transport mean free path. Eq. 4.9
m	Distance traversed by a neutron that starts off-center in the sphere in Fig. 6.7
$N(E)\,dE$	Flux of neutrons between energy E and energy E + dE in the fission spectrum
$n_k(r,\theta)\,d\omega$	Number of neutrons per cubic centimeter that have their kth collision at position r before escaping from the sphere and whose direction of motion after this kth collision is in solid angle $d\omega$ at angle θ
$P(r,\theta)$	Probability that a neutron which starts at position r at an angle θ with the radius will escape from the sphere without making any further collisions. Eq. 3.4
$P(r)$	Average escape probability of a neutron starting at position r, assuming isotropic scattering. Eq. 3.5
P_n	Average escape probability for neutrons emerging from the nth elastic collision. Eqs. 3.8 and 3.12
P_n^*	Defined by Eq. 6.6
P^{**}	Defined by Eq. 6.7
P_n^n, $\bar{P}_n$	Escape probabilities after the nth elastic collision, considering an absorbing detector in the middle of the sphere. Section 6.3
${}^1p^{180}$, ${}^2p^{180}$, p^{180}, P_Ω, P_A	Defined in Section 6.3
$P(E')\,dE'$	Probability of neutrons escaping from the shell after only elastic collisions and having an energy between E′ and E′ + dE′. Section 6.5
P_i^S, P_i^D	Probabilities of emission of the neutron source and detection of the neutron counter in energy group i per unit volume of source and detector, respectively. For example, P_1^{37} is the detector probability in group i for Np^{237} counter.
$p(z)\,dz$	Probability that the total path through the shell of a neutron originating at the sphere center is between z and z + dz, considering only elastic collisions. Section 4.4 and Eq. 4.28
Q_0	Number of neutrons escaping from the sphere with no collisions. Eq. 6.19
q_i	Total number of neutrons escaping from the shell in group i. Section 8.2 and Eq. 8.22
R	Perpendicular distance from detector center to line joining points (x_0,y_0) and (x,y,z). Fig. 6.7

r_1	Inside radius of sphere
r_2	Outside radius of sphere
$\bar{r}$	Defined by Eq. 6.40
r_{12}	Distance between dV_1 and dV_2 in Fig. 8.1
S	Ratio of elastic transport cross section to total elastic cross section, σ_{et}/σ_{el}. Eq. 3.38
S_i^{n+1}	Number of group i neutrons produced on the n + 1 collision in a shell. Eq. 8.13
T_n	Number of neutrons escaping from a sphere after n elastic transport collisions. Eqs. 2.3, 3.2, 3.42, and 3.43
T_n'	Same as T_n but describing the first collision with the total cross section, not the transport cross section
V_d	Detector volume, used especially in Section 6.2
V_s	Source volume
W, W′	Finite detector size correction factors. Eqs. 6.22 and 6.25
W_2	Probability of a second inelastic collision in thin shell approximation. Eq. 2.6
X	Shell thickness, $r_2 - r_1$
Y	Effective shell thickness for case of very sharply peaked elastic scattering angular distribution. Eq. 4.27
$y(r,\theta)$	Distance traveled through the shell material to the edge of the shell by a neutron scattered at point r through angle θ. Eq. 2.9
$\langle y(r) \rangle$	Average of $y(r,\theta)$ over angle θ. Eq. 2.10
$\langle y \rangle$	Average of $y(r,\theta)$ over angle θ and r. Eq. 2.16
y_1	One half the cylindrical detector height in the finite detector size correction
Z	$(r - r_1) = XZ$. Eq. 2.13

Greek Alphabet

$\langle \alpha^2(r) \rangle$	Statistical average of α^2 over all possible neutron paths taken at position r. Eq. 4.34
δ	Phase shift. Eq. 3.19
Δ	Reduced efficiency for counter asymmetry correction. Section 6.4
$\Delta\sigma$	Error in inelastic cross section because of effect of energy loss on elastic collisions. Eqs. 6.37, 6.41, and 6.42
$\langle \theta^2 \rangle$	Average squared deflection of a neutron on an elastic collision
λ_d	Mean free path for neutron detection in counter
μ	Cosine θ
ν_i	Average number of neutrons per fission produced by a neutron in energy group i
π_1	The escape probability after the first elastic collision if total cross sections are used to specify the number of first collisions. Eqs. 4.5 and 5.15
σ_t, σ_{in}, σ_{el}, σ_{tr}, σ_{et}	One group total, inelastic collision (capture plus inelastic scattering), elastic, transport, and elastic transport cross sections
σ_i^{tr}, σ_i^{in}, σ_i^{c}, σ_i^{et}	Transport, inelastic scattering, capture, and elastic transport cross sections for energy group i. For this multi-group notation, inelastic scattering and capture are separated
$\sigma^D(E)$	Neutron detector sensitivity for energy E

$\hat{\sigma}_{el}$,	Average effective elastic cross section for a continuous spectrum counting in a threshold detector. Eq. 7.8
$\overline{\overline{\sigma_t}}$, $\overline{\overline{\sigma_{in}}}$, $\overline{\overline{\sigma_{el}}}$	Average total, inelastic collision, and elastic cross sections for continuous spectrum neutrons counting in a given threshold detector. Eqs. 7.7, 7.5, and 6.38, respectively.
σ_{ji}	Inelastic scattering cross section from energy group j to group i
ϕ, ϕ^r	Flux at arbitrary point in space. Section 6.2
ϕ_i	Fraction of neutrons from central source in sphere in energy group i, in our case f_i. Section 8.2
ϕ_m	Normal mode flux in sphere. Eq. 3.19
Ψ	Integrated one group flux over the volume of the sphere. Neutrons in this flux must have made at least one elastic collision. Section 3.6 and Eq. 3.48
Ψ_i	Integrated flux of energy group i over the volume of the sphere. Neutrons in this flux have made from zero to an infinite number of collisions

Chapter 1

INTRODUCTION

1.1 Purposes of the Investigation

A great need exists for information on the inelastic scattering of fast neutrons, both for the theory of the compound nucleus and for the calculation of the degradation of fission neutrons in a material. The present investigation was undertaken primarily to supply information of an integral nature on the inelastic scattering of fission spectrum neutrons. At the same time, results are obtained on the energy dependence of inelastic cross sections in various regions of the periodic table.

The "sphere method" was used in these experiments because it appeared to be the method most compatible with experimental conditions at the reactor. By detailed theoretical investigations, it was shown that this method permits a very accurate evaluation of the inelastic cross section.

1.2 Reciprocity Theorem

The experimental work discussed in this report was performed with an external fission source and a detector which was surrounded with a sphere of material for a transmission determination. In the theoretical treatment, however, we will assume that the source is inside the sphere and the detector outside. This is a considerable convenience for following the paths of neutrons from the shell. It has been shown in LA-1428[1] that one can obtain the same sphere transmission by surrounding either the source or the detector. Specifically, the reciprocity theorem states: The number of neutrons coming from an isotropic source at the center of a spherical shell of matter and detected in an isotropic detector outside the sphere is equal to the number detected if the positions of source and detector are interchanged.

It should be pointed out that if one performs experiments with a large anisotropic counter inside a sphere and an anisotropic source outside the sphere, the transmission computed by assuming an internal source must be done as follows: The internal source must have the same shape and absorption characteristics as the counter it replaces, and the external counter must have the same shape and characteristic angular sensitivity as the source it replaces.

1.3 The Sphere Method

The method of spherical shells has been used by a large number of experimenters. Qualitatively the method works as follows:

If we place an isotropic threshold neutron detector at a large distance from an isotropic source and count with and without a sphere of material surrounding the source, the resulting transmission

$$T = \frac{\text{counts (sphere on)}}{\text{counts (sphere off)}}$$

is a measure of the amount of inelastic scattering.

We can think of this as follows: With only elastic scattering in a shell, a transmission of unity will be obtained, because of spherical symmetry. Therefore, when both elastic and inelastic collisions occur in the shell, one might tend to believe that the number of inelastic collisions is more or less independent of the elastic cross section. If this were true, the elastic scatterings would again give essentially no effect, and only the inelastic cross section would be important in determining the sphere transmission.

On the basis of this argument, it has often been assumed that the transmission is given by an exponential

$$T = e^{-\sigma_{in} X} \tag{1.1}$$

where X is the shell thickness. In particular, this has been assumed by Phillips et al.[2] at Los Alamos in scattering experiments with 14 Mev neutrons. They justify the use of the exponential by pointing out that the elastic scattering angular distribution has a very pronounced forward peak at 14 Mev. This means that an elastic scattering does not lengthen the paths traveled by neutrons in escaping from the sphere and, hence, does not act like a scattering at all. Therefore, the inelastic cross section only is important in determining the transmission of a sphere. Also, they have varied the sphere thickness over a limited range and have observed essentially the same inelastic cross section at all thicknesses.

The argument of Phillips et al.[2] may be reasonably well justified at 14 Mev (since the inelastic cross section is large and the elastic transport cross section small). However, it certainly is not sufficient at lower energies, around 1 Mev, where the elastic cross section, as well as the average scattering angle, is much larger. Equation 1.1 will break down when the inelastic cross section becomes small compared to the elastic transport cross section, and this is the rule, rather than the exception, at energies around 1 Mev.

Of course, in any case, the first term in the expansion of Eq. 1.1 in a power series will be valid, viz.

$$T = 1 - \sigma_{in} X \tag{1.2}$$

for very thin shells, regardless of the elastic scattering cross section. For this reason, some experimenters have used very thin shells. The disadvantage of this is obvious; for the sake of statistical accuracy, shells with a transmission of 30 to 70 percent are desirable. Moreover, Eq. 1.2 does not indicate how thin the shells have to be for Eq. 1.2 to be valid. Our theory, in Chapter 2, will show that the shells need to be much thinner than might be expected.

It is clearly desirable to have a theory which is valid also for thicker shells. Several approaches to this problem have been advanced in the past. H. H. Barschall[3] has suggested the use of an effective path length through the shell instead of the thickness X in Eq. 1.1. Amaldi et al.[4] have formulated a correction factor F(X) for multiple scatterings. The shell transmission is written

$$T = F(X)\, e^{-\sigma_{in} X} \tag{1.3}$$

Szilard et al.[5] have used a method of interpreting sphere transmission data which is similar to the methods presented in Chapters 3 and 4. They conclude that the failure of their theory to give the same cross section for all shell thicknesses of the same element may be due to a "hardening" of the spectrum.

A tested theory to use in the evaluation of fairly thick spherical shells is clearly needed at present. This will be developed in Chapters 3 and 4. A large amount of experimental work was performed to test its validity under a wide variety of conditions.

In addition, cross sections for inelastic scattering from a fission neutron spectrum to a point below several detector energy thresholds have been measured and are discussed in Chapters 11, 12, 13, and 14 of this report. These measurements were performed for about 15 elements.

The meaning of the average inelastic cross sections, which were measured with energy threshold detectors and the fission neutron spectrum, is discussed in Chapter 7.

Chapter 2

THIN-SHELL THEORY

A theoretical analysis of the thin shell is particularly instructive because it shows, by a purely analytical argument, the large effect of elastic scattering on the transmission. To show this effect, it is clearly necessary to calculate the transmission at least up to order X^2, where X is the thickness of the shell; for, in the first order, the transmission is given by Eq. 1.2. It has been assumed in Eq. 1.2, as it will be in the following, that inelastic scattering is the only process which renders neutrons undetectable (i.e., that neutron capture is negligibly small). Otherwise, the capture cross section should be added to that for inelastic scattering.

To obtain Eq. 1.2, as well as equations in this chapter, we make use of the reciprocity theorem; i.e., we assume the source to be in the center of the spherical shell. The shell thickness is

$$X = r_2 - r_1 \tag{2.1}$$

where r_2 is the outer radius, and r_1 the inner radius. The macroscopic cross section, measured in cm^{-1}, is used for σ_{in} in Eq. 1.2, as it is for all cross sections in this report, unless otherwise indicated.

Elastic scattering has no influence on the transmission in the linear approximation Eq. 1.2 because in this approximation we have only one collision, which may be either elastic or inelastic, so that certainly T is of the form

$$T = 1 - (a\sigma_{el} + b\sigma_{in}) \tag{2.2}$$

where a and b are constant coefficients. But in the absence of inelastic scattering, elastic scattering does not change the number of neutrons transmitted, hence a = 0.

Now let us proceed to a better approximation. We will assume throughout that one neutron is emitted by the source. Then the number of neutrons which come out of the sphere without any collision is exactly

$$T_0 = e^{-\sigma_t X} \tag{2.3}$$

where σ_t is the total cross section. The number of first collisions is $1 - T_0$, and the number of inelastic first collisions is therefore

$$I_1 = \left(\frac{\sigma_{in}}{\sigma_t}\right)(1 - T_0) \tag{2.4}$$

Expanding up to order X^2, we get

$$I_1 = \sigma_{in} X - \frac{1}{2}\sigma_{in}\sigma_t X^2 + \ldots \tag{2.5}$$

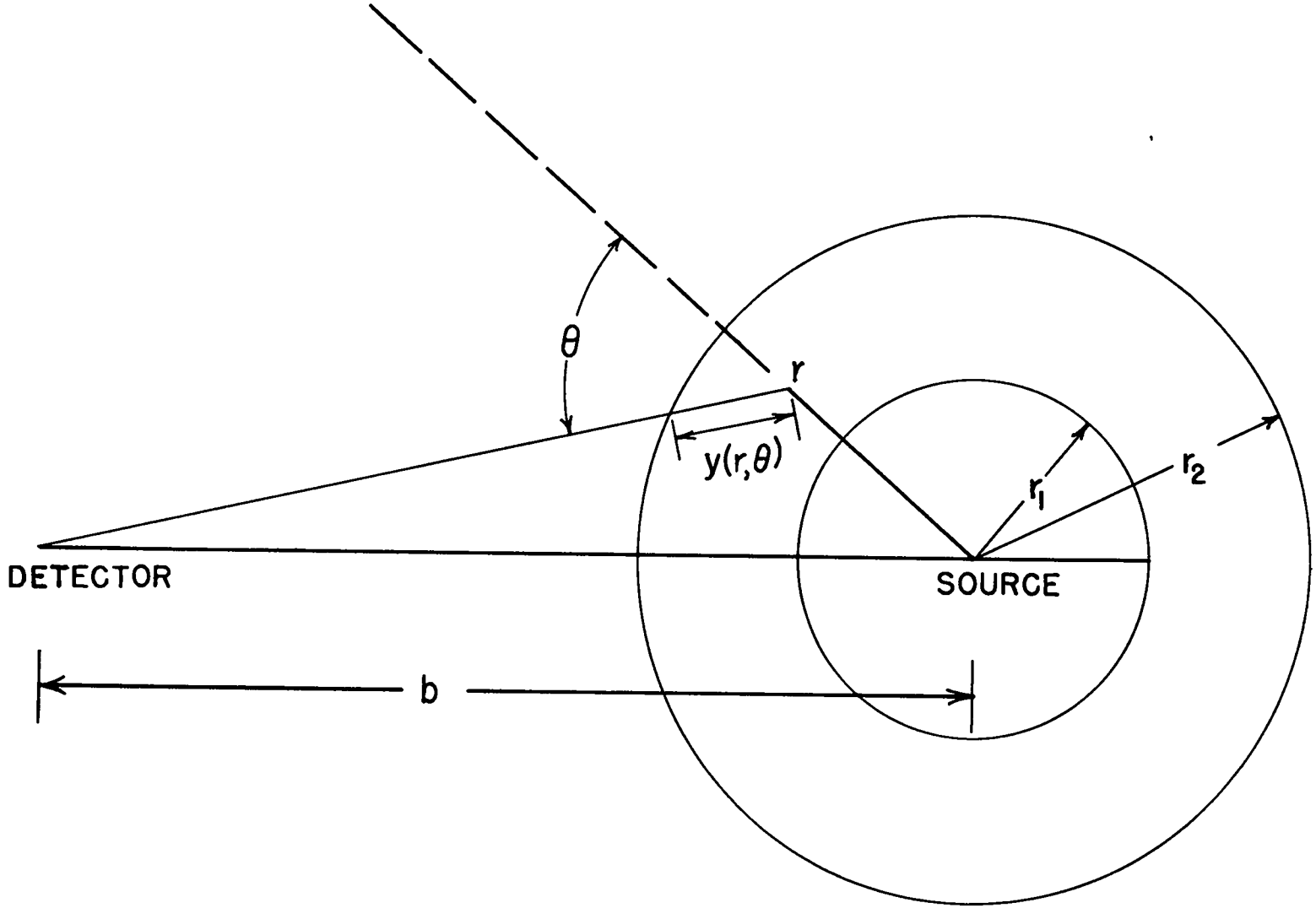

Fig. 2.1 Geometry used for analysis of sphere experiments.

We now wish to calculate, to order X^2, the number of neutrons which are elastically scattered on their first collision and then inelastically on the second. For the sake of generality, we assume that the elastic scattering is not isotropic, and define $\sigma(\theta)\, d\omega$ as the differential cross section for elastic scattering into solid angle $d\omega$ at angle θ. The elastic scattering is illustrated in Fig. 2.1.

The probability that a neutron, after its first elastic scattering at r, is subsequently scattered inelastically depends on the distance $y(r,\theta)$ which it has to travel after its first scattering, before escaping from the sphere. In our approximation, it is sufficient to set this probability equal to

$$W_2 = \sigma_{in}\, y(r,\theta) \tag{2.6}$$

Then the number of second inelastic scatterings is

$$I_2 = \sigma_{in} \int_0^{4\pi} \int_{r_1}^{r_2} \sigma_{el}(\theta)\, d\omega\, dr\, y(r,\theta) \tag{2.7}$$

This expression is, of course, proportional to X^2, and the transmission to order X^2 is

$$T = 1 - I_1 - I_2 \tag{2.8}$$

For an arbitrary angular distribution of elastic scattering, I_2 would have to be found numerically. However, to demonstrate the effect of elastic collisions, we shall calculate it with isotropic elastic scattering. We shall show in Chapter 4 that even for very anisotropic scattering it is a good approximation to replace the actual scattering by isotropic scattering, if at the same time the total cross section is replaced by the transport cross section. This makes the present calculation quite realistic. From geometry

$$y(r,\theta) = -\, r \cos\theta + \sqrt{r_2^2 - r^2 \sin^2\theta} - a\sqrt{r_1^2 - r^2 \sin^2\theta} \tag{2.9}$$

where $a = 2$ if $\cos\theta \leq -\sqrt{1 - \frac{r_1^2}{r^2}}$

and $a = 0$ if $\cos\theta \geq -\sqrt{1 - \frac{r_1^2}{r^2}}$

Geometrically, a = 2 if, and only if, the neutron path after scattering penetrates into the interior cavity of the shell (see Fig. 2.2).

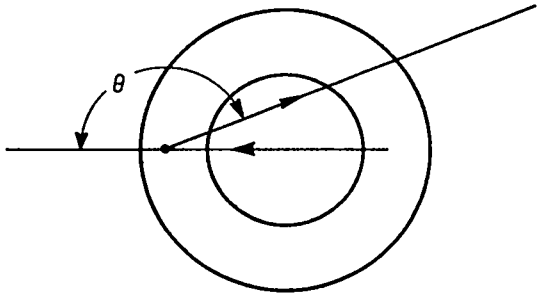

Fig. 2.2

If the scattering is isotropic, Eq. 2.9 can be averaged over solid angle and gives for any r

$$\langle y(r)\rangle = \frac{1}{4\pi} \int_0^{4\pi} y(r,\theta)\, d\omega$$

$$\langle y(r)\rangle = \frac{X}{2} + \frac{r_2^2 - r^2}{4r} \ln\left(\frac{r_2 + r}{r_2 - r}\right) + \frac{r^2 - r_1^2}{4r} \ln\left(\frac{r + r_1}{r - r_1}\right) \tag{2.10}$$

For simplicity, let us assume now that the shell is thin, not only compared to a mean free path, but also compared to its radius, i.e.

$$X \ll r_2 \tag{2.11}$$

Then Eq. 2.10 simplifies to

$$\langle y(r)\rangle = \frac{X}{2} + \frac{r_2 - r}{2} \ln\left(\frac{2r_2}{r_2 - r}\right) + \frac{r - r_1}{2} \ln\left(\frac{2r}{r - r_1}\right) \tag{2.12}$$

Let us now set

$$r - r_1 = XZ \tag{2.13}$$

where Z runs from zero to one. Then Eq. 2.12 may be written as

$$\langle y(r)\rangle = \frac{X}{2}\left[1 + \ln\left(\frac{2r_2}{X}\right) - Z \ln Z - (1 - Z) \ln (1 - Z)\right] \tag{2.14}$$

The two last terms in the square bracket always give a positive contribution, which varies from 0 at $Z = 0$ and 1, to ln 2 at $Z = \frac{1}{2}$. Even the maximum value, ln 2, is small compared with $\ln (2\, r_2/X)$ under the assumption of Eq. 2.11. Therefore we find: The average length of the path of a scattered neutron, $\langle y(r)\rangle$, is almost independent of the location of the scattering, r. It is largest if the scattering occurs in the middle of the shell, smallest if it occurs at the outer or inner edge. As a consequence, the probability of making an inelastic collision after an elastic one is almost independent of the point where the elastic collision occurs.

Some understanding of this result, and of the form of Eq. 2.14, may be obtained as follows: Consider the neutrons starting from r in direction θ, and those in direction $\pi - \theta$. The sum of their paths, for a thin shell, is approximately twice the path through a slab of thickness $\overline{X}$ at angle θ to the normal, i.e.

$$\frac{2X}{\cos\theta} \tag{2.15}$$

This is independent of Z, the starting position within the shell (Eq. 2.13). Averaging Eq. 2.15 over the solid angle gives a logarithmic divergence which is cut off by the sphericity when $\cos\theta \sim X/r_2$; hence the appearance of $\ln (r_2/X)$ in Eq. 2.14.

Averaging Eq. 2.14 over Z (i.e., over r) gives $+\frac{1}{4}$ from each of the two last terms and hence

$$\langle y\rangle = \frac{X}{2}\left[\frac{3}{2} + \ln\left(\frac{2r_2}{X}\right)\right] \equiv \frac{XL}{2} \tag{2.16}$$

where the factor L is clearly quite large, usually between 3 and 4, and largest for the thinnest shells. The number of second inelastic collisions (i.e., I_2, Eq. 2.7) is obtained using Eq. 2.16 for $\langle y\rangle$, the average path length in the shell after a collision

$$I_2 = \frac{1}{2}\sigma_{in}\sigma_{el} X^2 L \tag{2.17}$$

The transmission (Eq. 2.8) is then, to order X^2

$$T = 1 - \sigma_{in}X + \frac{1}{2}\sigma_{in}X^2(\sigma_t - \sigma_{el}L) + \ldots \tag{2.18}$$

For an anisotropic scattering angular distribution, instead of an isotropic, one should use the elastic transport cross section σ_{et} instead of σ_{el} in Eq. 2.18.

The coefficient of X^2 in this formula is very interesting indeed. If the scattering is almost entirely inelastic, then

$$T = 1 - \sigma_{in}X + \frac{1}{2}\sigma_{in}^2 X^2 + \ldots \tag{2.19}$$

which is the well-known expansion of the exponential. In this case, the X^2 term is positive, i.e., the curve of T vs X has the familiar upward bend (Fig. 2.3). But if the

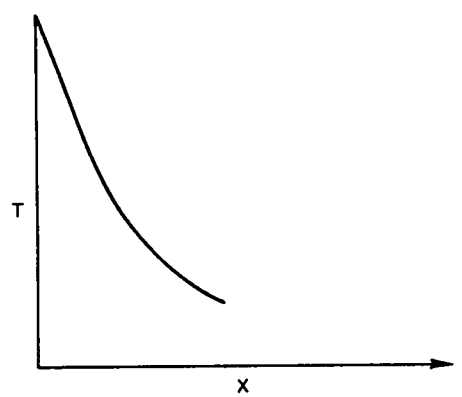

Fig. 2.3 — Scattering almost entirely inelastic.

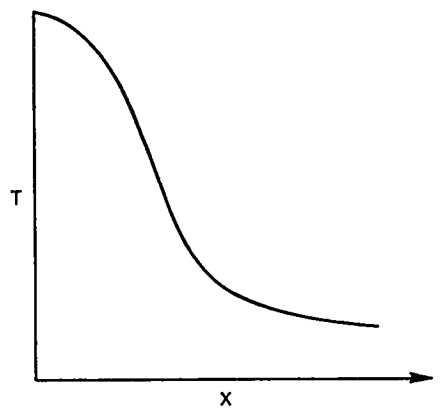

Fig. 2.4 — Scattering mostly elastic.

scattering is mostly elastic, then because of a large value of L, $\sigma_{el}L$ is greater than σ_{in}, and the X^2 term in Eq. 2.18 is negative. Then the curve of transmission vs thickness bends downward as illustrated in Fig. 2.4. Clearly, in this case, it must be entirely wrong to evaluate transmission experiments by assuming

$$T = e^{-\sigma_{in}X}$$

The choice of the exponential formula is particularly bad because the negative coefficient of X^2 in Eq. 2.18 is apt to be large, much larger than the positive factor in the "elementary" formula (Eq. 2.19), both because $L > 1$ and because $\sigma_{el} > \sigma_{in}$.

Obviously, the curve of T vs X cannot bend downward indefinitely. There must be an inflection point and finally a quasi-exponential behavior, caused by higher order terms as shown schematically in Fig. 2.4. Of course, at no point (except for extremely thin shells) can the inelastic cross section be derived from the transmission by the exponential formula.

The reason for the behavior of Eq. 2.18 is, of course, that the path of a neutron in the shell is greatly increased by elastic scattering. Suppose a neutron makes a collision at some point r in the shell: then, if it continued radially outward, it would still go a distance $r_2 - r$, and if we average this quantity over all scattering positions r, we get $\frac{1}{2}$ X. On the other hand, if the neutron is scattered in a random direction at r, then its average path in the shell before leaving is $\frac{1}{2}$ X L, according to Eq. 2.16, which is L times (3 to 4 times) longer. Clearly, by going more or less tangentially, the neutron must go a longer distance in the shell than if it went radially.

The coefficient of X^2 will be negative as long as

$$\frac{\sigma_{el}}{\sigma_t} > \frac{1}{L.} \tag{2.20}$$

Thus relatively small inelastic scattering ($\frac{1}{4}$ or $\frac{1}{3}$ of total) will suffice to make the transmission curve bend initially downward.

Let us examine now how thin the shell must be made if one wants to avoid multiple-scattering corrections: Assuming $\sigma_{el} > \sigma_{in}$, the parenthesis in Eq. 2.18 is about $-\sigma_{el}(L-1)$. Therefore, if the inelastic cross section is deduced from a measured transmission by means of the exponential formula (Eq. 1.1) or the linear formula (Eq. 1.2), the relative error in it, according to Eq. 2.18, will be

$$\frac{1}{2}\sigma_{el}(L-1)X \tag{2.21}$$

The inelastic cross section deduced from an elementary analysis will always be too large. If we want to make the error (Eq. 2.21) equal to 5 percent, and if $L = 4$, then the probability of an elastic scattering in the shell must be kept down to 3 percent. In the region of 1 or 2 Mev, σ_{in} is about $\frac{1}{2}$ or $\frac{1}{3}$ of σ_{el} for most substances; therefore the probability of inelastic scattering must be about 1 percent! To measure the transmission in such a case with sufficient accuracy is virtually impossible.

From the previous discussion it can be seen that the elementary formulas should not, in general, be used to evaluate sphere transmission experiments. A more nearly correct method of computing inelastic cross sections is to use Eq. 2.8 or 2.18. These equations, however, have a limited range of application and should not be used in the case of a thick shell. Some specific examples in which transmissions computed according to Eq. 2.18 are compared with transmissions determined from a more detailed theory are given in Chapter 4.

Chapter 3

THICK-SHELL THEORY AND ISOTROPIC SCATTERING

We shall now treat the case of a shell of arbitrary thickness in which an arbitrary number of collisions may take place. However, we shall still assume that the thickness is of the order of one mean free path, rather than many. This means that the density of neutrons from the source will not fall off too much from the inside of the shell to the outside—an assumption which will be useful in the theory. The case of very thick shells could be treated by diffusion theory, but it has practical importance for measurements only when it is desired to measure extremely small absorption cross sections.

The theory will be greatly simplified if we assume isotropic scattering. As will be shown in Chapter 4, this assumption is a good approximation if the elastic transport cross section is used for the elastic scattering cross section. The error thus made in the inelastic cross section is of the order of 1 percent. We shall, therefore, use in this section the total transport cross section σ_{tr} and the elastic transport cross section σ_{et}, rather than the total cross section σ_t and the total elastic cross section σ_{el}. We further assume, as before, that the detector does not respond to inelastically scattered neutrons.

3.1 Number of Second Collisions

Let us consider the neutrons which have suffered one elastic collision in the shell. Their number (for one source neutron) is, similar to Eq. 2.4

$$E_1 = \frac{\sigma_{et}}{\sigma_{tr}} (1 - T_0) \tag{3.1}$$

with

$$T_0 = e^{-\sigma_n X} \tag{3.2}$$

The fraction which suffer their first collision between r and r + dr is

$$f_1(r)\, dr = \frac{e^{-\sigma_n (r - r_1)} \sigma_{tr}\, dr}{1 - T_0} \tag{3.3}$$

A neutron which starts at position r at an angle θ with the radius will have a probability

$$P(r,\theta) = e^{-\sigma_n\, y(r,\theta)} \tag{3.4}$$

of escaping from the sphere without making any further collisions. Here $y(r,\theta)$ is the distance travelled in the shell (if there is no collision), as shown in Figs. 2.1 and 2.2 and as calculated in Eq. 2.9. If the scattering is isotropic, we are interested in the average escape probability of a neutron starting at r

$$P(r) = \frac{1}{4\pi} \int_0^{4\pi} P(r,\theta)\, d\omega \tag{3.5}$$

The probability that such a neutron makes at least a second collision is then $1 - P(r)$, and the probability that this neutron makes a second collision which is inelastic, is

$$\frac{\sigma_{in}}{\sigma_{tr}} [1 - P(r)] \tag{3.6}$$

The total number of inelastic second scatterings is then

$$I_2 = E_1 \frac{\sigma_{in}}{\sigma_{tr}} \int_{r_1}^{r_2} f_1(r)\, dr\, [1 - P(r)] \tag{3.7}$$

It is convenient to introduce the average escape probability for neutrons emerging from first collisions

$$P_1 = \int_{r_1}^{r_2} f_1(r)\, dr\, P(r) \tag{3.8}$$

Then, if we remember that by definition

$$\int_{r_1}^{r_2} f_1(r)\, dr = 1 \tag{3.9}$$

we find

$$I_2 = E_1 \frac{\sigma_{in}}{\sigma_{tr}} (1 - P_1) \tag{3.10}$$

3.2 Number of Third and Higher Order Collisions

The number of second elastic collisions is

$$E_2 = E_1 \frac{\sigma_{et}}{\sigma_{tr}} (1 - P_1) \tag{3.11}$$

Suppose we knew the spatial distribution of these neutrons, $f_2(r)\, dr$. Then we could define an average escape probability for neutrons after the second collision

$$P_2 = \int_{r_1}^{r_2} f_2(r)\, dr\, P(r) \tag{3.12}$$

The number of neutrons which are inelastically scattered on their third collision is then

$$\begin{aligned} I_3 &= E_2 \frac{\sigma_{in}}{\sigma_{tr}} (1 - P_2) \\ &= E_1 \frac{\sigma_{in}}{\sigma_{tr}} \frac{\sigma_{et}}{\sigma_{tr}} (1 - P_1)(1 - P_2) \end{aligned} \tag{3.13}$$

This may be continued in an obvious way, giving for inelastic collisions on the n + 1 collision:

$$I_{n+1} = E_1 \frac{\sigma_{in}}{\sigma_{tr}} \left(\frac{\sigma_{et}}{\sigma_{tr}}\right)^{n-1} (1 - P_1)(1 - P_2) \ldots (1 - P_n) \tag{3.14}$$

The difficulty here lies clearly in the calculation of spatial neutron distributions. It is possible, though troublesome, to obtain this for the second collisions, $f_2(r)$, but it would be

prohibitive to try to calculate the distributions for higher collisions. However, two circumstances help at this crucial point:

(1) The spatial distribution of successive collisions converges to a limiting distribution which we shall call $f_m(r)$, and this convergence is quite rapid. This will be discussed in Section 3.3.

(2) The escape probability P(r) does not depend very much on r, and therefore the average escape probability P_n is not very sensitive to the assumed distribution function $f_n(r)$.

Concerning statement 2, we remember the result of Eq. 2.14 which showed, at least for a thin shell, that $1 - P(r)$ [actually $\langle y(r) \rangle$ in Eq. 2.14] varies only by about 20 percent from maximum to minimum as a function of r. Any "reasonable" distribution function $f_n(r)$ of the starting points of the neutrons will give the same average $(1 - P)$ within a few percent.

For thicker shells, of the order of one mean free path, the dependence on r may be slightly greater. Consider, for example, neutrons starting at the outer and inner edges of the shell, r_2 and r_1, respectively. They will, on the whole, follow the same paths, such as that shown in Fig. 3.1.

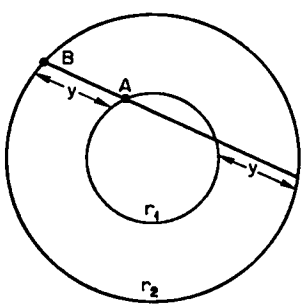

Fig. 3.1

Let y be the length of a typical path through the material on one traversal of the shell. Then the probability of a collision within the shell is

$$1 - P(r_1,\theta) = 1 - e^{-\sigma_{tr} y} \cdot \tag{3.15}$$

if the neutron starts from the inside (point A) going either "up" or "down." If it starts from the outside (point B) and goes "up," the neutron will not traverse any material, giving zero collision probability, while if it starts "down," we get

$$1 - P'(r_2,\theta) = 1 - e^{-2\sigma_{tr} y} \tag{3.16}$$

The average between "up" and "down" is

$$1 - P(r_2,\theta) = \frac{1}{2}(1 - e^{-2\sigma_{tr} y}) \tag{3.17}$$

If we expand Eqs. 3.15 and 3.17 in powers of y, the linear terms are equal

$$1 - P(r_1,\theta) = 1 - P(r_2,\theta) = \sigma_{tr} y \tag{3.18}$$

This corresponds to the result in Eq. 2.14, where the inner and outer edge gave equal values of $\langle y(r) \rangle$. However, for thicker shells, Eq. 3.15 is clearly greater than Eq. 3.17. The maximum collision probability, which for thin shells lies at the middle of the shell, moves with increasing shell thickness towards the inside edge. At the same time, the variation of $1 - P(r)$ with r is apt to increase, but even for very thick shells it is not likely to exceed a factor of 2 (compare Eqs. 3.15 and 3.17).

In Fig. 3.2 we give $1 - P(r)$ as a function of r for some typical cases.

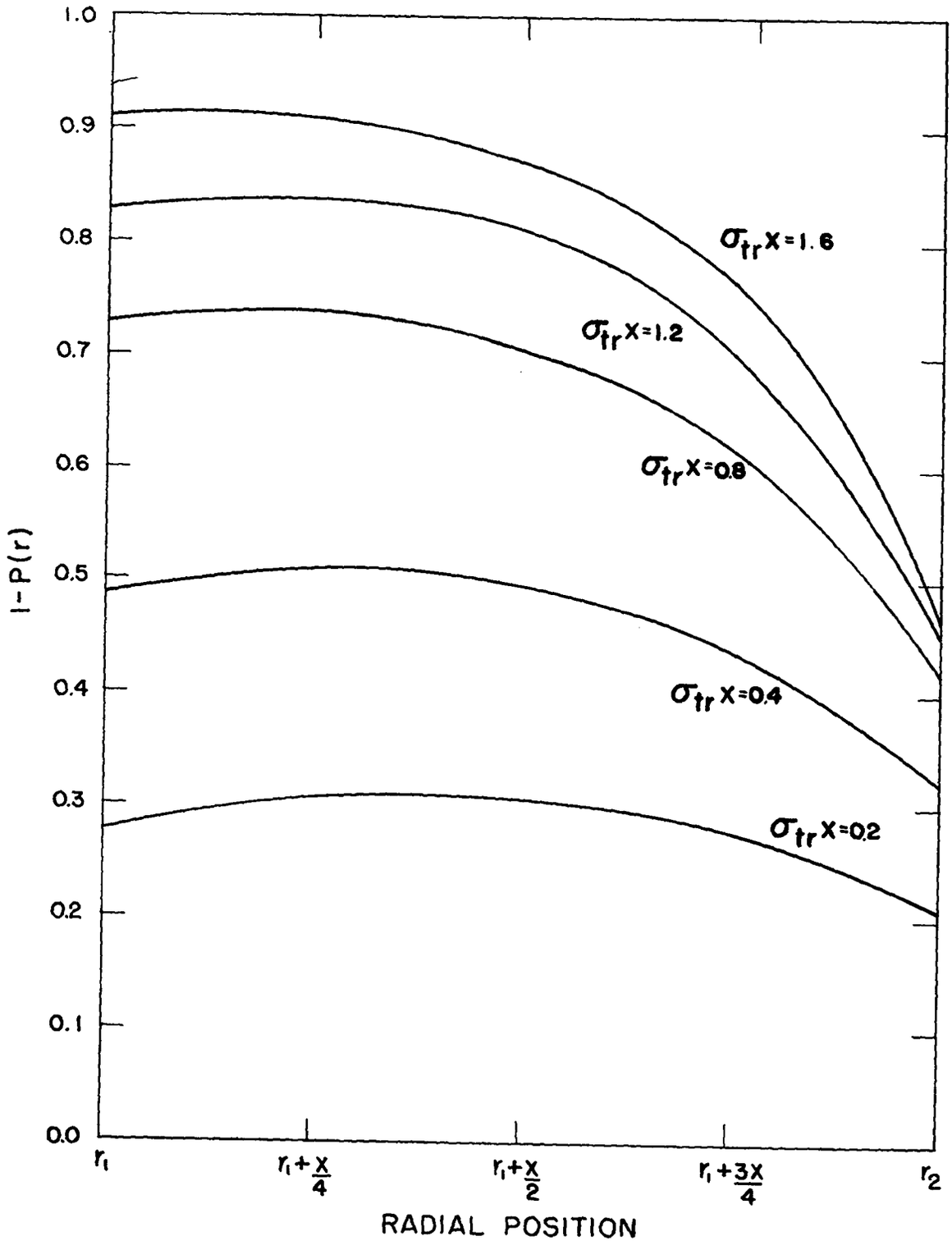

Fig. 3.2—Plot of 1 – P(r), the probability of making another collision for neutrons scattered isotropically at various points in spherical shells, with $r_1/r_2 = 0.8$.

3.3 Normal Mode Distribution

Statement 1 (page 28) claims that the spatial distribution of the nth collision, $f_n(r)$, tends to a limit as n increases. To see this, and to calculate this limit, let us make the following consideration: For given f_n, the spatial distribution of the next collisions, $f_{n+1}(r)$, is completely determined, and does not change if we increase the absolute number of neutrons emitted in each of the nth collisions. Imagine this is done, e.g., by ascribing to the material a fictitious fission cross section, such that in each collision not one neutron is emitted, but g neutrons.* Then we can choose g in such a way that, in the limit of large n, the total number of neutrons making an nth and the n + 1 collision is the same. Then our shell will be just critical, and the spatial distribution of neutrons will be that characteristic of a critical assembly of the given shell geometry, i.e., the fundamental normal mode of the shell. We have shown, then, that also in our actual problem, with only elastic and inelastic collisions and no fission, the neutron distribution tends toward the normal mode.

This argument does not show, of course, how many collisions are required to reach the normal mode. This depends on the deviation of the distribution of first collisions, $f_1(r)$, from the normal mode. Fortunately, this deviation usually is not very great, especially if the thickness of the shell is not more than about one mean free path. In Fig. 3.3 we compare the distribution of first collisions with the normal mode and with a histogram of the distribution of neutrons that have made a second collision for a typical case. All collision distributions are normalized to one collision in the shell. If f_1 does not differ much from f_m, then f_2, f_3, etc., will, of course, be even closer to f_m.

To calculate the normal mode distribution, we use the method of the extrapolated end point. We assume that within the shell the neutron flux distribution is

$$\phi_m \propto \frac{\sin k\,(r + \delta)}{r} \tag{3.19}$$

where k is related in the usual manner of integral theory to the fictitious number of neutrons produced per collision, g, viz.

$$\frac{k/\sigma_{tr}}{\arctan\left(\frac{k}{\sigma_{tr}}\right)} = g \tag{3.20}$$

and all distances are in centimeters.

To determine k and the "phase shift" δ, we use the following boundary conditions:

(1) At the inner radius, we assume the slope of ϕ_m to be zero

$$\frac{d\phi_m}{dr} = 0 \qquad \text{at } r_1 \tag{3.21}$$

$$kr_1 \cot\left[k(r_1 + \delta)\right] = 1 \tag{3.22}$$

This boundary condition is not exact but should ensure reasonably well that there is no net flux, except for source neutrons, through the inner surface of the sphere r_1.

(2) At the outer radius, we have the condition of the extrapolated end point

$$\sin k(r_2 + \delta + D) = 0 \tag{3.23}$$

*g is usually denoted by 1 + f in neutron diffusion theory. This f is not used explicitly in this report.

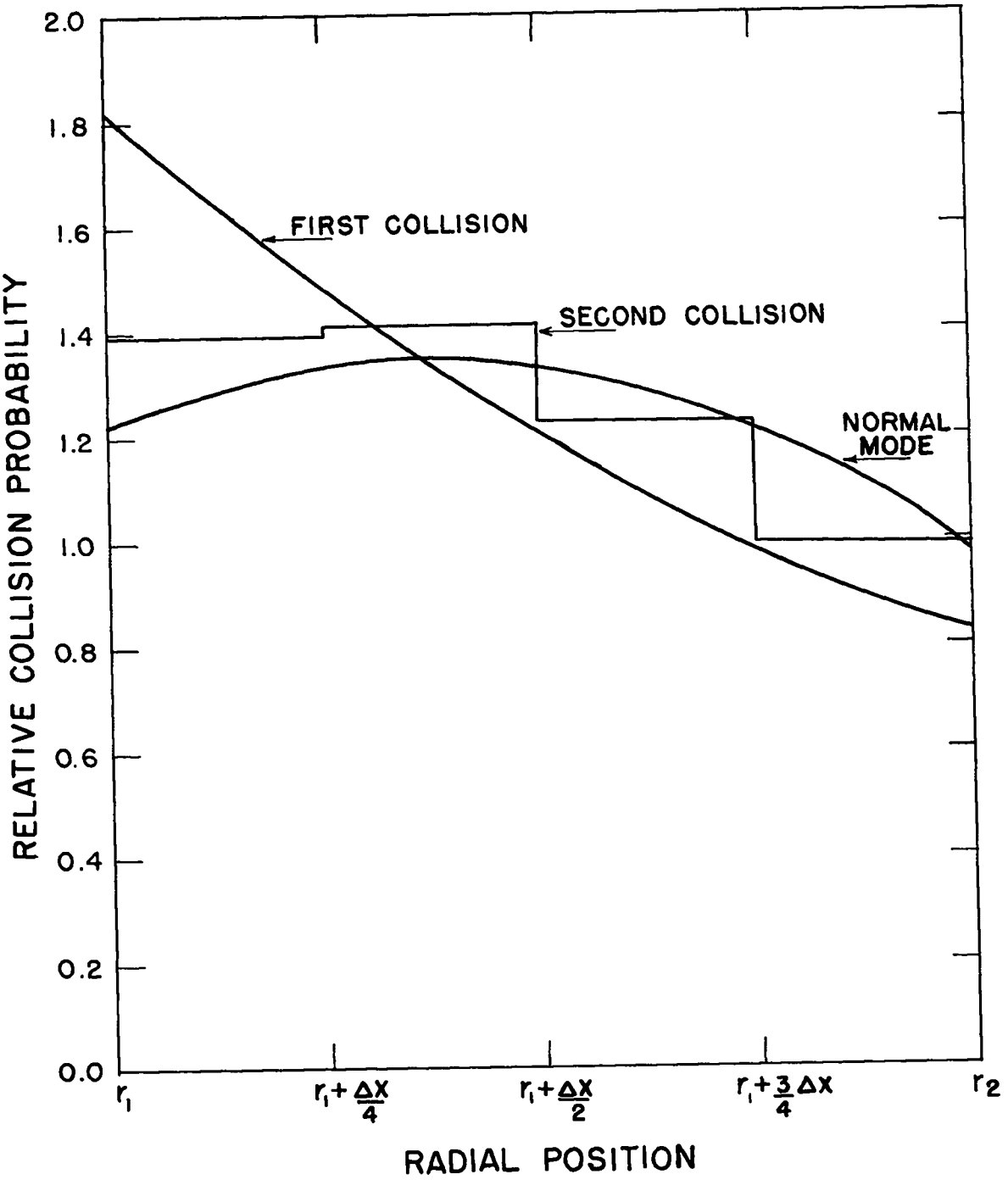

Figure 3.3 — Radial distribution of neutrons that have made first collisions, second collisions, and normal mode collisions for a shell with $\sigma_{tr}X = 0.8$ and $r_1/r_2 = 0.8$.

where D is the extrapolation distance for which Frankel and Nelson give the very good approximate formula*

$$D = \frac{0.71}{g\,\sigma_{tr}} \tag{3.24}$$

From Eq. 3.23, we have $k(r_2 + \delta + D) = \pi$, and Eq. 3.22 becomes

$$kr_1 \cot [\pi - k(X + D)] = 1 \tag{3.25}$$

It may be noted that

$$kD = 0.71 \arctan\left(\frac{k}{\sigma_{tr}}\right) \tag{3.26}$$

Rearranging Eq. 3.25 and substituting Eq. 3.26

$$kX + 0.71 \arctan\left(\frac{k}{\sigma_{tr}}\right) + \arctan (kr_1) = \pi \tag{3.27}$$

In practice, Eq. 3.27 was solved numerically by assuming values of k until the desired X and r_1 would satisfy the equation.

For very thin shells, k becomes large, and $\arctan (k/\sigma_{tr}) = \pi/2$. Then the phase of the sine at the outer edge is

$$k(r_2 + \delta) = \pi - kD = 1.29\left(\frac{\pi}{2}\right) = 116^\circ \tag{3.28}$$

which is now independent of X. If $X \ll r_1$, then the phase at the inner edge is

$$k(r_1 + \delta) = \frac{\pi}{2} - \frac{1}{kr_1} \tag{3.29}$$

and therefore

$$kX = 0.29\frac{\pi}{2} + \frac{1}{kr_1} = 0.45 + \frac{1}{kr_1} \tag{3.30}$$

from which k is easily determined.

With the neutron distribution given by the normal mode $r^2\phi_m$ (ϕ_m from Eq. 3.19) the escape probability can be calculated. In all cases we have considered, P_m does not differ greatly from P_1, the escape probability after one collision. This problem is considered in more detail in Section 5.4.

3.4 Calculation of Transmission

If we assume that all higher escape probabilities are equal to that for the normal mode

$$P_2 = P_3 = \ldots = P_m \tag{3.31}$$

according to Eq. 3.14, the inelastic collision probabilities after the first collision ($n \geq 1$, $n + 1$ = collision number) are given by

*This formula appeared originally in 1944 in a Los Alamos Scientific Laboratory report, now available as AECD-3497.

$$I_{n+1} = E_1\left(\frac{\sigma_{in}}{\sigma_{tr}}\right)(1-P_1)\left(\frac{\sigma_{et}}{\sigma_{tr}}\right)^{n-1}(1-P_m)^{n-1} \tag{3.32}$$

This series can be summed and gives

$$\sum_{n=1}^{\infty} I_{n+1} = \frac{E_1(\sigma_{in}/\sigma_{tr})(1-P_1)}{1-(\sigma_{et}/\sigma_{tr})(1-P_m)} \tag{3.33}$$

$$= \frac{E_1\sigma_{in}(1-P_1)}{\sigma_{in}+\sigma_{et}P_m} \tag{3.34}$$

We insert E_1 from Eq. 3.1 and the first inelastic collisions from Eq. 2.4 and find thus the total number of inelastic collisions, which is equal to the number of neutrons which fail to be transmitted

$$1-T = (1-T_0)\frac{\sigma_{in}}{\sigma_{tr}}\left[1+\frac{\sigma_{et}(1-P_1)}{\sigma_{in}+\sigma_{et}P_m}\right] \tag{3.35}$$

Since we have actually computed curves of escape probability for neutrons which have made a second elastic transport collision, an alternate and slightly more accurate formula for sphere transmission is

$$1-T = (1-T_0)\frac{\sigma_{in}}{\sigma_{tr}}\left[1+\frac{\sigma_{et}}{\sigma_{tr}}(1-P_1)+\frac{(1-P_1)(1-P_2)\sigma_{et}^2}{\sigma_{tr}(\sigma_{in}+\sigma_{et}P_m)}\right] \tag{3.36}$$

Equations 3.35 and 3.36 are our final formulas. These formulas can be simplified if we assume that the escape probability is the same for the first collision, second collision, and the normal mode: $P_1 = P_2 = P_m$. Then Eqs. 3.35 and 3.36 reduce to

$$1-T = (1-T_0)\left(\frac{\sigma_{in}}{\sigma_{in}+\sigma_{et}P_m}\right) \tag{3.37}$$

This formula allows a simple physical interpretation. The total number of neutrons which "are supplied" to the shell is $1-T_0$. These can be removed from the shell by two processes, either by inelastic scattering, or by escape. In a given collision, the probability of inelastic scattering is σ_{in}, that of elastic scattering followed by escape is $\sigma_{et}P_m$. This gives for the fraction scattered inelastically the expression in Eq. 3.37.

3.5 Analysis of Experiments

Let us assume the total transport cross section σ_{tr} is known, and σ_{in} is to be determined. Then we first calculate P_1 and P_m as a function of σ_{tr}, r_1 and r_2; this is done in Chapter 5. $T_0 = e^{-\sigma_{tr}X}$ is immediately obtained. Experiment gives $1-T$. Since $\sigma_{et} = \sigma_{tr} - \sigma_{in}$, Eq. 3.35 contains only the one unknown σ_{in}, for which it can easily be solved.

In practice, other experiments give not σ_{tr}, but the total cross section σ_t. In addition, Jurney and Zabel[6,15] have measured the angular distribution of the elastically scattered neutrons (for most of the neutron spectra and elements of interest here). From these data we can obtain the ratio of elastic transport to total elastic cross section, viz.

$$S = \frac{\sigma_{et}}{\sigma_{el}} = \frac{\int_0^{\pi}\sigma_{el}(\theta)\,(1-\cos\theta)\,\sin\theta\,d\theta}{\int_0^{\pi}\sigma_{el}(\theta)\,\sin\theta\,d\theta} \tag{3.38}$$

We then write

$$\sigma_{et} = (\sigma_t - \sigma_{in})\,S$$
$$\sigma_{tr} = \sigma_{et} + \sigma_{in} \tag{3.39}$$

which reduces all cross sections in Eqs. 3.35, 3.36, and 3.37 to the measured σ_t and the unknown σ_{in}. The escape probabilities P_1, P_2, and P_m, as well as T_0, depend on σ_{tr} and thus become functions of the unknown σ_{in}. The best way to solve Eq. 3.35 is then by trial and error, i.e., to calculate the right hand side for a few assumed values of σ_{in} until agreement with the observed $1 - T$ is achieved.

3.6 Alternative Derivation

Instead of considering inelastic scattering on the second, third, and subsequent collisions, we may introduce the total flux of neutrons in the shell which have suffered at least one elastic collision. Let us integrate this flux over the entire volume of the shell, and call the result Ψ, assuming that the source emits one neutron per second. The spatial distribution of the collisions is again assumed to be $f_m(r)\,dr$ so that $\Psi f_m/4\pi r^2$ is the actual flux (per square centimeter per second) at r. The number of transport collisions per cubic centimeter per second is then $\Psi\sigma_{tr}f_m/4\pi r^2$, and the total number of second or higher collisions per second is

$$C_{tot} = \Psi\sigma_{tr} \tag{3.40}$$

because of the normalization of f_m.

Of the collisions (Eq. 3.40), the number

$$C_{in} = \Psi\sigma_{in} \tag{3.41}$$

will be inelastic, and $\Psi\sigma_{et}$ elastic. Of the latter neutrons, a fraction P_m will escape, so that the number of neutrons escaping after two or more elastic transport collisions is

$$T_{>2} = \Psi\sigma_{et}P_m \tag{3.42}$$

To this we add the neutrons escaping after one elastic scattering

$$T_1 = (1 - T_0)\left(\frac{\sigma_{et}}{\sigma_{tr}}\right)P_1 \tag{3.43}$$

and the number escaping without any scattering, T_0. This gives for the total transmission

$$T = T_0 + T_1 + T_{>2} \tag{3.44}$$

This expression for the transmission still contains in $T_{>2}$, the unknown integrated flux Ψ.

To eliminate Ψ, we note that we can also calculate the total number of inelastically scattered neutrons, which, of course, equals $1 - T$. We know that Eq. 3.41 represents the total number of inelastic collisions on the second collision or later. We need only add the number of first inelastic collisions

$$I_1 = (1 - T_0)\left(\frac{\sigma_{in}}{\sigma_{tr}}\right) \tag{3.45}$$

which gives

$$1 - T = (1 - T_0)\left(\frac{\sigma_{in}}{\sigma_{tr}}\right) + \Psi\sigma_{in} \tag{3.46}$$

On the other hand, Eqs. 3.42 to 3.44 give

$$1 - T = (1 - T_0)\left(1 - \frac{\sigma_{et}\,P_1}{\sigma_{tr}}\right) - \Psi\sigma_{et}P_m \tag{3.47}$$

Equating the two expressions for $1 - T$ gives

$$\Psi = \frac{(1 - T_0)\sigma_{et}(1 - P_1)}{\sigma_{tr}(\sigma_{in} + \sigma_{et} P_m)} \tag{3.48}$$

and inserting this into Eq. 3.46 gives

$$1 - T = (1 - T_0)\left(\frac{\sigma_{in}}{\sigma_{tr}}\right)\left[1 + \frac{\sigma_{et}(1 - P_1)}{\sigma_{in} + \sigma_{et} P_m}\right] \tag{3.49}$$

This is identical with Eq. 3.35. The present derivation is the mathematical extension of the physical argument at the end of Section 3.4.

Chapter 4

ANISOTROPIC SCATTERING AND JUSTIFICATION OF TRANSPORT APPROXIMATION

4.1 Outline of Methods

In principle, the theory with anisotropic scattering is simple. The number of neutrons elastically scattered on the first collision in the shell at position r into direction θ is

$$\sigma_{el}(\theta)\, d\omega\, dr\, e^{-\sigma_t(r-r_1)} \tag{4.1}$$

where now the total cross section is used rather than the transport. The fraction of these which suffer a second collision is $[1 - P(r,\theta)]$, where P is given by Eq. 3.4. Therefore the total number of second collisions that are preceded by first elastic collisions is

$$C_2 = \int_{r_1}^{r_2} e^{-\sigma_t(r-r_1)}\, dr\ \ \sigma_{el}(\theta)\, d\omega[1 - P(r_1\theta)] \tag{4.2}$$

Of these, $C_2(\sigma_{in}/\sigma_t)$ are inelastic, the rest elastic. The latter again have a certain angular distribution, more complicated than after the first collision, and their further fate may be treated similarly.

In calculating the total transmission, it must be remembered that the number of neutrons transmitted without collisions is now

$$T_0' = e^{-\sigma_t(r_2-r_1)} \tag{4.3}$$

rather than T_0 (Eq. 3.2), i.e., here also the total cross section must be substituted for the transport. Likewise, the number of inelastic scatterings on the first collision is

$$I_1' = \frac{\sigma_{in}}{\sigma_t}(1 - T_0'). \tag{4.4}$$

Both T_0' and I_1' are less than their transport-theory counterparts, T_0 and I_1.

To calculate the number of second and higher order collisions, two different methods have been chosen, viz.

(a) The angular distribution of elastic scattering has been taken into account on all collisions. In this case, the only feasible method is Monte Carlo. The results of Monte Carlo calculations for typical cases will be given below; the method of calculation is described in LA-1583.[7]

(b) We have assumed that, after the second collision, the neutrons are distributed randomly in direction, and according to the normal mode (Section 3.3) in space. Then, after the first collision, we can use the theory of Chapter 3, i.e., isotropic elastic scattering and transport cross sections. To be in accord with the assumption of isotropic second scattering, we must then also calculate the escape probability $P(r,\theta)$ in Eq. 4.2 by using the transport cross

section. The total cross section and the actual angular distribution are used only in the description of the first collision.

The formula for transmission of a sphere in this approximation is then (similar to Eq. 3.36)

$$1 - T = (1 - T_0') \frac{\sigma_{in}}{\sigma_t} \left[1 + \frac{\sigma_{et}}{\sigma_{tr}} (1 - \pi_1) + \frac{(1 - \pi_1)(1 - P_2)\, \sigma_{et}^2}{\sigma_{tr}\, (\sigma_{in} + \sigma_{et}\, P_m)} \right] \tag{4.5}$$

The computation of the escape probability π_1, essentially $1 - C_2$ (Eq. 4.2) except for the normalization $\sigma_t/(1 - T_0')\sigma_{el}$, is discussed in Section 5.5.

To qualitatively justify the procedure (b), we note that those neutrons which are scattered through large angles on their first collision will afterwards travel long distances through the material and will thus have an enhanced chance of making a second collision. Moreover, the radius vector from the source to the point of second scattering is more or less randomly oriented relative to the radius vector to the point of first scattering, if the neutron has a long path between first and second collisions. Considering both of these arguments, we conclude that, even though the differential scattering cross section $\sigma_{el}(\theta)$ is strongly peaked forward, the flux of neutrons available for second collisions will be approximately random in direction relative to the radial direction at the point of second collision. Therefore, the neutrons emerging from the second collision will also tend to be isotropic in orientation relative to the radius vector.

Procedures (a) and (b) can then be compared with:

(c) Theory using the transport cross section and isotropic elastic scattering for the first and all later collisions, i.e., use the method of Chapter 3.

4.2 Numerical Test of Transport Theory

To test the transport theory, we have calculated the transmission for 11 different cases, using both the "correct" procedure (b) and the transport procedure. Four different angular distributions for elastic scattering were used in the computations in examples 1 to 8. Three assumed distributions were of the form

$$\sigma_{el}(\theta) = a_0 + a_1 \cos\theta + a_2 \cos^2\theta + a_3 \cos^3\theta + a_4 \cos^4\theta + a_5 \cos^5\theta \tag{4.6}$$

The coefficients were assumed as follows:

	Cases 1–5	Case 6	Cases 7–8
a_0	0.115	0.059	0.311
a_1	0.066	0.030	0.625
a_2	−0.250	−0.258	−2.283
a_3	−0.382	0.010	−3.827
a_4	0.954	1.210	4.107
a_5	1.040	0.953	5.394

Thus, cases 1 to 5 correspond to a moderate peak in the forward direction, 7 and 8 to a stronger peak, and 6 to an even more pronounced peak. In fact, cases 1 to 5 correspond rather closely to a measured distribution for fission neutrons in iron, and 7 and 8 to that for uranium.[6] The angular distribution used in case 6 was chosen from the continuum theory predictions[8] for about 4.0 Mev neutrons and A = 45. This is thought to be a rather extreme case, being far more forward peaked than almost all distributions used in our analysis and even much more forward peaked than distributions recently measured at 4.0 Mev neutron energy.[9] Various thicknesses of the shell and various ratios of inner to outer radius were considered and are listed in Table 4.1.

Table 4.1 — A COMPARISON OF VARIOUS METHODS OF COMPUTING SPHERE TRANSMISSION

Case	σ_t, barns	σ_{in}, barns	$\frac{\sigma_{et}}{\sigma_{el}}$	$\sigma_t X$	$\frac{r_i}{r_2}$	Transmission by method (a), Monte Carlo calculation	Transmission by method (b), angular distribution, first collision	Transmission by method (c), transport procedure	Transmission by method (d), thin shell theory, Eq. 2.18	$\frac{\sigma_{in}(b)-\sigma_{in}(c)}{\sigma_{in}(b)}$, %
1	3.15	0.717	0.58	0.172	0.895		0.9575	0.9569	0.9574	1.4
2	3.14	0.704	0.58	0.277	0.825		0.9312	0.9300	0.9306	1.7
3	3.17	0.72	0.58	0.551	0.798		0.8528	0.8509	0.8460	1.3
4	3.17	0.72	0.58	1.106	0.594	0.7087	0.7072	0.7043	0.6812	1.0
5	3.17	0.72	0.58	2.465	0.094	0.4632	0.4677	0.4643		0.6
6	3.17	0.72	0.300	2.465	0.094	0.519	0.513	0.510		0.6
7	7.6	2.6	0.402	0.50	0.400		0.8325	0.8305		1.2
8	7.6	2.6	0.402	1.38	0.600		0.5574	0.5554		0.5
9	3.17	0.72	1*	2.465	0.094	0.405	0.423	0.413		2.0
10	3.17	0.72	1*	1.6	0.80		0.5265	0.4772		10.0
11	3.17	0.72	1*	0.8	0.80		0.7718	0.7376		14.0

$$1^* = \frac{\sigma_{el}}{2}[\delta(0,\theta) + \delta(\pi,\theta)]$$

As an extremely unfavorable case for the transport approximation, we have also considered an angular distribution in which the neutrons are scattered either directly forward or directly backward, $\theta = 0$ or 180°, with equal probability. In this case, of course, transport and total cross section are equal (cases 9, 10, 11).

In the "reasonable" cases 1 to 8, the agreement between procedures (b) and (c) is very close indeed, as shown by Table 4.1. A good way to show the agreement is to calculate the transmission by the "correct" method (b), using the assumed thickness, cross sections and angular distribution, and then to deduce an apparent inelastic cross section from this calculated transmission by use of method (c). Table 4.1 shows that the inelastic cross section deduced from (c) agrees to within 2 percent (always in the same direction) with the "correct" cross section from method (b), for cases 1 through 8. It is also clear from the table that the method of Chapter 2, method (d), does not give accurate results below about 90 percent transmission for the cases tried. For the lowest transmission calculated using Eq. 2.18, the error made in inelastic cross section is about 10 percent.

In the abnormal cases 9, 10 and 11, the error is as great as 14 percent. This is not surprising. The assumed scattering in these cases, straight backward, does not give rise to a very long path of the neutrons through the shell, on the average, 3/2 times the thickness X. Half of the scattering is assumed to go forward and thus does not lengthen the path at all (average path after scattering = $\frac{1}{2}$ X). Averaging between backward and forward scattering gives a path after scattering equal to the shell thickness, far less than the average path after isotropic scattering (except in case 9, where the shell is almost solid). Therefore, using the transport assumption and the same cross sections, we expect much more chance for inelastic collisions after the first collision, and a much smaller transmission, than using the "correct" theory. This is borne out by Table 4.1. Conversely, if the inelastic cross section is deduced from the "calculated" transmission by the transport method (c) as described in the last paragraph, we get values that are too small. Fortunately, experimental angular distributions ordinarily do not have the behavior assumed in cases 9, 10, and 11, but are commonly peaked in the forward direction.

To test the accuracy of method (b), E. D. Cashwell and C. J. Everett of LASL Group T-8, and J. M. Kister, Group T-7, have run four problems on the Los Alamos MANIAC with the Monte Carlo method,[7] taking into account the exact angular distribution in all collisions, i.e., method (a). The three angular distributions used, as well as other specifications of the problem, are listed in Table 4.1.

The Monte Carlo transmissions were compared with those calculated from method (b), and the agreement was within 2 percent. The corresponding maximum error in the deduced inelastic cross section is about 2 percent (case 9, non-realistic angular distribution). We consider this as an excellent empirical justification of method (b). Considering, then, method (b) as established, the calculations reported in Table 4.1 justify also method (c), i.e., the use of the transport cross section even for the first collision, for a realistic angular distribution of elastic scattering.

4.3 Analytical Justification

The considerations of the last section may be regarded as a justification of the transport approximation by empirical mathematics. However, a more general and theoretical argument is desirable.

As is well known, the concept of the transport cross section was developed originally in differential diffusion theory. In the limits of that theory, i.e., when there are many collisions before absorption or escape, the neutron flux at a given point in space may be written as a function of direction in the form

$$f(r,\alpha) = A(r) + B(r) \cos \alpha \qquad (4.7)$$

where α is the angle between r and the direction of motion of the neutron. Under these conditions, i.e., when all higher spherical harmonics are absent from the angular distribution, the

entire influence of scattering on the neutron distribution can be described by the transport cross section. Indeed, the net number of neutrons elastically scattered into the direction α is

$$\begin{aligned} C &= -\sigma_{el}\ f(r,\alpha) + \int \sigma_{el}(\theta)\, f(r,\alpha')\, \frac{d\Omega'}{4\pi} \\ &= B(r) \int \sigma_{el}(\theta)\, (\cos\alpha' - \cos\alpha)\, \frac{d\Omega'}{4\pi} \\ &= -B(r)\cos\alpha \int \sigma_{el}(\theta)\, (1-\cos\theta)\, \frac{d\Omega'}{4\pi} \end{aligned} \tag{4.8}$$

The first term in the first line represents the neutrons scattered out, the second those scattered in from direction α'. In the second line, Eq. 4.7 has been used; in the last, well known relations of spherical trigonometry. The last integral is the elastic transport cross section. In the further development of diffusion theory, only σ_{tr} occurs; e.g., the diffusion coefficient is

$$D_0 = \tfrac{1}{3}\, l_{tr}\, v \tag{4.9}$$

where l_{tr} is the transport mean free path and v is the neutron velocity.

The distribution (Eq. 4.7) will be established whenever there are many collisions. In our problem, then, the use of the transport cross section will be valid within the same limits in which the normal mode solution is valid, i.e., for shell thickness large compared with a mean free path. Thus, the transport approximation is exact within the limits where the multiple scattering is most important.

Let us now investigate the opposite limit, that of a thin shell. The number of first inelastic collisions is, as in Eq. 2.5

$$I_1' = \sigma_{in} X - \tfrac{1}{2}\, \sigma_{in}\sigma_t X^2 + \ldots \tag{4.10}$$

The number of second inelastic collisions is given by Eq. 2.7,

$$I_2' = \sigma_{in} \int_{r_1}^{r_2} \int_0^{4\pi} \sigma_{el}(\theta)\, d\omega\, dr\, y(r,\theta) \tag{4.11}$$

which can also be derived from Eq. 4.2. The length of chord $y(r,\theta)$ is given by Eq. 2.9. Except for very small $|\cos\theta|$, Eq. 2.9 may be written for a thin shell in the form

$$\begin{aligned} y(r,\theta) &= \frac{r_2 - r}{\cos\theta} \qquad \text{if } \cos\theta > 0 \\ y(r,\theta) &= \frac{X + r - r_1}{|\cos\theta|} \qquad \text{if } \cos\theta < 0 \end{aligned} \tag{4.12}$$

This means essentially that the curvature of the shell is neglected.

Let us now expand $\sigma_{el}(\theta)$ (cross section for scattering per unit solid angle) in powers of $\cos\theta$,

$$\sigma_{el}(\theta) = a_0 + a_1\cos\theta + a_2\cos^2\theta + a_3\cos^3\theta + \ldots \tag{4.13}$$

Inserting this into Eq. 4.11 we see that we can use the approximation of Eq. 4.12 for y, together with every term in Eq. 4.13 except the first. The first term, on the other hand, has been integrated in Eqs. 2.14 and 2.16. Therefore, we can evaluate Eq. 4.11 in good approximation, and noting that $\langle r_2 - r\rangle = \langle r - r_1\rangle = \tfrac{1}{2} X$, we get

$$I_2' = \tfrac{1}{2}\, \sigma_{in} X^2 \left[a_0 L - a_1 + a_2 - \sum_{\substack{n \\ \text{odd}}} \frac{a_n}{n} + \sum_{\substack{n \\ \text{even}}} \frac{2}{n} a_n \right] \tag{4.14}$$

Adding this to Eq. 4.10, we get to order X^2

$$I' = I_1' + I_2' = \sigma_{in} X \left(1 - \frac{\sigma_{in} X}{2}\right) + \frac{1}{2}\sigma_{in} X^2 \left[a_0(L-1) - a_1 + \frac{2}{3} a_2 - \sum_{\substack{n \\ \text{odd}}} \frac{a_n}{n} + \sum_{\substack{n \\ \text{even}}} \left(\frac{2}{n} - \frac{1}{n+1}\right) a_n \right] \quad (4.15)$$

where we have used the expression for the total elastic cross section corresponding to Eq. 4.13

$$\sigma_{el} = a_0 + \sum_{\substack{n \\ \text{even}}} \frac{1}{n+1} a_n \quad (4.16)$$

The elastic transport cross section is

$$\sigma_{et} = a_0 - \frac{1}{3} a_1 + \frac{1}{3} a_2 - \sum_{\substack{n \\ \text{odd}}} \frac{1}{n+2} a_n + \sum_{\substack{n \\ \text{even}}} \frac{1}{n+1} a_n \quad (4.17)$$

Now our old Eq. 2.18 gives, if σ_{et} is substituted for σ_{el}

$$I = 1 - T = \sigma_{in} X \left(1 - \frac{1}{2}\sigma_{in} X\right) + \frac{1}{2}\sigma_{in}\sigma_{et} X^2 (L-1) \quad (4.18)$$

In other words, if we use the transport cross section, the bracket in the "correct" result (Eq. 4.15) is replaced by Eq. 4.17, multiplied by $L - 1$. Reasonable values of L are between 3 and 4, corresponding to r_1/r_2 between 0.55 and 0.85, Eq. 2.16. Choosing $L = 4$, the bracket in Eq. 4.15 is

$$3a_0 - a_1 + \frac{2}{3} a_2 - 0.33a_3 + 0.30a_4 - 0.20a_5 \quad (4.19)$$

whereas the transport theory gives for this case

$$3a_0 - a_1 + a_2 - 0.6a_3 + 0.6a_4 - 0.429a_5 \quad (4.20)$$

Thus for $L = 4$, the coefficient of a_1 is correctly* given by transport theory. If the angular distribution is just $a_0 + a_1 \cos\theta$, we would therefore get the correct result by using the transport cross section theory. With most measured angular distributions of elastic scattering, the "correct" result (Eq. 4.19) is likely to be smaller by 10 percent or so than the transport result (Eq. 4.20). For angular distributions requiring high order terms (a_n) in the cosine expansion (Eq. 4.13), the discrepancy between the exact and transport theory is increased.

Thus we see that even in the limit of very thin shells, the transport theory is quite a good approximation, especially if we remember that the bracket in Eq. 4.15 occurs only in a correction term. Since the transport theory is a good approximation for thin shells and is exact for thick ones, it is not surprising that it is very good for intermediate thicknesses, in accord with Table 4.1. Even the sign of the error can be understood: We have seen that the elastic transport cross section, used in Eq. 2.18 or 4.18, predicts too high an inelastic scattering for a given cross section, and hence too low a sphere transmission. This agrees with Table 4.1.

Since Eq. 4.18 predicts slightly too much inelastic scattering, it follows that σ_{et} is slightly larger than a true effective elastic cross section would be. The use of the total elastic cross section σ_{el} in Eq. 4.18 would greatly aggravate this error; in fact, the factor $(1 - \cos\theta)$ does not reduce the cross section quite enough.

* The coefficient of a_0 is, of course, always correct.

In view of the above discussions of inelastic scattering, it is important to note that the evaluation of experiments with the transport cross section gives a lower limit to the inelastic scattering cross section and as we have shown, a very close limit.

4.4 Small Angle Limit

An interesting special case is that of a very sharp forward peak in the differential cross section for elastic scattering. This is not relevant for our own experiments at energies around 1 to 6 Mev, where there is always considerable elastic scattering through 90° and more, but it is important at high energies, such as 14 Mev. We shall treat this case also analytically. We shall assume throughout that the shell is thin compared to its radius and that we have effectively plane geometry. In the beginning, we shall assume further that $\sigma_t X \ll 1$; then we can use the approximations of Chapter 2. Later on, we shall relax this condition.

Using Eq. 2.9 for small angles θ, we find (see Eq. 4.12)

$$y(r,\theta) = (r_2 - r)\left(1 + \frac{1}{2}\theta^2\right) \tag{4.21}$$

If the neutron had proceeded forward, the path length would have been $r_2 - r$, so that the increase of path is $1/2(r_2 - r)\ \theta^2$, as is geometrically obvious.

The sum of first and second inelastic collisions is, to order X^2, similar to Eqs. 2.18 and 4.15

$$I_1 + I_2 = \sigma_{in} X - \frac{1}{2}\sigma_{in}\sigma_t X^2 + \sigma_{el} X\left[\frac{\sigma_{in} X}{2}\left(1 + \frac{<\theta^2>}{2}\right)\right] \tag{4.22}$$

where $<\theta^2>$ is the average of θ^2 over all elastic collisions. In the last term, $\sigma_{el} X$ is the probability of a first elastic collision, to order X. This is multiplied by the probability of a second inelastic collision, which is σ_{in} times the average of Eq. 4.21 over r. Equation 4.22 may be rewritten

$$I_1 + I_2 = \sigma_{in} X\left(1 - \frac{\sigma_{in} X}{2} + \frac{1}{4}\cdot\sigma_{el} <\theta^2> X\right) \tag{4.23}$$

Now for small scattering angles

$$\sigma_{et} = \int_0^{4\pi} \sigma_{el}(\theta)\ (1 - \cos\theta)\ d\omega = \frac{\sigma_{el} <\theta^2>}{2} \tag{4.24}$$

so that the total number of inelastically scattered neutrons is

$$1 - T = I_1 + I_2 = \sigma_{in} X\left(1 - \frac{\sigma_{in} X}{2} + \frac{\sigma_{et} X}{2}\right) \tag{4.25}$$

To accuracy X^2, this may be written in the form

$$T = e^{-\sigma_{in} Y} \tag{4.26}$$

We define an effective thickness Y by

$$Y = X\left(1 + \frac{1}{2}\sigma_{et} X\right) \tag{4.27}$$

The last factor describes the lengthening of the path due to elastic collisions.

We can now generalize this result to greater thickness of the shell. For this purpose, let us separate the effects of elastic and inelastic scattering. All that the elastic scattering does is to lengthen the path of the neutrons. Let p(z) dz be the probability that the total path through the shell of a neutron, originating at the sphere center, is between z and z + dz, if there is only elastic scattering of the correct cross section and angular distribution. In principle, p(z) can be calculated; clearly, p(z) = 0 if z < X and p is normalized so that

$$\int_0^\infty p(z)\, dz = 1 \tag{4.28}$$

Now consider the inelastic scattering. The probability that a neutron will not be inelastically scattered if it travels a distance z, is $e^{-\sigma_{in} z}$. Hence, with no approximations, the total probability of transmission without making inelastic collisions is

$$T = \int_0^\infty p(z)\, e^{-\sigma_{in} z}\, dz \tag{4.29}$$

Now let us make our assumption that the scattering angles are small. Then, in general, the path length z will be not much greater than the shell thickness X. Precisely, we assume that

$$\sigma_{in}\,(z - X) \ll 1 \tag{4.30}$$

for all important values of z. Then we may expand Eq. 4.29 as follows

$$\begin{aligned} T &= e^{-\sigma_{in} X} \int p(z)\, e^{-\sigma_{in}(z-X)}\, dz \\ &= e^{-\sigma_{in} X} \int p(z)\, dz\, [1 - \sigma_{in}(z - X) + \ldots.] \\ &= e^{-\sigma_{in} X}\, [1 - \sigma_{in} \langle z - X \rangle + \ldots] \\ &\approx e^{-\sigma_{in} Y} \end{aligned} \tag{4.31}$$

where

$$Y = \langle z \rangle \tag{4.32}$$

neglecting terms of order $\sigma_{in}^2 (z - X)^2$ (assumption of Eq. 4.30).

Thus, if Eq. 4.30 is true, we need only find the average length of path due to elastic scattering.

We thus calculate the average path length of a neutron which does not suffer inelastic collisions, assuming that the neutron starts at the center of the sphere. The distance that an average neutron travels in going from r to r + dr is

$$dY = \frac{dr}{\langle \cos \alpha \rangle} = dr \left(1 + \frac{\langle \alpha^2(r) \rangle}{2} + \ldots\right) \tag{4.33}$$

where α is the angle between neutron direction and radius vector, and $\langle \alpha^2(r) \rangle$ is the statistical average of α^2 over all possible neutron paths, taken at position r. As is well known, α^2 increases linearly with the distance the neutron has already traveled. Explicitly

$$\begin{aligned} \langle \alpha^2(r) \rangle &= \sigma_{el}\ \ (r - r_1) \langle \theta^2 \rangle \\ &= 2(r - r_1)\, \sigma_{et} \end{aligned} \tag{4.34}$$

where $\langle \theta^2 \rangle$ is the average over the deflections in one collision, and, on the right hand side, the distance traveled has been put equal to $r - r_1$. Inserting in Eq. 4.33 and integrating over r, the total average path length of the neutron becomes

$$Y = X\left(1 + \frac{1}{2}\sigma_{et}X\right) \tag{4.35}$$

in exact agreement with the thin-shell formula (4.27).

Thus, Eqs. 4.26 and 4.27 have been established if only (1) $< \alpha^2 >$ remains small, and (2) the condition of Eq. 4.30 is fulfilled. Condition 1, according to Eq. 4.34, means

$$\sigma_{et}X \ll 1 \tag{4.36}$$

replacing z by its average Y, (Eq. 4.35) means

$$\sigma_{in}\sigma_{et}X^2 \ll 1 \tag{4.37}$$

In practice, for 14 Mev neutrons, $\sigma_{in} \gg \sigma_{et}$; hence, if Eq. 4.37 is fulfilled, Eq. 4.36 will be true a fortiori. On the other hand, for the same reason it is not necessary that $\sigma_{in}X$ be small; in other words, the average number of inelastic scatterings may well be larger than 1. In practice, again, $\sigma_{el} \propto \sigma_{in}$, so $\sigma_{el}X$ may also be larger than one. In fact, the number of elastic collisions in the shell is totally irrelevant, as long as the deflection in each of them is small so that Eqs. 4.36 and 4.37 remain true.

We shall now compare the results of the small angle limit (Eqs. 4.25, 4.26, 4.31) with the transport theory as summarized in Eq. 4.18. Equation 4.25 differs from Eq. 4.18 only by the absence of the factor $L - 1$. Since L is, in general, equal to 3 or 4, the effect of elastic scattering in the correct formula (Eq. 4.25) is smaller than in the transport formula (Eq. 4.18) by a numerical factor of 2 or 3. This is understandable because great lengthening of the path occurs only for scattering between say, 60° and 150°, and such large angles are specifically excluded by condition 1, above.

We see that the error of transport theory is in the same direction as in the general case discussed in Section 4.3, but much greater. In both cases, transport theory overestimates the enhancement of the number of inelastically scattered neutrons by elastic collisions. However, in the case of very fast neutrons, the whole enhancing effect of elastic scattering is very small, even if it is overestimated by the use of transport theory. Thus the discrepancy between correct and transport theory in this limit is not very important. However, if high accuracy is desired, the use of Eqs. 4.26 and 4.27 is recommended at 14 Mev, and at intermediate energies (6 to 10 Mev) the result will lie between the values of Eqs. 4.26 and 4.27 and those of the transport theory used in the bulk of this paper.

Chapter 5

DETERMINATION OF ESCAPE PROBABILITIES

5.1 Escape Probability After First Transport Collision (P_1)

The escape probability after the first transport collision, P_1, is defined by Eq. 3.8

$$P_1 = \int_{r_1}^{r_2} f_1(r)\, dr\, P(r)$$

where $f_1(r)\, dr$ is the first collision distribution in the spherical shell, given by Eq. 3.3, and $P(r)$ is the escape probability from the shell as a function of radius (Eq. 3.5). The quantity $P(r,\theta)$ in Eq. 3.5 is defined in Eq. 3.4. The integral, which we will do by numerical methods, is thus

$$P_1 = \frac{\int_{r_1}^{r_2} \int_{-1}^{+1} e^{-(r-r_1)} dr\, e^{-y(r,\mu)}\, d\mu}{2(1 - T_0)} \tag{5.1}$$

where all distances are now expressed in transport mean free paths and the new variable $\mu = \cos\theta$ is introduced; $y(r,\mu)$, as in Eq. 2.9, is

$$y(r,\mu) = -r\mu + \sqrt{r_2^2 + r^2\mu^2 - r^2} - a\sqrt{r_1^2 + r^2\mu^2 - r^2}$$

where $a = 2$ if $-\sqrt{1 - \frac{r_1^2}{r^2}} \geq \mu \geq -1$

$a = 0$ if $1 \geq \mu \geq -\sqrt{1 - \frac{r_1^2}{r^2}}$

Isotropic elastic scattering is assumed in Eq. 5.1 because we are now treating only transport collisions.

To completely specify P_1 it is only necessary to give the values of two parameters since these will fix r_1 and r_2: (1) the shell thickness in transport mean free paths $\sigma_{tr} X$, and (2) the ratio of inside to outside shell radius r_1/r_2, or K. Then

$$r_1 = \frac{K(\sigma_{tr}X)}{1-K}$$

$$r_2 = \frac{(\sigma_{tr}X)}{1-K} \qquad (5.2)$$

The determination of the proper transport cross section to use for a given incident neutron energy is discussed in Section 3.5.

The integration of Eq. 5.1 was done numerically on the CPC (Card Program Calculator) machines at Los Alamos for a variety of choices of $\sigma_{tr}X$ and K. The results are graphed in Fig. 5.1. Simpson's rule was used to perform both the μ and r integrals. In most of the computations, five equally spaced values of r and 21 values of μ varying from 1 to -1 were chosen. To determine whether P_1 could be obtained to sufficient accuracy by calculating P(r) at five points in the shell and combining these values, P(r) was also calculated for nine equally spaced values of r and these nine values were combined to form P_1. The P_1 values computed by the two methods were compared for a number of shells and were found to differ by 0.3 percent in the worst case. To check whether a sufficient number of intervals was chosen for the μ integration, the number of values of μ was increased from 21 to 41 in some typical cases, with the result that $P(r)_{41}$ was at most 0.1 percent different from $P(r)_{21}$. Some of the numerical integrals were performed using both the trapezoidal rule and Simpson's rule. The results of the two methods agreed to 0.1 percent. It is thought, however, in view of the smooth nature of the curves for $P(r,\theta)$ and P(r), that Simpson's rule gives a slightly better approximation to the correct answer. The small differences mentioned above are not the result of carrying too few places in the machine computation. In all of the numerical computations eight places were carried. In view of these uncertainties the values of P_1 calculated on the CPC machines are thought to be uncertain to ≤ 0.4 percent.

To construct each of the curves for a fixed K in Fig. 5.1, five values of $\sigma_{tr}X$ were chosen ($\sigma_{tr}X = 0.2$, 0.4, 0.8, 1.2, and 1.6). Smooth curves were drawn through these points and the origin. For an arbitrary shell, K and $\sigma_{tr}X$ usually require an escape probability somewhere between the computed points. To obtain this escape probability, one reads P_1 for each K at the desired $\sigma_{tr}X$. These values can then be plotted as a function of K and a smooth curve drawn through the points. P_1 at the desired K can then be read from this curve. P_1 determined by interpolation between computed points was within 1 percent of values actually calculated on the computing machine for several cases.

It can be shown that

$$\frac{\delta\sigma_{in}}{\sigma_{in}} \cong \frac{\delta P}{P} \qquad (5.3)$$

For most of the experimental work reported herein, $\delta\sigma_{in}/\sigma_{in}$ (the error in inelastic cross section due to an error in computation of escape probability) is less than 1 percent, although for some of the measurements taken with the Np^{237} detector $\delta\sigma_{in}/\sigma_{in}$ is about 2 percent. This is, however, about $\frac{1}{5}$ of the statistical counting error in these cases and is thus not very significant.

In Section 3.2 it is pointed out that P(r) should not depend very much on r in a spherical shell. Curves of some typical examples of $1 - P(r)$, computed by the above methods, are given in Fig. 3.2 to illustrate this point. As expected, the magnitude of $1 - P(r)$ changes more from the inside to the outside radius of the shell for a thick shell than it does for a thin shell.

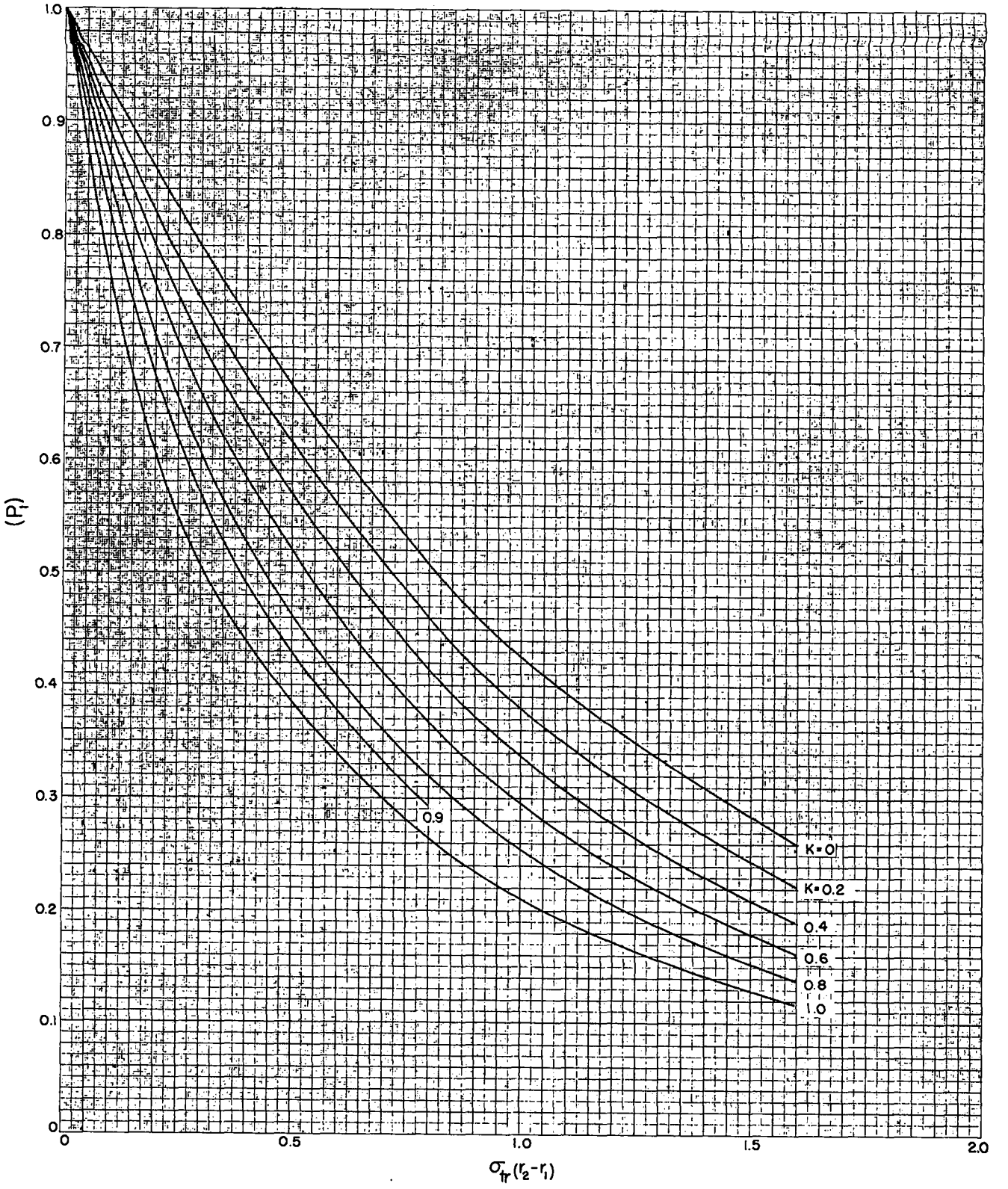

Fig. 5.1 — Plot of P_1, the escape probability from a spherical shell after the first elastic collision.

5.2 Escape Probability After a Second Transport Collision (P_2)

The escape probability after a second transport collision, P_2, is computed from Eq. 3.12. The relative probability $[f_2(r)\,dr]$ of a second elastic collision between r and r + dr is yet to be determined. We shall now endeavor to find this probability for a finite size Δr.

Thus we write

$$f_2(r_j)\,\Delta r_j = \frac{\int_{r_1}^{r_2}\int_{-1}^{1} e^{-(r-r_1)}\,d\mu\,dr\,G(\theta,r,r_j,r_{j+1})}{\int_{r_1}^{r_2}\int_{-1}^{1} e^{-(r-r_1)}\,d\mu\,dr\,[1-P_1]} \tag{5.4}$$

where r_j is the inner radius of the subshell in question and r_{j+1} is the outer radius in transport mean free paths. Thus

$$\Delta r_j = r_{j+1} - r_j$$

$G(\theta,r,r_j,r_{j+1})$ is the probability of a second collision in the subshell between r_j and r_{j+1}, if a neutron scatters on its first collision at a position r and through an angle θ. The numerator in Eq. 5.4 is then the number of second collisions in the spherical subshell Δr_j, and the denominator is just the total second collision rate. To minimize computing effort, a four-region distribution function was decided upon, i.e., $\Delta r_j = (r_2 - r_1)/4$. The geometry is shown in Fig. 5.2. To describe $G(\theta,r,r_j, r_{j+1})$, we define the following quantities

$$\begin{aligned} a(r,j,\mu) &= r\mu - \sqrt{r_j^2 - r^2 + r^2\mu^2} \\ b(r,j,\mu) &= r\mu + \sqrt{r_j^2 - r^2 + r^2\mu^2} \\ c(\mu,r) &= 2\sqrt{r_1^2 - r^2 + r^2\mu^2} \end{aligned} \tag{5.5}$$

Of course, $\mu = \cos\theta$, and distances are expressed in transport mean free paths.

Case A

$r \le r_j$

(i) $1 \ge \mu \ge -\sqrt{1 - \frac{r_1^2}{r^2}}$

$$G(\mu,r,r_j,r_{j+1}) = e^{a(j)} - e^{a(j+1)} \tag{5.6}$$

(ii) $-1 \le \mu \le -\sqrt{1 - \frac{r_1^2}{r^2}}$

$$G(\mu,r,r_j,r_{j+1}) = e^{a(j)+c} - e^{a(j+1)+c} \tag{5.7}$$

Case B

$r \ge r_{j+1}$

(i) $1 \ge \mu \ge -\sqrt{1 - \frac{r_{j+1}^2}{r^2}}$

$$G = 0 \tag{5.8}$$

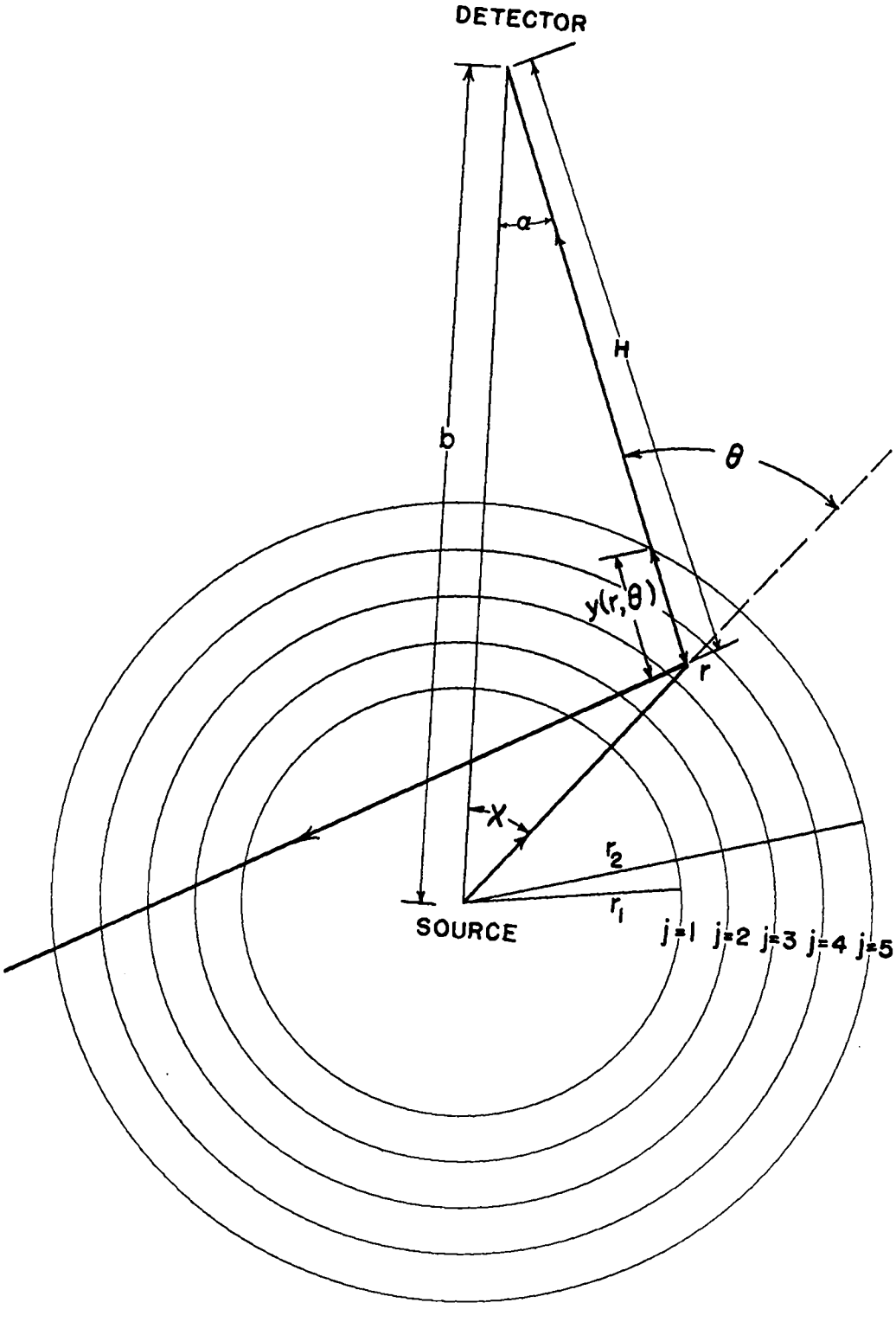

Fig. 5.2—Geometrical arrangement showing the spherical shells used in computing P_2.

(ii) $$-\sqrt{1-\frac{r_{j+1}^2}{r^2}} \geq \mu \geq -\sqrt{1-\frac{r_j^2}{r^2}}$$

$$G = e^{b(j+1)} - e^{a(j+1)} \qquad (5.9)$$

(iii) $$-\sqrt{1-\frac{r_j^2}{r^2}} \geq \mu \geq -\sqrt{1-\frac{r_i^2}{r^2}}$$

$$G = e^{b(j+1)} - e^{b(j)} + e^{a(j)} - e^{a(j+1)} \qquad (5.10)$$

(iv) $$-\sqrt{1-\frac{r_i^2}{r^2}} \geq \mu \geq -1$$

$$G = e^{b(j+1)} - e^{b(j)} + e^{a(j)+c} - e^{a(j+1)+c} \qquad (5.11)$$

To evaluate Eq. 5.4, the μ integral was done first using 21 values of μ between +1 and −1 at each r. The integrand was evaluated for five values of radial position r, and the final P_2 was obtained using Simpson's rule to combine these values of the integrand. These numerical integrals were performed on the CPC machines for several choices of the two parameters necessary to describe a spherical shell: $K = r_1/r_2$ and $\sigma_{tr}X$. To obtain a complete four-region distribution function, six hours of machine computing time was required. From Eq. 5.4 it is clear that

$$\sum_{j=1}^{4} f_2(r_j)\,\Delta r_j = 1 \qquad (5.12)$$

This allows one to check the results of the second collision probability calculation against the probability of a second collision computed in another way, namely, $1 - P_1$. The $1 - P_1$ value is, of course, not computed by the methods of this section but by those of Section 5.1. In 12 cases which were compared, the probabilities of a second collision computed by both methods were essentially the same.

In Fig. 3.3, the second collision distribution in a typical case is compared with the first collision distribution and with the normal mode. One may see that even for the second collision, the distribution function is beginning to resemble closely the normal mode.

Curves of second collision escape probability P_2 are given in Fig. 5.3 for the two parameters K and $\sigma_{tr}X$. Values of P_2 obtained from these curves are probably subject to slightly more error than values read from Fig. 5.1 because the collision distribution here is somewhat less well determined. The question of whether it is necessary to refine the shell theory to the extent of including P_2 is discussed in Section 5.4.

5.3 Escape Probability After a Third or Later Transport Collision (P_m)

Escape probability after a third or later transport collision, P_m, may be calculated using Eq. 3.12 with the normal mode collision distribution function $f_m(r)\,dr$ replacing $f_2(r)\,dr$. The justifications for using the normal mode for third and higher order collisions are discussed in Section 3.3. The appropriate distribution function is given by

$$f_m(r) = \frac{c}{r} \sin k(r + \delta), \qquad (5.13)$$

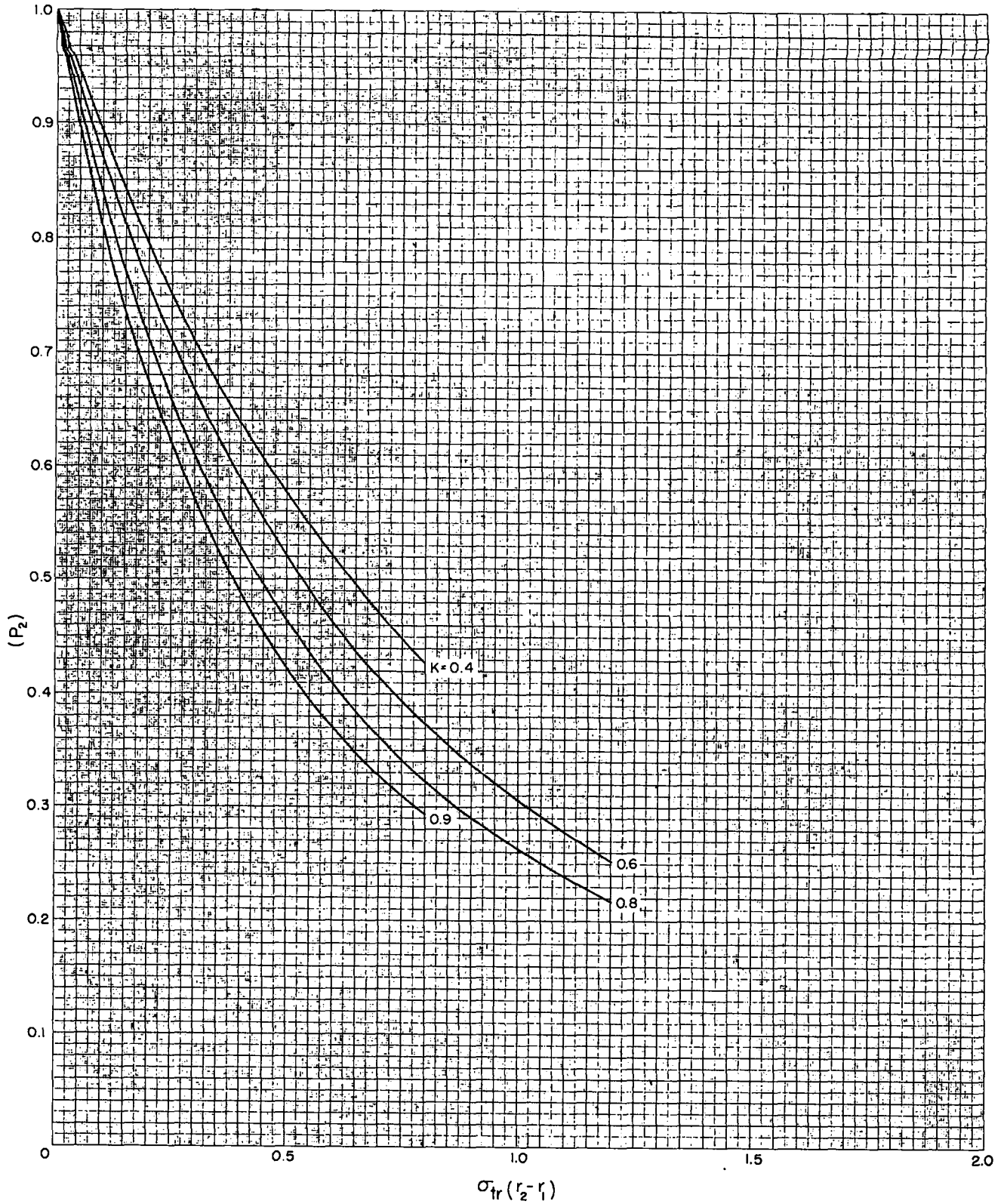

Fig. 5.3 — Plot of P_2, the escape probability after a second elastic collision.

where c is just a normalization constant. A solution of Eq. 3.27 gives k, and δ is determined from Eq. 3.22. P_m resulting from integration over the normal mode distribution is believed to be determined ultimately to the same accuracy as P_1, i.e., to ~0.4 percent. Curves of P_m for the two parameters K and $\sigma_{tr}X$ are given in Fig. 5.4.

5.4 Importance of Collision Distribution

If the escape probabilities P_1, P_2, and P_m are compared as in Table 5.1, it is observed that for the same shell parameters the three values are not drastically different. This is not unexpected in view of the considerations given in Section 3.2. However, if one replaces P_2 by P_m in the transmission formula for a spherical shell, an error of 1 or 2 percent may occur in the calculated inelastic cross section, especially for thick, nearly solid, shells. It is thus usually desirable to include P_2 in the transmission formula (Eq. 3.36). If one cannot obtain P_2 from Fig. 5.3, for a particular case it is possible to estimate P_2 quite well by assuming it is the average of P_1 and P_m.

TABLE 5.1—ESCAPE PROBABILITIES FROM SPHERICAL SHELLS AFTER FIRST, SECOND, AND NORMAL MODE COLLISIONS

K	$\sigma_{tr}X$	P_1	P_2	P_m
0.9	0.2	0.675	0.673	
0.9	0.4	0.491	0.488	
0.9	0.8	0.293	0.293	
0.8	0.2	0.711	0.710	
0.8	0.4	0.527	0.528	0.531
0.8	0.8	0.319	0.322	0.329
0.8	1.2	0.207	0.217	0.224
0.8	1.6	0.139		0.1625
0.6	0.2	0.756	0.758	
0.6	0.4	0.585	0.588	0.593
0.6	0.8	0.367	0.373	0.386
0.6	1.2	0.243	0.252	0.269
0.6	1.6	0.163		0.197
0.4	0.2	0.790	0.794	
0.4	0.4	0.632	0.638	0.647
0.4	0.8	0.415	0.426	0.444
0.4	1.2	0.279		0.321
0.4	1.6	0.191		0.241

The fact that the collision distribution does not drastically affect the average probability of escape from a spherical shell has an interesting consequence. It occasionally occurs that the spatial distribution of neutrons making a particular kind of collision (inelastic scattering, for example) is influenced by one cross section (that for a "fast" neutron), and the escape probability from a point in the sphere after this collision is influenced by another cross section (that for a "slower" neutron). The average escape probability desired has the form

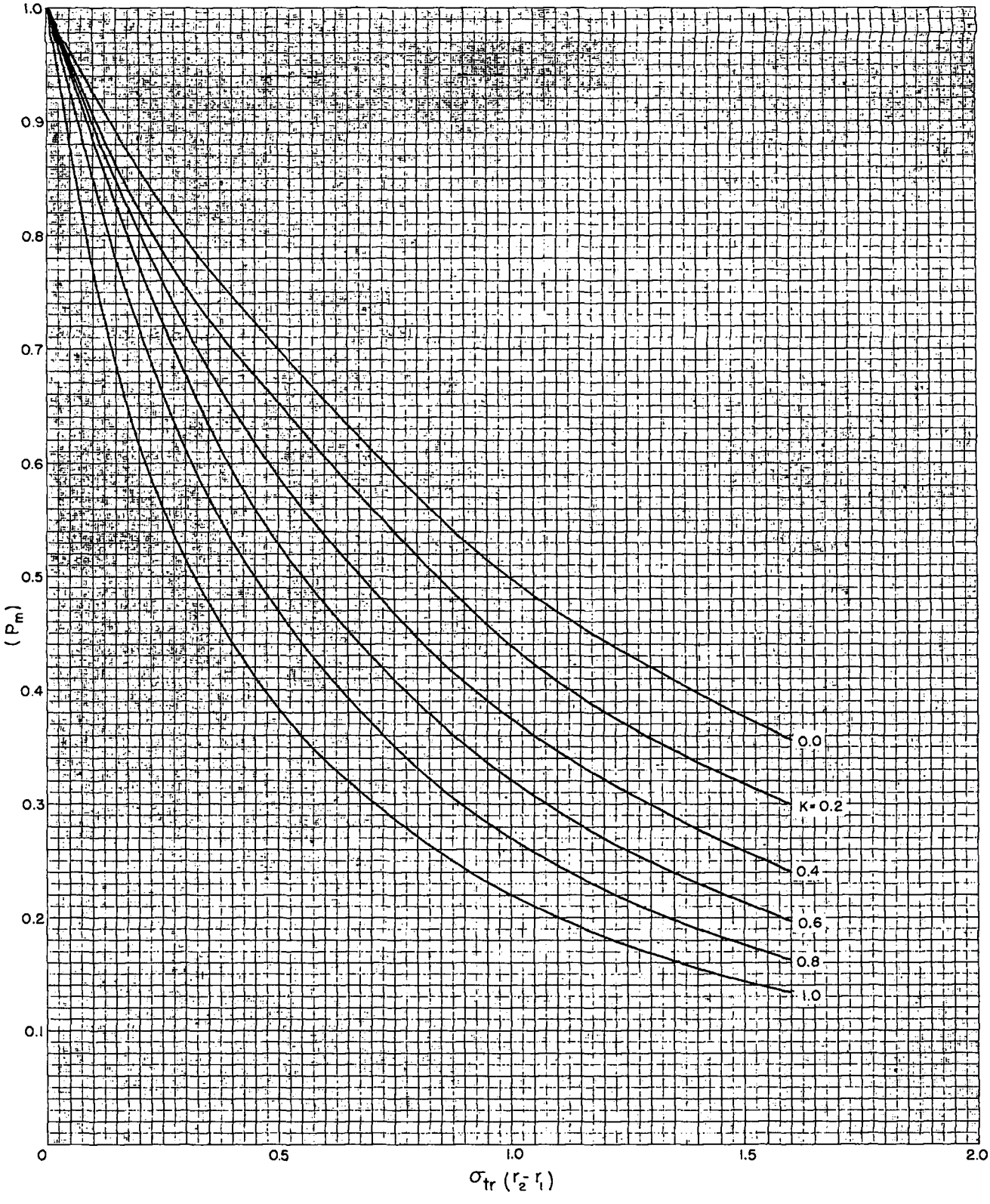

Fig. 5.4 — Plot of P_m, the escape probability after a third or later transport collision.

$$P_n = \frac{\int_{r_1}^{r_2}\int_0^{4\pi} f_n(\sigma_1^{tr},r)d\omega\ dr\ e^{-\sigma_2^{tr}y(r,\theta)}}{\int_{r_1}^{r_2}\int_0^{4\pi} f_n(\sigma_1^{tr},r)\ d\omega\ dr} \tag{5.14}$$

where f_n is f_1, f_2, or f_m. Since collision distribution does not markedly influence the average escape probability per collision, a fairly accurate value of P_n may be obtained by using the function $f_n(\sigma_2^{tr},r)$ instead of $f_n(\sigma_1^{tr},r)$ and by then referring to the existing curves in Figs. 5.1, 5.3, or 5.4.

5.5 Escape Probability, Including the Elastic Scattering Angular Distribution Explicitly

In Section 4.1, an approximate theory (termed the "correct" theory) for sphere transmission is given, in which one includes the elastic scattering angular distribution explicitly. One solves for the inelastic cross section, using Eq. 4.5. We will now discuss the method used to determine the quantity π_1 needed in Eq. 4.5. As mentioned before,

$$\pi_1 = \frac{(1 - C_2)\sigma_t}{\sigma_{el}(1 - T_0')}$$

where C_2 is given by Eq. 4.2. Specifically

$$\pi_1 = \frac{\int_{r_1}^{r_2}\int_0^{4\pi} e^{-\sigma_t(r-r_1)}\ \sigma_{el}(\theta)\ d\omega\ dr\ e^{-\sigma_{tr}y(r,\theta)}}{\int_{r_1}^{r_2}\int_0^{4\pi} e^{-\sigma_t(r-r_1)}\ \sigma_{el}(\theta)\ d\omega\ dr} \tag{5.15}$$

where $y(r,\theta)$ is given by Eq. 2.9, and all distances are in centimeters.

To check whether both Eqs. 4.5 and 3.36 give the same result for sphere transmission (with the same input conditions), computations using the "correct" theory (Eq. 4.5) were carried out in complete detail for two angular distributions. These two angular distributions had been measured for iron and normal uranium with a "28" (U^{238}) threshold detector and with a beam of fission neutrons from the Los Alamos Fast Reactor by Jurney and Zabel.[6] So that one can make comparisons of shells of various sizes, general sets of curves were prepared of π_1 for these two angular distributions. Other than the specific angular distribution, one needs three parameters to specify Eq. 5.15: $\sigma_t X$, σ_{tr}/σ_t, and r_1/r_2. To indicate how one prepares the general sets of curves of π_1, we have included the set for the iron angular distribution, Figs. 5.5, 5.6, and 5.7. To determine π_1 for a specific sphere one must do a double interpolation using values read from these figures.

The π_1 values were computed using the same general coding for the CPC machine as used for previous sections of this chapter. The accuracy of this computation is thus the same as mentioned in Section 5.1.

Table 4.1 indicates that for reasonable angular distributions of elastic scattering, one does not gain a significant amount of accuracy in the determination of the inelastic cross section by using this analysis in preference to the simpler analysis of Chapter 3.

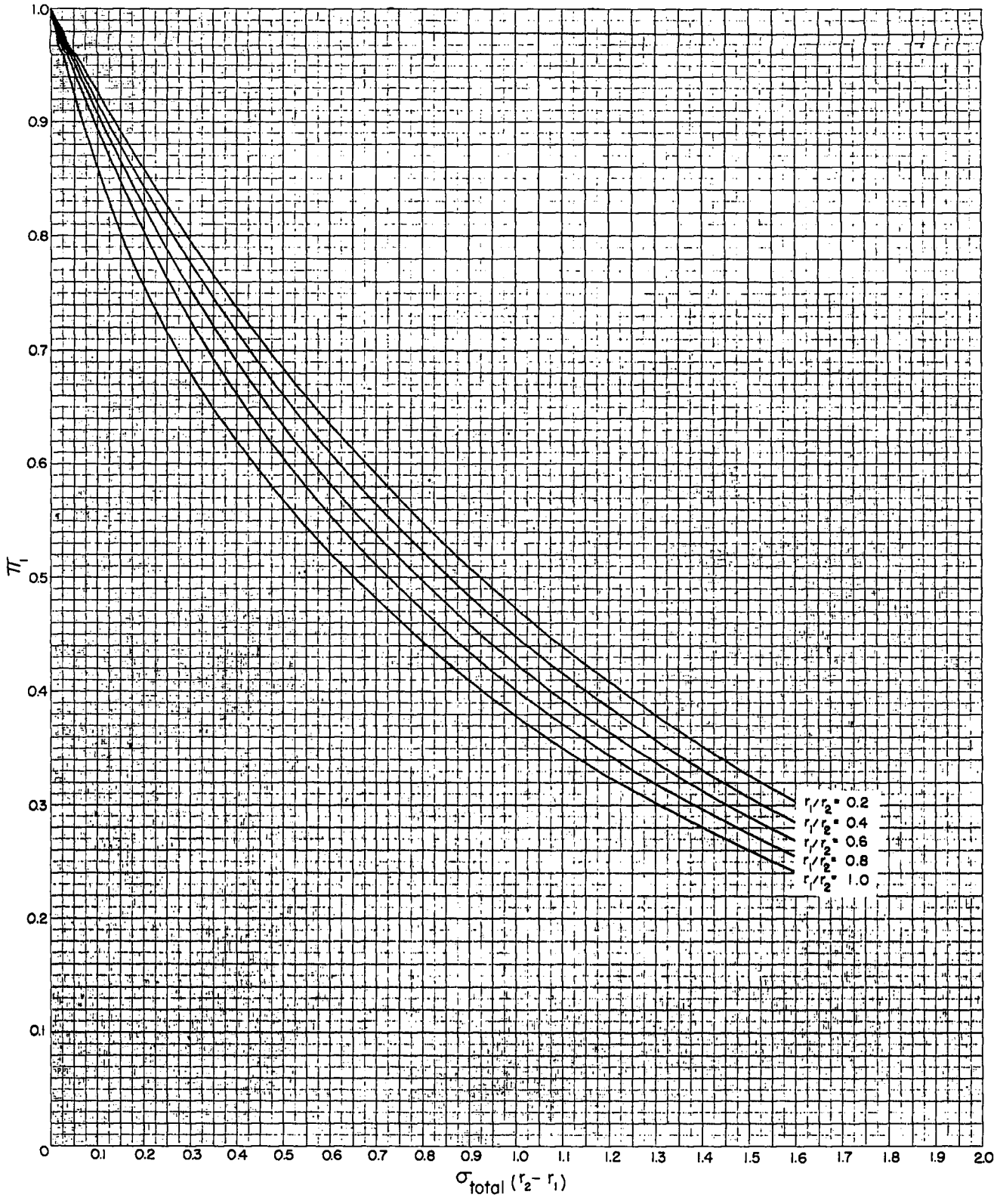

Fig. 5.5 — Plot of π_1 for iron angular distribution, measured with "28" detector, when $\sigma_{tr}/\sigma_t = 1.0$.

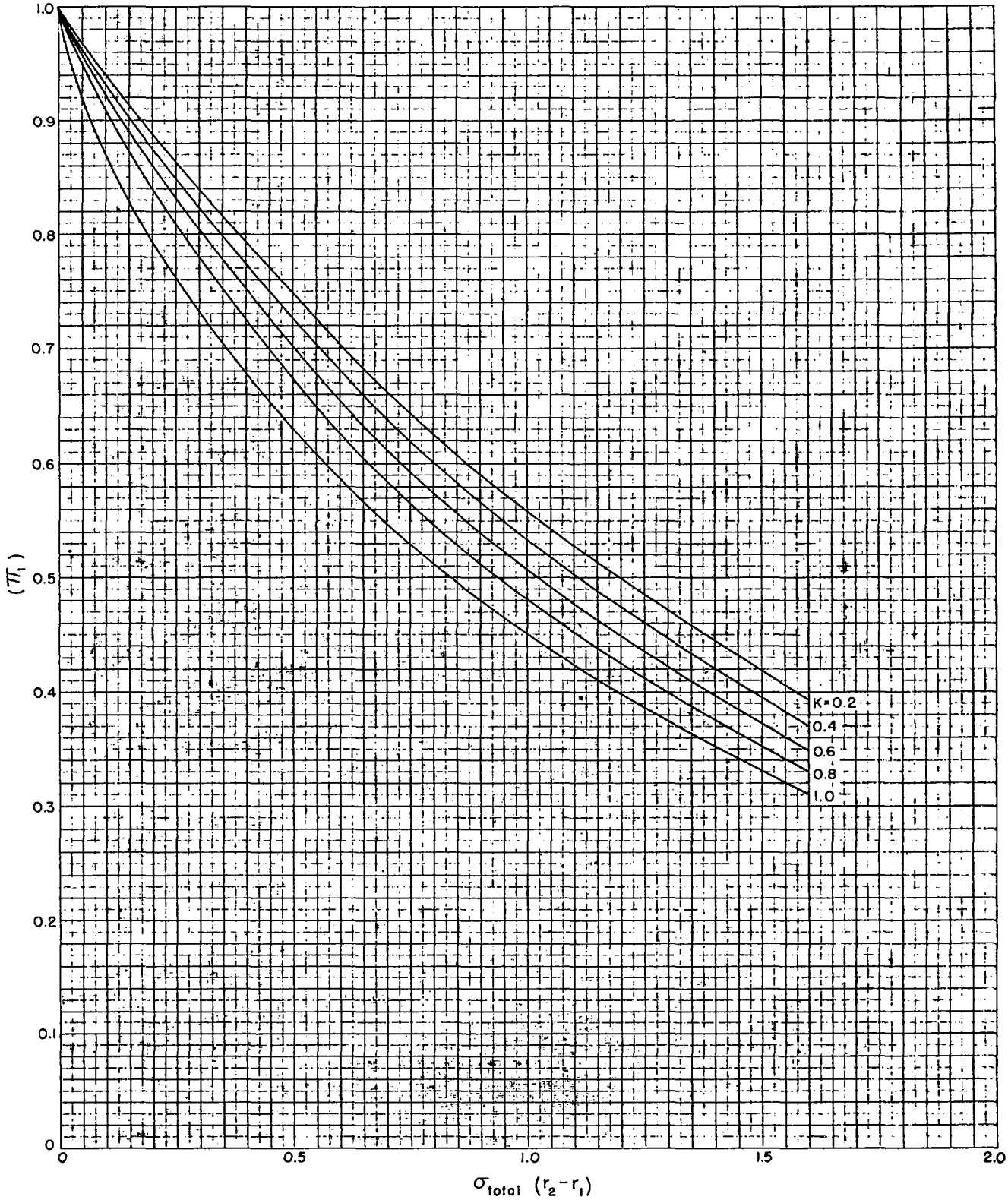

Fig. 5.6—Plot of π_1 for iron angular distribution, measured with "28" detector, when $\sigma_{tr}/\sigma_t = 0.75$.

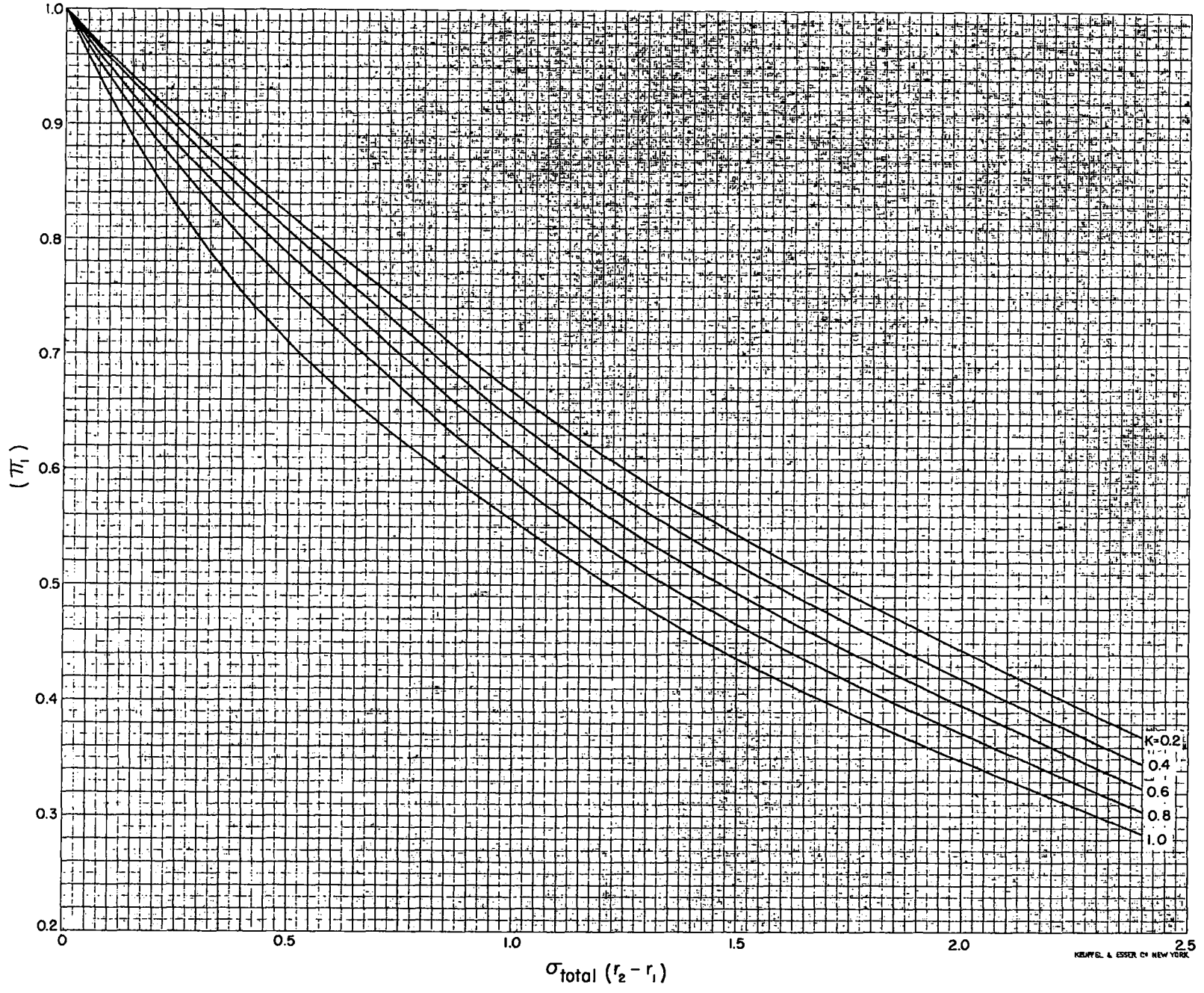

Fig. 5.7—Plot of π_1 for iron angular distribution, measured with "28" detector, when $\sigma_{tr}/\sigma_t = 0.50$.

Chapter 6

CORRECTIONS

Assumptions included in the derivation of transmission T in Chapters 3 and 4 are that the internal source is a point, non-absorbing isotropic emitter; the detector is small and isotropic; and the source-to-detector distance is large, relative to the sphere radius. By the reciprocity theorem, these assumptions are equivalent to the set: The internal detector is a point, non-absorbing isotropic detector; the external source is a small isotropic emitter; and the source-to-detector distance is large, compared with the sphere radius. The latter set of assumptions is of primary concern to us since an external neutron source was used in the execution of the experimental work.

Since a fission neutron source produced with thermal neutrons is an isotropic emitter, we are interested in the following variations from ideal conditions: finite source-to-detector distance, finite counter size, absorptions in the counter material, and angular variation of sensitivity of the counter. In addition to the above corrections, one needs also to consider the effect of losses of energy on elastic collisions, with the resultant decrease in counting efficiency in the neutron detector. The corrections derived in this chapter should be made to the observed transmission before comparing it to the theoretical transmission calculated under the ideal conditions assumed in Chapters 3 to 5. If intensity permits favorable geometrical conditions, these corrections will be quite small. Since this was true in our experiments, these small corrections are all treated independently and are only first order approximations. The availability and use of these corrections does not in any sense obviate the necessity of starting out with a relatively clean experiment.

6.1 Finite Distance Between Source and Detector

The characteristics of the finite distance effect are discussed in LA-1428[1] and LA-740.[2] The problem here will be to continue the description of the effect from Section 3, LA-1428, so that an approximate correction term for it can be computed along with the escape probabilities (Eqs. 3.8 and 3.12, Chapter 5) on the CPC machine.

The reason for the finite distance effect can be best understood when one thinks of the source inside of the sphere and the detector outside. Then it is evident that all the neutrons which are recorded in the detector with the sphere on, do not come from the same position as the recorded neutrons do with the sphere off. Thus, on the average, neutrons which have shell collisions have a slightly different probability of passing through the counter (solid angle) than neutrons that come directly from the source. In Chapters 3 and 4, we implicitly assumed that all neutrons of the initial energy, whether they had made elastic collisions in the shell or not, had the same chance of passing through the detector.

In Section 3 of LA-1428, the quantity $n(r, \theta)\, dV\, d\omega$ is introduced and is there defined as the number of neutrons which have their last collision before escaping from the spherical shell in the volume element dV at position r, and whose direction of motion immediately after this last collision is in solid angle $d\omega$ at an angle θ with the radius. Then

$$n(r,\theta) = n_1(r,\theta) + n_2(r,\theta) + n_m(r,\theta)$$

where $n_1(r,\theta)$ includes only those neutrons whose last collision in the shell is their first collision, $n_2(r,\theta)$ includes only those neutrons whose last collision is their second, and $n_m(r,\theta)$ includes all neutrons whose last collision is the third or higher. Then Eq. 25 for T′ (the sphere transmission with the finite distance effect) in LA-1428[1] can be rewritten as follows

$$T' = \int_{r_1}^{r_2} dV \int_0^{\pi} \frac{2\pi \sin\theta \, d\theta \, [n_1(r,\theta) + n_2(r,\theta) + n_m(r,\theta)]}{\sqrt{1 - \frac{r^2}{b^2}\sin^2\theta}} \tag{6.1}$$

Expanding the square root in the denominator of a characteristic term, one obtains

$$\int_{r_1}^{r_2} dV \int_0^{\pi} \frac{2\pi \sin\theta \, d\theta \, n_n(r,\theta)}{\sqrt{1 - \frac{r^2}{b^2}\sin^2\theta}} = \int_{r_1}^{r_2} dV \int_0^{\pi} 2\pi \sin\theta \, d\theta \, n_n(r,\theta) \left(1 + \frac{1}{2}\frac{r^2}{b^2}\sin^2\theta + \frac{3}{8}\frac{r^4}{b^4}\sin^4\theta + \ldots\right) \tag{6.2}$$

In the nomenclature of this report

$$\int dV \int 2\pi \sin\theta \, d\theta \, n_n(r,\theta) = E_n P_n \tag{6.3}$$

the number of neutrons escaping from the sphere after the nth collision. E_n is the total number of neutrons which have made n elastic collisions and P_n their average escape probability as calculated in the manner of Eq. 3.8 or 3.12

$$P_n = \frac{1}{4\pi} \int_0^{4\pi} \int_{r_1}^{r_2} f_n(r) \, dr \, P(r,\theta) \, d\omega \tag{6.4}$$

We may also write

$$2\pi \int_{r_1}^{r_2} dV \int_0^{\pi} n_n(r,\theta) \, r^2 \sin^3\theta \, d\theta \equiv E_n P_n^* \tag{6.5}$$

where

$$P_n^* = \frac{1}{4\pi} \int_0^{4\pi} \int_{r_1}^{r_2} f_n(r) \, r^2 \, dr \sin^2\theta \, P(r,\theta) \, d\omega \tag{6.6}$$

Similarly

$$P_n^{**} = \frac{1}{4\pi} \int_0^{4\pi} \int_{r_1}^{r_2} f_n(r) \, r^4 \, dr \sin^4\theta \, P(r,\theta) \, d\omega \tag{6.7}$$

Introducing these quantities into Eq. 6.1, one obtains for the observed transmission

$$T' = T + \frac{1}{2b^2}\left[E_1 P_1^* + E_2 P_2^* + E_m P_m^*\right] + \frac{3}{8b^4}\left[E_1 P_1^{**} + E_2 P_2^{**} + E_m P_m^{**}\right] + \ldots \tag{6.8}$$

The term to be subtracted from the observed transmission to correct for the finite source to detector distance is, for the analysis of Chapter 3

$$J_1 = (1 - T_0)\left(\frac{\sigma_{et}}{\sigma_{tr}}\right)\left\{\left(\frac{P_1^*}{2b^2} + \frac{3P_1^{**}}{8b^4}\right) + \frac{\sigma_{et}}{\sigma_{tr}}(1 - P_1)\left[\frac{P_2^*}{2b^2} + \frac{3P_2^{**}}{8b^4}\right] + \frac{(1 - P_1)(1 - P_2)\,\sigma_{et}^2}{\sigma_{tr}\,(\sigma_{in} + \sigma_{et}P_m)}\left[\frac{P_m^*}{2b^2} + \frac{3P_m^{**}}{8b^4}\right]\right\} \tag{6.9}$$

For the analysis of Chapter 4, the correction term is

$$J_1 = (1 - T_0)\left(\frac{\sigma_{el}}{\sigma_t}\right)\left\{\left(\frac{\pi_1^*}{2b^2} + \frac{3\pi_1^{**}}{8b^4}\right) + \frac{\sigma_{et}}{\sigma_{tr}}(1 - \pi_1)\left(\frac{P_2^*}{2b^2} + \frac{3P_2^{**}}{8b^4}\right) + \frac{(1 - \pi_1)(1 - P_2)\sigma_{et}^2}{\sigma_{tr}(\sigma_{in} + \sigma_{et}\,P_m)}\left[\frac{P_m^*}{2b^2} + \frac{3P_m^{**}}{8b^4}\right]\right\} \tag{6.10}$$

In most of the geometrical situations encountered in this investigation, the quantities P_1^{**}, P_2^{**}, and P_m^{**} were fairly small. However, an approximate correction was usually made for these terms. Ignoring the exponentials present in the integral Equations 6.6 and 6.7 and assuming spherically symmetric elastic scattering, it can be shown that

$$\frac{P_n^{**}}{P_n^*} \cong 0.48\,\frac{(r_2^5 - r_1^5)}{(r_2^3 - r_1^3)} \tag{6.11}$$

6.1.1 Finite Distance Correction for Analysis of Chapter 3

The quantities P_1^*, P_2^*, and P_n^* were calculated on the CPC using Eq. 6.6. It was necessary to modify only the integration of P_1, P_2, and P_m discussed in Chapter 5 to include the additional factor ($r^2 \sin^2\theta$) at each point in the integration. The integration of P_n^* proceeded concurrently with that of P_n on the computing machines. Simpson's rule was used for both the r and θ integrations. Twenty-one equally spaced values of $\cos\theta$ between 1 and -1 and five equally spaced values of r between r_1 and r_2 were used. The error introduced in P_n^* by the numerical methods, mentioned above, is estimated to be ≤2 percent. This is considerably greater accuracy than is required in the correction term, since b^2 is known to a few percent at best.

To calculate the correction factor for the finite distance effect from Eq. 6.9, one first obtains trial transport cross sections in the manner of Section 3.5. The $(1 - K)P_1^*$, $(1 - K)P_2^*$, and $(1 - K)P_m^*$ values are then read from Figs. 6.1, 6.2, and 6.3, respectively (or obtained by interpolation). As in Chapter 5, the only parameters necessary to fix P_n^* are K or r_1/r_2, and the sphere thickness in transport mean free paths. The distance between the centers of source and detector, b, must be expressed in transport mean free paths because r in Eq. 6.6 is expressed in these units. When the source-to-detector distance is approximately equal to the sphere diameter, it becomes necessary to include P^{**} in the correction terms (Eq. 6.11). Of course, if J_1 is large, one must recompute it for each new trial σ_{in} and subtract it from the observed transmission.

6.1.2 Finite Distance Effect Correction for Analysis of Chapter 4

If one decides to calculate the correction for finite source to counter distance using the more exact Eq. 6.10, P_2^* and P_m^* can be obtained from Eq. 6.6 (Figs. 6.2 and 6.3). In addition, π_1^* must be computed including the desired angular distribution. If in Eq. 6.6 one replaces $d\omega/4\pi$ by $[\sigma_{el}(\theta)\,d\omega]/\sigma_{el}$ the desired π_1^* will be obtained. However, π_1^* is determined by three parameters: the shell thickness in transport mean free paths, K or r_1/r_2, and σ_{tr}/σ_t, since $f_1(r)\,dr$ is a function of σ_t and $P(r,\theta)$ is a function of σ_{tr}.

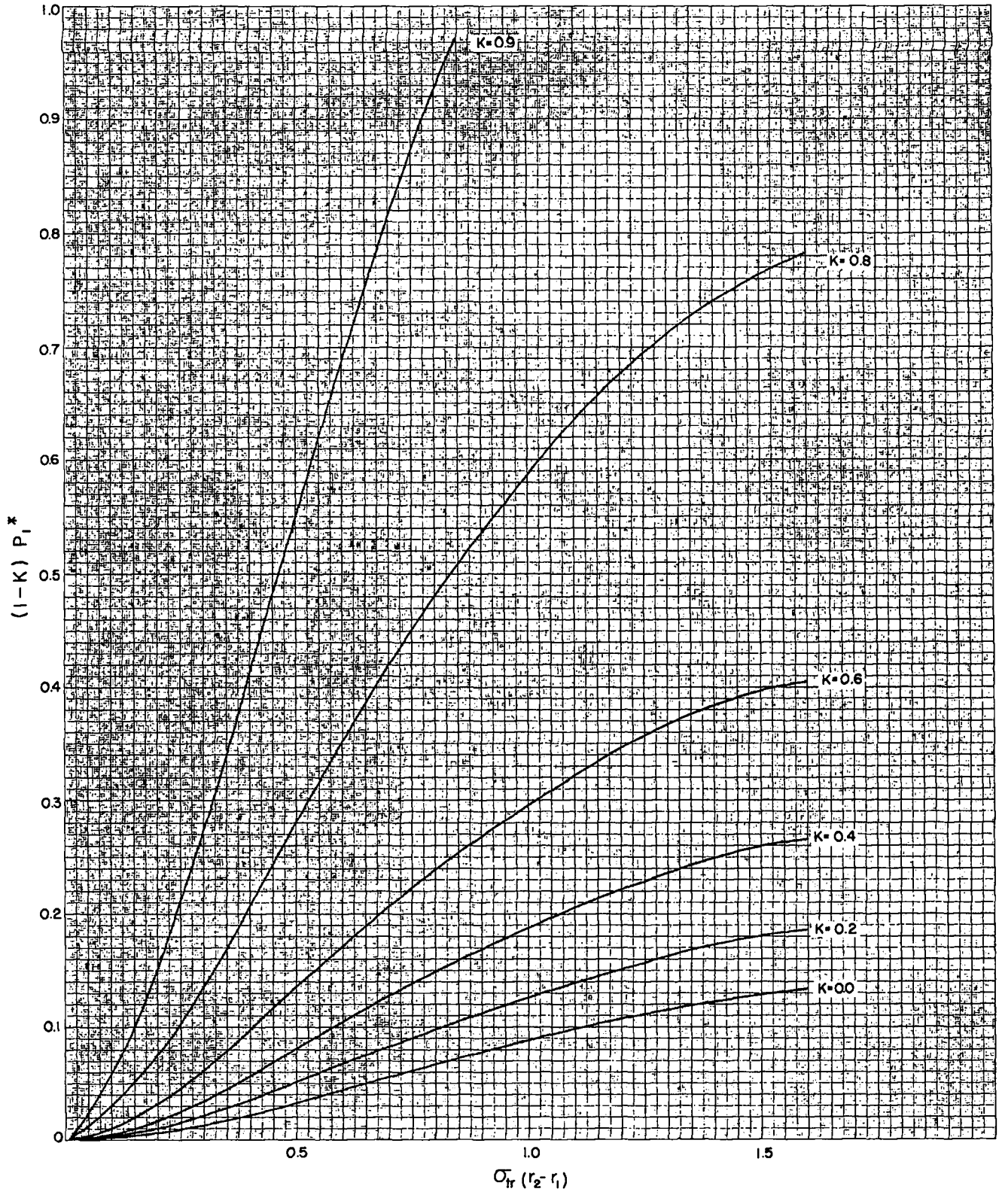

Fig. 6.1 — Plot of $(1-K)P_1^*$, finite distance effect correction for escape probability, assuming spherically symmetric scattering, and exponential collision distribution.

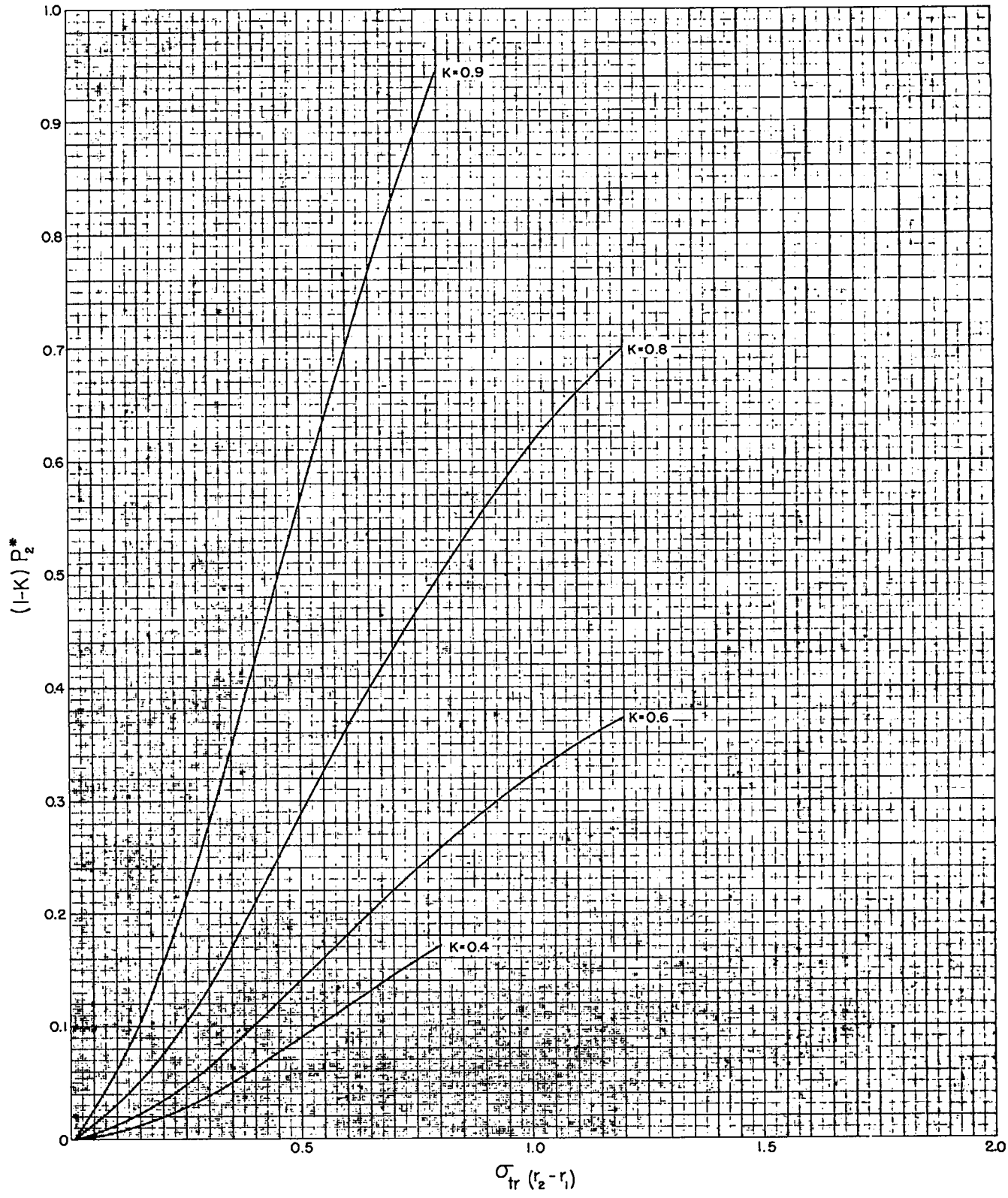

Fig. 6.2 — Plot of $(1-K)P_2^*$, finite distance effect correction for escape probability, assuming spherically symmetric scattering and second collision distribution.

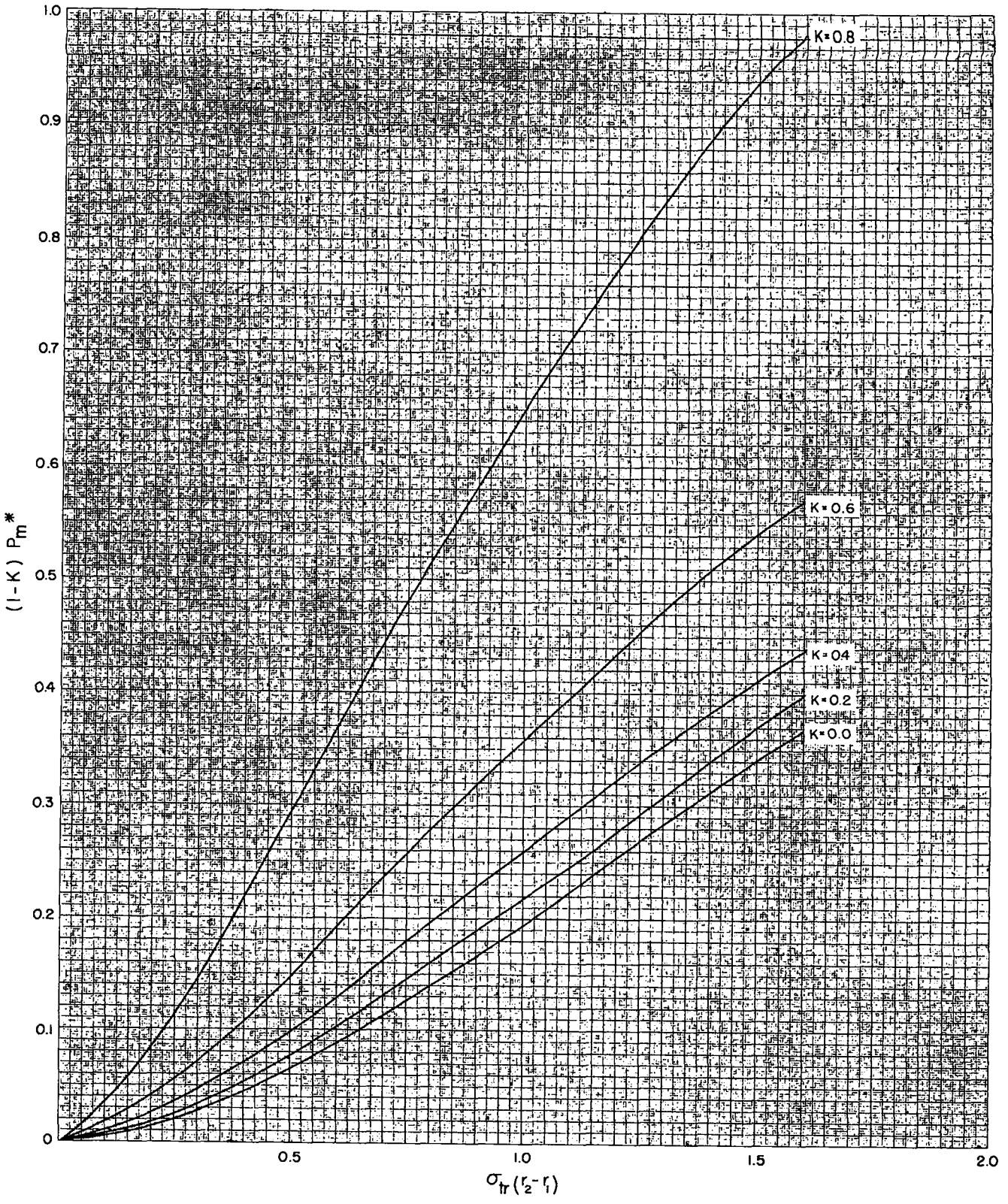

Fig. 6.3 — Plot of $(1-K)P_m^*$, finite distance effect correction for escape probability, assuming spherically symmetric scattering and normal mode collision distribution.

In practice, a great deal more computational effort is required to evaluate π_l^* than P_l^*, just as more work is required to find π_l instead of P_l. This is true because π_l^* must be found by actual machine calculation each time the elastic scattering angular distribution is changed, whereas, in principle, a general set of curves applicable to any angular distribution can be prepared for P_l^* by machine computation once and for all. It is thus desirable to use Eq. 6.9 instead of Eq. 6.10 if one is certain of the accuracy of the transport analysis. Clearly, when either the elastic scattering is spherically symmetric or is concentrated in a delta function in the forward direction (the two opposite extremes), Eqs. 6.9 and 6.10 give the same result. Between these extremes one can not be sure without actually comparing the results. To check this point, the curves of π_l^* in Figs. 6.4, 6.5 and 6.6 were prepared, including explicitly the angular distribution for elastic scattering from iron measured with a "28" counter using a beam of fast neutrons from the Los Alamos Fast Reactor.[6] This angular distribution is characterized by $\sigma_{et}/\sigma_{el} = 0.58$, which is approximately midway between the two extremes. A comparison of typical J_l values computed from Eqs. 6.9 and 6.10 indicates that an error of, in general, less than 10 percent is made in J_l by using Eq. 6.9. The entire correction to σ_{in} for finite distance of source and detector is less than 10 percent in most cases to be considered.

6.2 Finite Counter Size Correction Factors

Throughout the experimental investigation discussed in this report we used cylindrical spiral fission chambers or cylindrical rolls of aluminum foil. To compute the effect of a finite counter, uniformly sensitive throughout, we replace it by a non-absorbing source distributed uniformly in the same volume (see Section 1.2). The finite source size introduces three types of effects:

(a) The flux of neutrons at a detecting point in space is not specified exactly by the distance between the center of the source and the detecting point.

(b) Neutrons from the source go through the sphere obliquely, with a greater path length than the thickness, thus increasing the probability of a first collision in the shell.

(c) The distribution of neutrons which have made a first collision in the shell is changed somewhat from an exponential. Therefore, the escape probability after the first collision will be changed. This third effect is totally neglected because small changes in the collision distribution in a spherical shell do not appreciably change the escape probability after the collision (Section 3.2).

We must compute: (1) the flux of neutrons that have had no collisions in the shell, at the detecting point on the X axis (Fig. 6.7); (2) the flux at the detecting point on the X axis with no sphere; and (3) the total number of neutrons that make at least one collision in the shell. The escape probability after the first collision is considered unchanged [effect (c)], and P_2 and P_m are also considered unchanged.

We will now compute (3), the total number of neutrons that make at least one collision in the shell. Referring to Fig. 6.7, let us determine the flux of neutrons at an arbitrary point in space x_o, y_o. We will first find this flux $d\phi$, which is due to an element of source volume dV at position x, y, and z. We consider a cylindrical source and choose Y to be the axis of the cylinder. All collisions will be described by transport cross sections as in Chapter 3. Then

$$d\phi = \frac{Q\, dV\, e^{-\sigma_{tr} m}}{4\pi H^2 V_s} \tag{6.12}$$

V_s = total volume of source
H = distance between points (x_o, y_o) and (x,y,z)
b = distance between center of source and point (x_o, y_o)

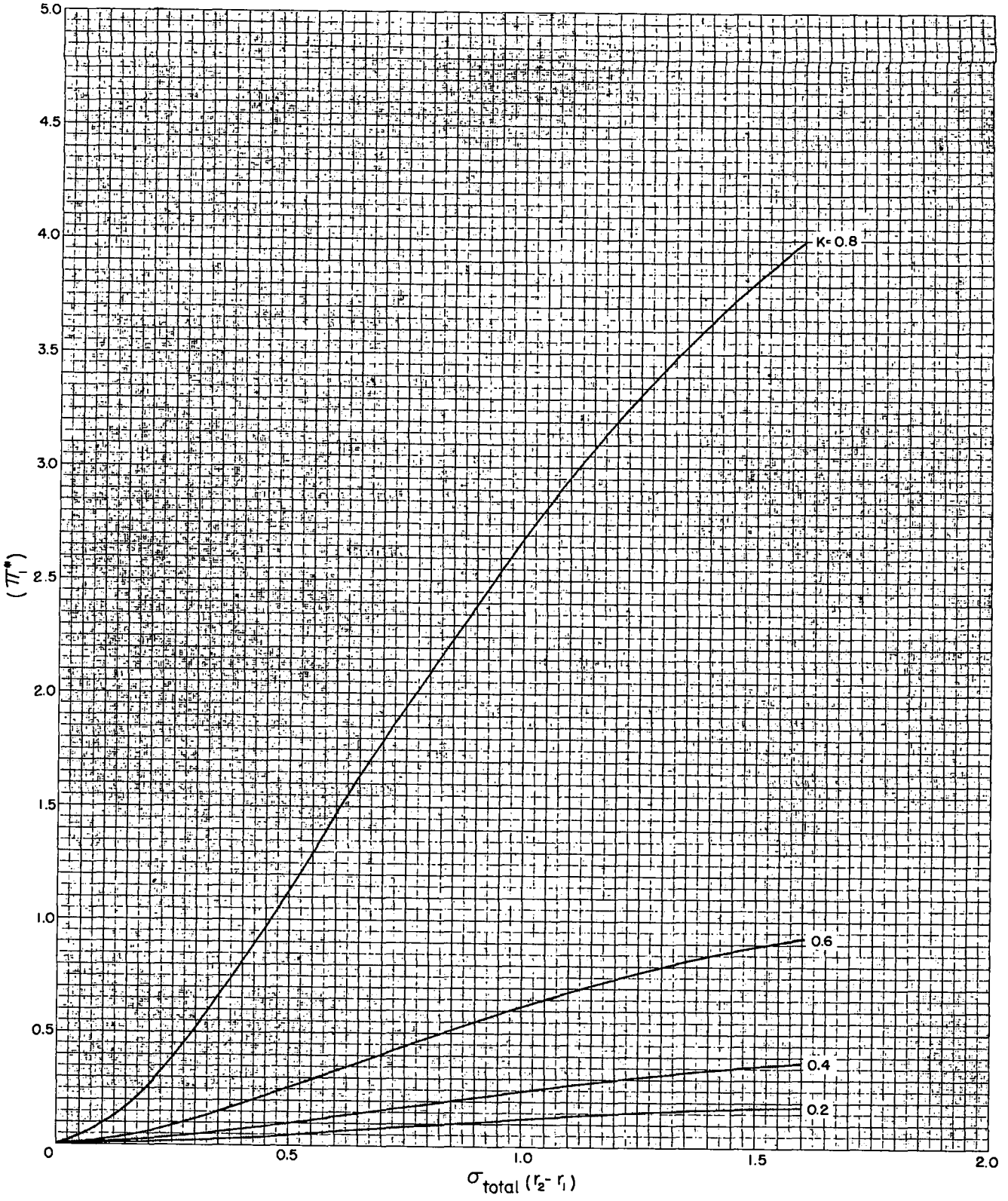

Fig. 6.4 — Finite distance effect for escape probability π_1^*, including iron angular distribution measured with "28" counter and exponential collision distribution when $\sigma_{tr}/\sigma_t = 1$.

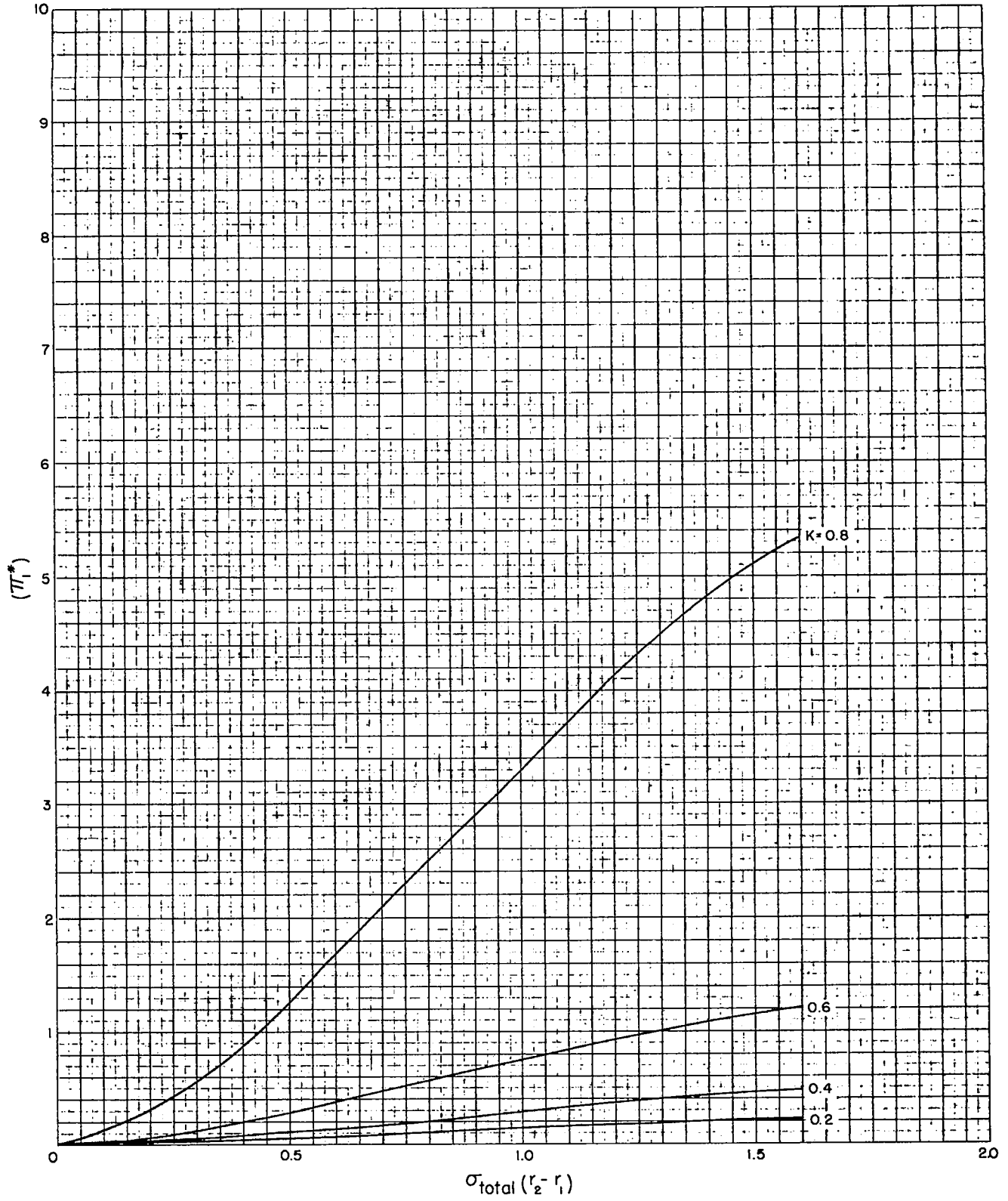

Fig. 6.5 — Finite distance effect for escape probability π_1^*, including iron angular distribution measured with "28" counter and exponential collision distribution, when $\sigma_{tr}/\sigma_t = 0.75$.

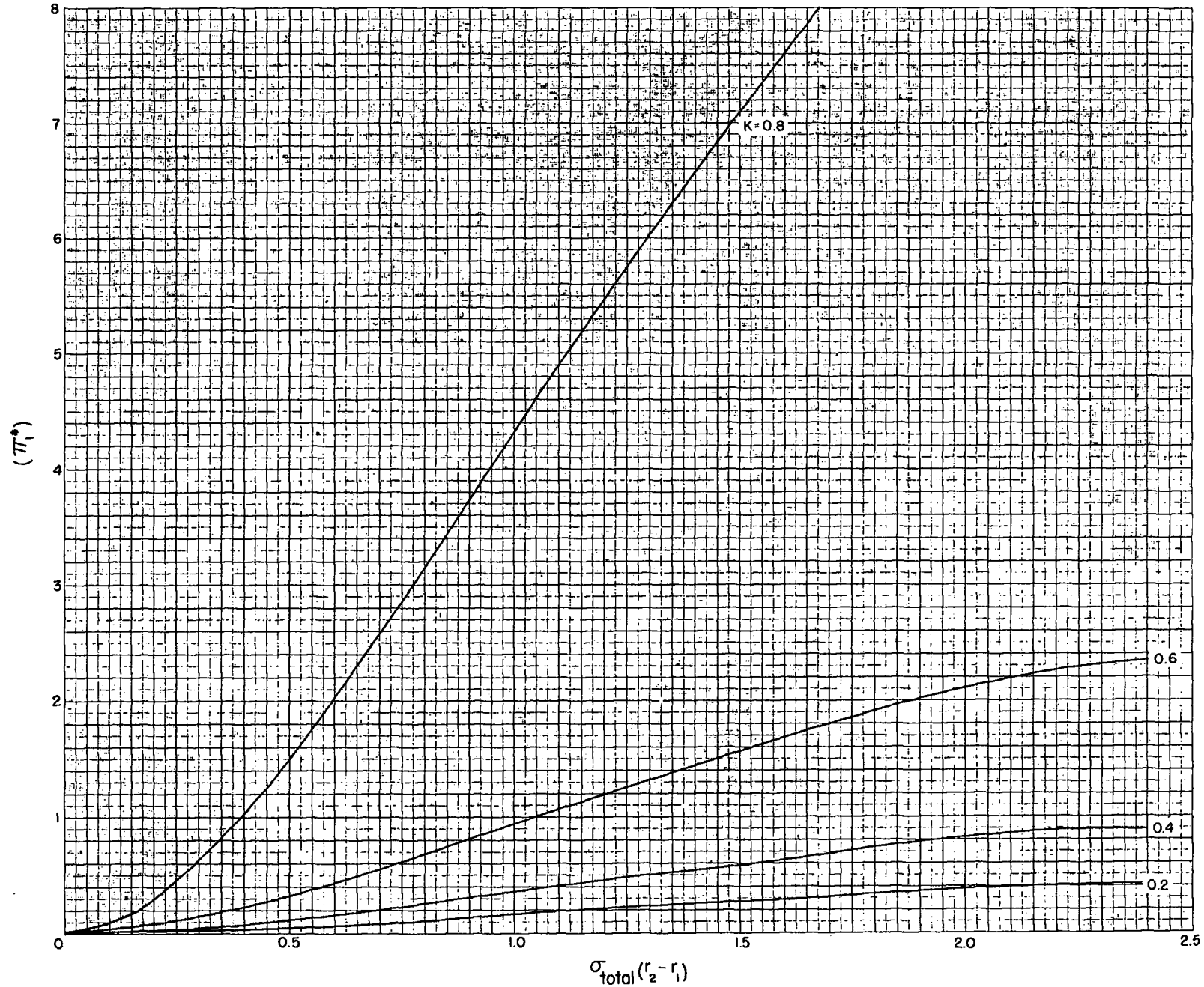

Fig. 6.6 — Finite distance effect for escape probability π_1^*, including iron angular distribution measured with "28" counter and exponential collision distribution, when $\sigma_{tr}/\sigma_t = 0.50$.

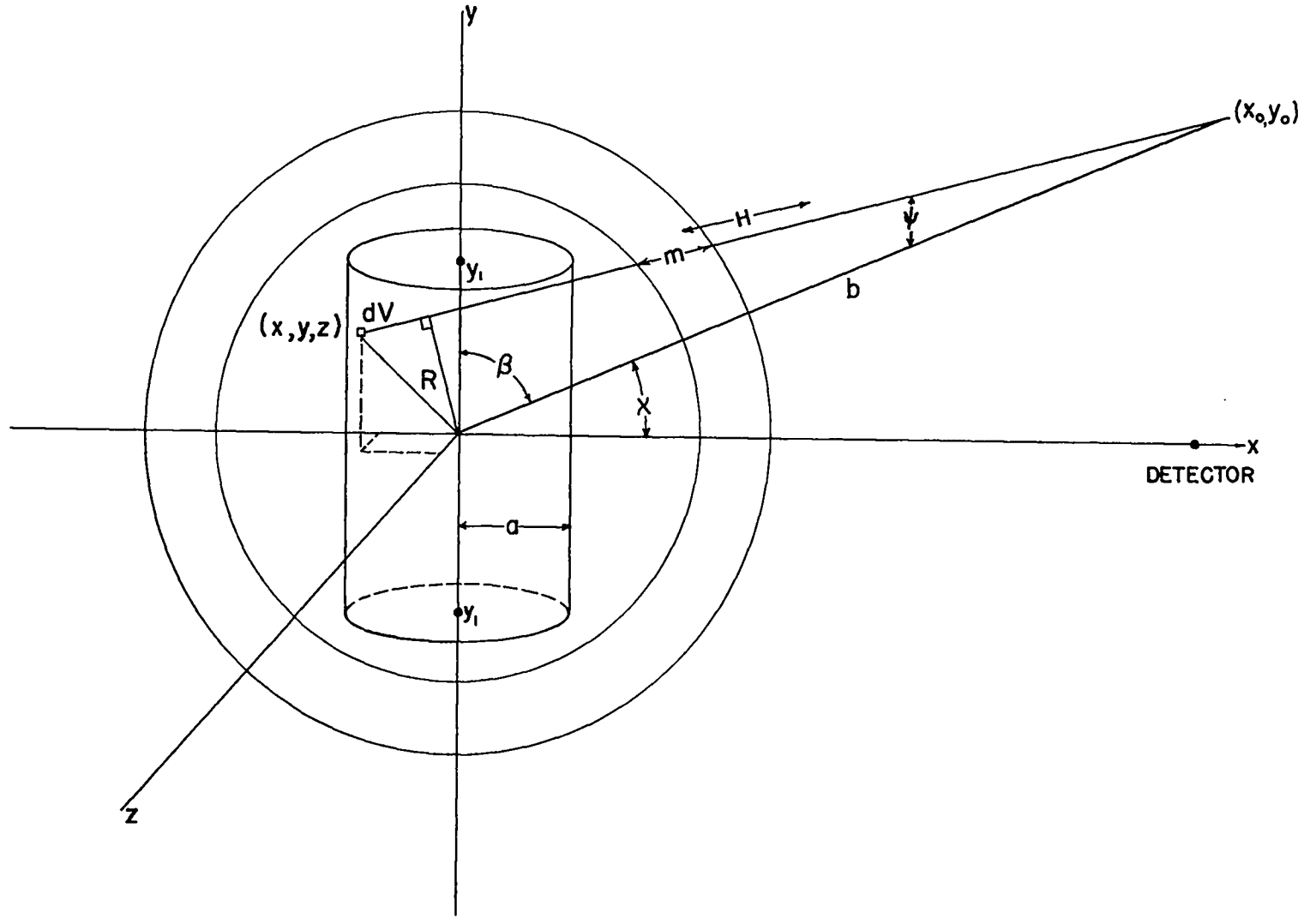

Fig. 6.7—Geometrical arrangement showing a cylindrical neutron source inside a sphere. This cylindrical source simulates in the numerical analysis the cylindrical detector actually used for the measurements.

$$H^2 = (x_o - x)^2 + (y_o - y)^2 + z^2 \tag{6.13}$$

Q = source strength

Inverting

$$\frac{1}{H^2} = \frac{1}{b^2}\left[1 + \frac{2(x_o x + y_o y)}{b^2} - \frac{(x^2 + y^2 + z^2)}{b^2} + \frac{4(x_o x + y_o y)^2}{b^4} + \ldots\right]$$

and

$$m = \sqrt{r_2^2 - R^2} - \sqrt{r_1^2 - R^2}$$

Expanding the square roots

$$m = r_2 - r_1 + \frac{R^2}{2}\left(\frac{1}{r_1} - \frac{1}{r_2}\right) + \frac{R^4}{8}\left(\frac{1}{r_1^3} - \frac{1}{r_2^3}\right) + \ldots$$

It can be shown geometrically that

$$R^2 = \frac{(xy_o - yx_o)^2}{b^2} + z^2 + \ldots \tag{6.14}$$

Substituting these quantities and the X of Eq. 2.1 into Eq. 6.12,

$$d\phi = \frac{Q\,dV}{4\pi b^2 V_s}\left[1 + \frac{2(x_o x + y_o y)}{b^2} - \frac{(x^2 + y^2 + z^2)}{b^2} + \frac{4(x_o x + y_o y)^2}{b^4}\right] \times e^{-\sigma_u X}\left[1 - \frac{\sigma_{tr}}{2}\left(\frac{1}{r_1} - \frac{1}{r_2}\right)\left(\frac{(xy_o - yx_o)^2}{b^2} + z^2 + \ldots\right) + \ldots\right] \tag{6.15}$$

The radial flux at point x_o, y_o is needed to compute the total number of neutrons escaping from a spherical surface concentric with source and sphere. It is

$$d\phi^r = d\phi \cos\psi$$

$d\phi$ is given by Eq. 6.15 and

$$\cos\psi = \frac{\sqrt{b^2 - R^2}}{b} \cong 1 - \frac{1}{2}\frac{R^2}{b^2} + \ldots$$

$$d\phi^r = \frac{Q\,dV}{4\pi b^2 V_s}\left[1 + \frac{2(x_o x + y_o y)}{b^2} - \frac{(x^2 + y^2 + z^2)}{b^2} + \frac{4(x_o x + y_o y)^2}{b^4}\right] \times e^{-\sigma_u X}\left[1 - \left(\frac{\sigma_{tr}}{2}\left[\frac{1}{r_1} - \frac{1}{r_2}\right] + \frac{1}{2b^2}\right)\left(\frac{(y_o x - x_o y)^2}{b^2} + z^2\right)\right] \tag{6.16}$$

We will call the radius of our cylindrical counter a, and its height, $2y_1$. We can then perform the source volume integrations of Eqs. 6.15 and 6.16. Terms containing the first powers, x, y, or xy integrate to zero, and the quadratic terms give

$$\int\int\int dv\, x^2 = \int\int\int dv\, z^2 = V_s \frac{a^2}{4}$$
$$\int\int\int dv\, y^2 = V_s \frac{y_i^2}{3} \tag{6.17}$$

If this is used, for instance, in Eq. 6.16 we get

$$\phi^r = \frac{Q}{4\pi b^2} e^{-\sigma_{tr} X}\left[1 - \frac{a^2}{2b^2}\left(\frac{5}{4} + \frac{y_o^2}{4b^2} - \frac{2x_o^2}{b^2}\right) - \frac{y_i^2}{3b^2}\left(1 - \frac{4y_o^2}{b^2} + \frac{x_o^2}{2b^2}\right)\right.$$
$$\left. - \frac{\sigma_{tr}}{2}\left(\frac{1}{r_1} - \frac{1}{r_2}\right)\left\{\frac{a^2}{4}\left(1 + \frac{y_o^2}{b^2}\right) + \frac{y_i^2 x_o^2}{3b^2}\right\}\right] \tag{6.18}$$

We can now calculate the number of neutrons which have made at least one collision in the shell. For this purpose, we subtract from the source Q the total number of neutrons escaping from the shell with no collisions. The latter is

$$\int \phi^r\, 2\pi\, b^2 \sin\beta\, d\beta \equiv Q_0 \tag{6.19}$$

where ϕ^r is given by Eq. 6.18. The integration in Eq. 6.19 goes over the angular coordinates of x_o and y_o. It can be seen that the average of y_o^2/b^2 is 1/3 and that of x_o^2/b^2 is 2/3. Then the terms without σ_{tr} in the bracket of Eq. 6.18 integrate to zero—as indeed they should, because for $\sigma_{tr} = 0$ the total radial flux out of the sphere must be Q. The result is

$$Q_0 = Q\, e^{-\sigma_{tr} X} - Q\, e^{-\sigma_{tr} X} \frac{\sigma_{tr}}{2}\left(\frac{1}{r_1} - \frac{1}{r_2}\right)\left(\frac{a^2}{3} + \frac{2y_i^2}{9}\right) \tag{6.20}$$

The number of neutrons which have made at least one collision is then (quantity 3, page 64)

$$(3) = Q - Q_0 = Q(1 - e^{-\sigma_{tr} X} + W) \tag{6.21}$$

where

$$W = \frac{\sigma_{tr}}{2}\left(\frac{1}{r_1} - \frac{1}{r_2}\right)\left(\frac{a^2}{3} + \frac{2y_i^2}{9}\right) e^{-\sigma_{tr} X} \tag{6.22}$$

Next we calculate the total (not the radial) flux at the detector. For our analysis the detector is located on the x axis, so that $y_o = o$ and $x_o = b$. We calculate the flux first without a sphere around the source. In this case, the exponential and the last bracket in Eq. 6.15 should be omitted, and we obtain after integrating over counter volume (quantity 2)

$$(2) = \phi(\text{sphere off}) = \frac{Q}{4\pi b^2}\left(1 + \frac{a^2}{2b^2} - \frac{y_i^2}{3b^2}\right) \tag{6.23}$$

The flux of neutrons which have made no collisions, at the same point on the x axis with the sphere on (quantity 1), is obtained by integrating Eq. 6.15 including all terms over the source volume, giving

$$\phi(\text{sphere on}) = \frac{Q}{4\pi b^2}\left[e^{-\sigma_{tr} X} - W'\right] \tag{6.24}$$

where

$$W' = e^{-\sigma_{tr}X}\left[\frac{y_i^2}{3b^2} - \frac{a^2}{2b^2} + \frac{\sigma_{tr}}{2}\left(\frac{1}{r_1} - \frac{1}{r_2}\right)\left(\frac{y_i^2}{3} + \frac{a^2}{4}\right)\right] \tag{6.25}$$

We formulate the correction term to be added to the observed transmission as follows: The counting rate in the detector with the sphere off is ϕ(sphere off) V_d/λ_d, where ϕ(sphere off) is given by Eq. 6.23. The counting rate in the detector with sphere on, due to neutrons that have made no collisions, is ϕ(sphere on) V_d/λ_d, where ϕ(sphere on) is given by Eq. 6.24. The counting rate in the detector due to neutrons that have made one or more elastic collisions is ϕ(collision) V_d/λ_d, where

$$\phi(\text{collision}) = \frac{Q}{4\pi b^2}\left[1 - e^{-\sigma_{tr}X} + W\right]\frac{\sigma_{et}}{\sigma_{tr}}\left[P_1 + (1 - P_1)\frac{\sigma_{et}P_2}{\sigma_{tr}} + \frac{(1 - P_1)(1 - P_2)\sigma_{et}^2 P_m}{\sigma_{tr}(\sigma_{in} + \sigma_{et}P_m)}\right] \tag{6.26}$$

neglecting the finite distance effect. Then the sphere transmission, corrected for counter size, is

$$\frac{\phi(\text{sphere on}) + \phi(\text{collision})}{\phi(\text{sphere off})}$$

The term to add to the observed transmission to correct for finite counter size is then

$$J_2 = \left[\frac{a^2}{2b^2} - \frac{y_i^2}{3b^2}\right]T_{obs} + W' - W\frac{\sigma_{et}}{\sigma_{tr}}\left[P_1 + (1 - P_1)\frac{\sigma_{et}}{\sigma_{tr}}P_2 + \frac{(1 - P_1)(1 - P_2)\sigma_{et}^2 P_m}{\sigma_{tr}(\sigma_{in} + \sigma_{et}P_m)}\right] \tag{6.27}$$

If one includes the angular distribution of elastically scattered neutrons in the analysis of the first collision, as in Chapter 4, the correction term is as follows

$$J_2 = \left[\frac{a^2}{2b^2} - \frac{y_i^2}{3b^2}\right]T_{obs} + W' - W\frac{\sigma_{el}}{\sigma_t}\left[\pi_1 + (1 - \pi_1)\frac{\sigma_{et}}{\sigma_{tr}}P_2 + \frac{(1 - \pi_1)(1 - P_2)\sigma_{et}^2 P_m}{\sigma_{tr}(\sigma_{in} + \sigma_{et}P_m)}\right] \tag{6.28}$$

where W and W′ are computed from Eqs. 6.22 and 6.25 respectively by replacing σ_{tr} with σ_t. The correction terms of Eqs. 6.27 and 6.28 are quite small ($\leq$0.002) for this experimental work and the next terms in the expansion of H and m in Eq. 6.13 are unnecessary.

6.3 Absorption in the Counter

To compute the effect of absorption in the counter, the absorbing counter is replaced with an absorbing source. We next assume that elastic scatterings in this source can be neglected since the neutron's direction only is changed and not its energy or probability of a collision in the shell. Since the absorption correction is usually very small, we will consider it independently of the previous corrections (Sections 6.1 and 6.2). We will merely make the necessary changes in the typical transmission formulas derived in Chapter 3. The number of neutrons escaping from the shell with no collisions has the same form as before, except that the source strength is now the number of neutrons escaping from the source per second. This redefinition does not affect the transmission formula. However, all escape probabilities and collision probabilities now depend on the probability of an absorption in the source.

An equivalent way of writing Eq. 3.36 is

$$T = T_0 + (1 - T_0)\frac{\sigma_{et}}{\sigma_{tr}}\left[P_1 + (1 - P_1)\frac{\sigma_{et}}{\sigma_{tr}}P_2 + \frac{(1 - P_1)(1 - P_2)\sigma_{et}^2 P_m}{\sigma_{tr}(\sigma_{in} + \sigma_{et}P_m)}\right] \tag{6.29}$$

where P_n is the average probability of escape after the nth collision and $(1 - P_n)$ is the average probability of making another collision in the shell after the nth collision. The effect under consideration necessitates changes in P_n and $(1 - P_n)$ as follows

$$P_n \rightarrow \bar{\bar{P}}_n = P_n - P_\Omega P_A P^{180} \tag{6.30}$$

and

$$(1 - P_n) \rightarrow (1 - \bar{\bar{P}}_n) = 1 - P_n - P_\Omega P_A \, {}^1P^{180}(1 - {}^2P^{180}) \tag{6.31}$$

where

P_Ω = relative probability that a neutron goes in an average solid angle Ω (the solid angle required to pass through the source after a collision, Fig. 6.8).
P_A = average probability of an absorption in the source per incident neutron.
${}^1P^{180}$ = probability that a neutron, if initially scattered into solid angle Ω, will penetrate into the cavity.
${}^2P^{180}$ = probability that a neutron escapes on the opposite side of the sphere after it traverses the cavity.
$P^{180} = ({}^1P^{180})({}^2P^{180})$

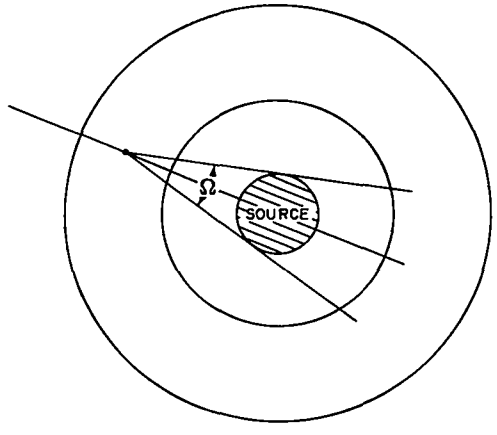

Fig. 6.8

One then introduces these changes into Eq. 6.29 to obtain the formula for the spherical shell transmission including an absorbing source

$$T = T_0 + (1 - T_0)\frac{\sigma_{et}}{\sigma_{tr}}\left[\bar{\bar{P}}_1 + (1 - \bar{\bar{P}}_1)\frac{\sigma_{et}}{\sigma_{tr}}\bar{\bar{P}}_2 + \frac{(1 - \bar{\bar{P}}_1)(1 - \bar{\bar{P}}_2)\sigma_{et}^2 \bar{\bar{P}}_m}{\sigma_{tr}(\sigma_{in} + \sigma_{et}\bar{\bar{P}}_m)}\right] \tag{6.32}$$

Since this effect is small, it may be estimated by calculating the "escape probabilities" ${}^1P^{180}$ and ${}^2P^{180}$ at exactly 180°. P_Ω can be estimated using spherically symmetric elastic scattering.

This effect may be included in the evaluation of the transmission experiments, if desired. However, for detectors used in the experimental work discussed in this report, the effect of detector absorption does not appear to cause an error of more than 0.5 percent in inelastic cross section.

6.4 Angular Asymmetry of Counter

In deriving transmission formulas in Chapters 2, 3, and 4, we have assumed that the detector (source) inside the sphere was isotropic, but in practice this is not necessarily realized. To evaluate the situation with an asymmetric counter, we retain the counter inside the sphere. This correction, like that of Section 6.3, is small in practice for our experimental conditions and will be considered independently of all other corrections.

Let us assume that our detector has a reduced efficiency Δ over a solid angle Ω, and an efficiency of unity over a solid angle $(1 - \Omega)$. We shall further assume that neutrons elastically scattered in a sphere of material come into a central counter with equal probability from all angles. This latter condition is clearly questionable, but it should be most nearly realized if one considers transport collisions only.

Transmission equation 3.36, or its equivalent, Eq. 6.29, rewritten with the reduced efficiency region of the neutron detector directed away from the source, gives (no neutrons enter through this region with the sphere removed)

$$T(\text{away}) = e^{-\sigma_{tr}X} + (1 - e^{-\sigma_{tr}X})\frac{\sigma_{et}}{\sigma_{tr}}\left[P_1 + (1 - P_1)\frac{\sigma_{et}}{\sigma_{tr}}P_2 + \frac{(1 - P_1)(1 - P_2)\sigma_{et}^2 P_m}{\sigma_{tr}(\sigma_{in} + \sigma_{et}P_m)}\right] \times [(1 - \Omega) + \Omega\Delta] \tag{6.33}$$

This reduces to

$$T(\text{away}) = T - (1 - e^{-\sigma_{tr}X})\frac{\sigma_{et}}{\sigma_{tr}}\left[P_1 + (1 - P_1)\frac{\sigma_{et}}{\sigma_{tr}}P_2 + \frac{(1 - P_1)(1 - P_2)\sigma_{et}^2 P_m}{\sigma_{tr}(\sigma_{in} + \sigma_{et}P_m)}\right](1 - \Delta)\Omega \tag{6.34}$$

where T is given by Eq. 6.29. The transmission formula with the reduced efficiency region of the neutron detector directed toward the source is

$$T(\text{toward}) = T + (1 - e^{-\sigma_{tr}X})\frac{\sigma_{et}}{\sigma_{tr}}\left[P_1 + (1 - P_1)\frac{\sigma_{et}}{\sigma_{tr}}P_2 + \frac{(1 - P_1)(1 - P_2)\sigma_{et}^2 P_m}{\sigma_{tr}(\sigma_{in} + \sigma_{et}P_m)}\right] \times \frac{(1 - \Delta)(1 - \Omega)}{\Delta} \tag{6.35}$$

Eliminating T between Eqs. 6.34 and 6.35, we obtain

$$T(\text{toward}) = T(\text{away}) + (1 - e^{-\sigma_{tr}X})\frac{\sigma_{et}}{\sigma_{tr}}\left(\frac{1 - \Delta}{\Delta} - \frac{\Omega(1 - \Delta)^2}{\Delta}\right) \times \left[P_1 + (1 - P_1)\frac{\sigma_{et}}{\sigma_{tr}}P_2 + \frac{(1 - P_1)(1 - P_2)\sigma_{et}^2 P_m}{\sigma_{tr}(\sigma_{in} + \sigma_{et}P_m)}\right] \tag{6.36}$$

For typical values $\Omega = 0.1$ and $\Delta = 0.95$, the term $\Omega(1 - \Delta)^2/\Delta$ is very much less than $(1 - \Delta)/\Delta$ and may therefore be neglected in Eq. 6.36. Thus, Δ can be determined by measuring a sphere transmission with the reduced sensitivity region of the detector pointing toward the source and measuring the transmission of the same sphere with this reduced sensitivity region pointing away from the source. Also, Δ can be measured directly by placing the detector in a beam of fast neutrons and counting with the detector oriented at several angles with respect to the direction of the fast beam. Experiments of both types are discussed in Section 10.9.

Final cross sections reported in Chapters 11, 12, 13, and 14 were corrected for counter asymmetry, using Eq. 6.33. Our particular counter orientation dictated this choice. Corrections to the inelastic cross sections averaged around 1 percent and are assumed to be correct only to one-half their magnitude, due to uncertainties in $(1 - \Delta)$ and Ω.

6.5 Correction for Loss of Energy on Elastic Collisions

If one re-derives the first order transmission Equation 1.2 for a continuous spectrum neutron source as in Chapter 7, and a non-ideal threshold detector, including loss of energy on elastic collisions, one obtains an additional apparent inelastic cross section of the form

$$\Delta\sigma \approx \overline{\overline{\sigma_{el}}} \left[1 - \frac{\int_0^\infty \int_0^E N(E)\, dE\, \sigma_{el}(E \rightarrow E')\, dE'\, \sigma^D(E')}{\int_0^\infty N(E)\, dE\, \sigma_{el}(E)\, \sigma^D(E)} \right] \tag{6.37}$$

$\overline{\overline{\sigma_{el}}}$ is the average elastic cross section for the neutrons which count in the detector, given by

$$\overline{\overline{\sigma_{el}}} = \frac{\int_0^\infty N(E)\, dE\, \sigma^D(E)\, \sigma_{el}(E)}{\int_0^\infty N(E)\, dE\, \sigma^D(E)} \tag{6.38}$$

where

$N(E)\, dE$ = the energy distribution function for the continuous spectrum of interest, here the fission spectrum.

$\sigma_{el}(E \rightarrow E')\, dE'$ = the cross section for scattering elastically from energy E into an energy interval dE' at E'.

$\sigma^D(E)$ = the detection cross section for neutrons of energy E.

$\sigma_{el}(E)$ = the total elastic cross section at energy E.

The evaluation of Eq. 6.37 in its present form is impossible without far more experimental data than exist at present. One may, however, proceed further if one assumes that neutrons of all enegies to be considered in the integral in the numerator of Eq. 6.37 have the same angular distribution for elastic scattering, an average angular distribution. We next define a normalized angular distribution function $F(\theta)\, d\omega$ as the probability of scattering into solid angle $d\omega$ at angle θ. Then

$$\sigma_{el}(E)\, F(\theta)\, d\omega \equiv \sigma_{el}(E \rightarrow E')\, dE' \tag{6.39}$$

where E' and θ are related by the expression (for moderately heavy and heavy elements)

$$E' = E\left[\left(\frac{1+\bar{r}}{2}\right) + \left(\frac{1-\bar{r}}{2}\right)\cos\theta\right]$$

and

$$\bar{r} = \left(\frac{A-1}{A+1}\right)^2 \tag{6.40}$$

where A is the atomic weight of the target nucleus. Substituting the left side of Eq. 6.39 into Eq. 6.37 and removing $\sigma_{el}(E)$ from both numerator and denominator, since we will assume this varies slowly with energy, we obtain

$$\Delta\sigma = \overline{\overline{\sigma_{el}}} \left[1 - \frac{\int_0^\infty \int_0^{4\pi} N(E)\, dE\, F(\theta)\, d\omega\, \sigma^D(E')}{\int_0^\infty N(E)\, dE\, \sigma^D(E)} \right] \tag{6.41}$$

This may be evaluated now, numerically as has been done in a trial case, or Eq. 6.41 may be simplified even further. If one now finds the average energy $\bar{E}$ after an elastic collision, the bracket in Eq. 6.41 may be simplified. Equation 6.41 becomes

$$\Delta\sigma = \overline{\overline{\sigma_{el}}} \left[1 - \frac{\int_0^\infty N(E)\, dE\, \sigma^D(\overline{E})}{\int_0^\infty N(E)\, dE\, \sigma^D(E)} \right] \tag{6.42}$$

The average energy after an elastic collision is obtained from

$$\int_0^{4\pi} F(\theta)\, d\omega\, \frac{E'(\theta)}{E} = \frac{\overline{E}}{E} \tag{6.43}$$

For the comparison of the more involved Eq. 6.41 with Eq. 6.42, we selected the angular distribution function measured by Jurney and Zabel with a "28" detector, and a nickel scattering sample, for the continuous, essentially fission, spectrum from the Los Alamos Fast Reactor. The bracket in Eq. 6.41 gave 0.0167 and in Eq. 6.42 gave 0.0180. This indicates that the approximate method (Eq. 6.42) gives acceptable results for this correction.

To further check that the correction made with Eq. 6.42 was reasonable, the Monte Carlo problem coded for the Los Alamos MANIAC computer was revised by E. D. Cashwell, C. J. Everett, and J. M. Kister, to include the energy loss on each elastic collision which a neutron suffers before escaping from the shell. This problem is, of course, done by assuming that only one initial neutron energy is present. The neutrons leaving the sphere were classified into 54 energy groups non-uniformly distributed from the initial energy to zero energy.

Case 5, Table 4.1, was recalculated on the computing machine, and the energy spectrum of neutrons leaving this thick iron shell after only the elastic collisions P(E') dE' was determined. The true shell transmission is related to the observed shell transmission by

$$T_{obs} = T_{true} \left[\frac{\int_0^\infty \int_0^E N(E)\, dE\, T(E)\, P(E')\, d(E')\, \sigma^D(E')}{\int_0^\infty N(E)\, dE\, T(E)\, \sigma^D(E)} \right] \tag{6.44}$$

where

$$\int_0^E P(E')\, dE' = 1$$

T(E) is the shell transmission as a function of neutron energy and is unknown. Since it occurs in both numerator and denominator, its effect was thought to be slight. Several reasonable functions were tried for T(E) and these changes, as expected, turned out to have negligible effects on the result. To check whether the Monte Carlo problem gives the same answer for the apparent inelastic cross section as does Eq. 6.42, one computes the bracket in Eq. 6.44 and solves for T_{true}. From T_{obs} one computes the true inelastic cross section, plus the apparent inelastic cross section $\Delta\sigma$; and from T_{true} one computes only the true inelastic cross section, using Eq. 3.36. Subtracting these numbers, one gets $\Delta\sigma = 0.047$ barns, and Eq. 6.42 gives $\Delta\sigma = 0.040$ barns, which is acceptable agreement. Of course, even the Monte Carlo problem suffers from some of the difficulties inherent in the simpler correction formulas. For example, we are still assuming the same elastic angular distribution function—an average —for all fission spectrum energies detected in our threshold detectors. To remove the apparent inelastic cross section in the numerical analysis of our data, Eq. 6.42 was used. The uncertainty in the correction was assumed to be 50 percent. This uncertainty is, however, probably quite a conservative estimate.

In the course of a recent investigation using the sphere method and a monoenergetic neutron source,[10] it was possible to make a more detailed study of the effect of losses of energy on elastic collisions. Two methods of correcting for this effect were compared: (1) a detailed Monte Carlo calculation and (2) essentially Eq. 6.42. The comparison is shown in Table 6.1. The elements studied are listed in the first column from the left. In the second column the

angular distribution shape factor σ_{et}/σ_{el} is listed to tell whether there is a large or small amount of forward scattering. The first four values listed are for 1 Mev neutrons, and the remaining are for 4 Mev neutrons. The cross section deduced from the monoenergetic sphere experiments before this correction is made is next listed. The cross sections after correction for this effect by the Monte Carlo method and by Eq. 6.42 are listed next. In the last column the ratio of these two cross sections is given. One can see that the Monte Carlo method is essential for light elements with nearly isotropic elastic scattering angular distributions, but is not essential for elements with atomic weights greater than aluminum, if the elastic scattering shape factor σ_{et}/σ_{el} is less than about 0.60. Part of the reason why the Monte Carlo results disagree a large amount percentagewise with Eq. 6.42 for light elements is that the inelastic cross sections are much smaller for these elements.

TABLE 6.1—COMPARISON OF CROSS SECTIONS CORRECTED FOR LOSSES OF ENERGY IN ELASTIC COLLISIONS BY MONTE CARLO METHOD AND BY EQ. 6.42

Element	$\frac{\sigma_{et}}{\sigma_{el}}$	σ_{in}, barns (uncorrected)	σ_{in}, barns (by Monte Carlo)	σ_{in}, barns (by Eq. 6.42)	$\frac{\sigma_{in}\text{ (by Monte Carlo)}}{\sigma_{in}\text{ (by Eq. 6.42)}}$
C	0.94	0.71	0.117	0.243	0.48
Al	0.73	0.21	0.04	0.09	0.44
Fe	0.80	0.47	0.419	0.439	0.96
Cu	0.88	0.27	0.192	0.222	0.86
Be	0.59	1.04	0.62	0.39	1.59
Al	0.54	1.10	0.75	0.73	1.03
Ti	0.38	1.45	1.27	1.24	1.02
Fe	0.37	1.53	1.35	1.37	0.99
Zn	0.39	1.75	1.67	1.68	1.00
Cu	0.39	1.68	1.59	1.55	1.03
Zr	0.49	1.73	1.56	1.53	1.02
Sn	0.42	2.22	2.17	2.13	1.02
Cd	0.42	2.22	2.18	2.13	1.02
Ag	0.42	2.10	2.05	2.02	1.02
Au	0.23	2.78	2.74	2.73	1.00
Pb	0.32	1.95	1.85	1.88	0.98

6.6 Treatment of a Non-isotropic Neutron Source

We are including this section on how to treat a non-isotropic external neutron source for those who may wish to use the sphere method with the neutron sources $Li^7(p,n)Be^7$, $D(d,n)He^3$, $T(p,n)He^3$, and $T(D,n)He^4$. The situation encountered with these sources is that the intensity falls off fairly rapidly with angle α in Fig. 5.2 (the detector being inside the sphere). The first step in the procedure is to fit these intensity variations as best one can with a function

$$W(\alpha) = A + B \cos^2 \alpha \tag{6.45}$$

where $W(0°) = 1$, or $A + B = 1$.

We next think of the neutron source being inside of the sphere and the detector outside, of course, now calling the source intensity variation the angular detection sensitivity of the external detector (reciprocity theorem). The transmission formula becomes now, analogous to Eq. 6.1

$$T' = \int_{r_1}^{r_2} dV \int_0^{\pi} 2\pi \sin\theta \, d\theta \, [n_1(r,\theta) + n_2(r,\theta) + n_m(r,\theta) \frac{W(\alpha)}{\cos\alpha} \tag{6.46}$$

α is not an independent variable, instead

$$\sin\alpha = \frac{r}{b} \sin\theta \tag{6.47}$$

Cos α is of course just another way of writing the obliquity factor

$$\sqrt{1 - \frac{r^2}{b^2} \sin^2\theta}$$

Performing a power series expansion of $W(\alpha)/\cos\alpha$ (cf. Eq. 6.45)

$$\frac{W(\alpha)}{\cos\alpha} = 1 + \frac{(A-B)\, r^2 \sin^2\theta}{2b^2} + \frac{(3A-B)\, r^4 \sin^4\theta}{8b^4} + \ldots \tag{6.48}$$

Now introducing Eq. 6.48 into Eq. 6.46 and using the definitions of P_n, P_n^*, and P_n^{**} of Eqs. 6.4, 6.6, and 6.7, respectively, we get the final transmission formula, which includes both the obliquity effect and the intensity fall-off effect

$$T' = T + \frac{(A-B)}{2b^2} [E_1 P_1^* + E_2 P_2^* + E_m P_m^*] + \frac{(3A-B)}{8b^4} [E_1 P_1^{**} + E_2 P_2^{**} + E_m P_m^{**}] + \ldots \tag{6.49}$$

P_n, P_n^*, and P_n^{**} are determined as in previous sections.

These considerations are, of course, not needed for the work of this report since our neutron source was an isotropic emitter.

Chapter 7

DETECTOR CHARACTERISTICS

In the experimental work presented in the following chapters, three neutron threshold detectors were used: Np^{237} and U^{238} fission detectors, and an $Al^{27}(n,p)Mg^{27}$ activation detector. The theory used to evaluate the experiments has been derived by assuming an ideal step function threshold detector and energy loss on all inelastic collisions sufficient to degrade the neutron below the ideal threshold.

Since there is no guarantee that a neutron will lose sufficient energy on an inelastic collision to go below the threshold, it is necessary to think of the elastic cross section used in the analysis as containing a contribution from those inelastic processes which leave the resultant neutron with an energy above the threshold. Furthermore, the threshold detectors used in the experiments do not have ideal responses, as shown in Fig. 7.1. It would be useful, however, to designate as the effective threshold of a non-ideal detector, the threshold energy at which an ideal step function detector would give the same response to the neutron spectrum as the non-ideal threshold detector.

For a reasonably flat neutron spectrum over the energy region of interest, this point is located so that area A equals area B in Fig. 7.2. Therefore, using non-ideal threshold detectors, one measures the cross section for collisions leading to energies below the effective detector threshold, instead of measuring average total inelastic cross sections. The effective energy threshold of a Np^{237} detector, according to the above definition, is 0.7 Mev, that of a U^{238} counter is 1.4 Mev, and that of the aluminum detector is about 5.0 Mev. This choice is influenced by the fact that the fission spectrum is far from flat over the sensitive range of the Al detector.

The measured inelastic cross sections may also be interpreted in another way, in terms of a certain average over the fission neutron spectrum. This average is obtained by deriving Eq. 1.2 for a continuous neutron spectrum. The energy losses on both elastic and inelastic collisions will be considered. Macroscopic cross sections (cross sections in cm^{-1}) are used here. We define now the following quantities:

$N(E)\,dE$ = flux of neutrons between E and E + dE in the fission spectrum

$\sigma_t(E)$, $\sigma_{el}(E)$, $\sigma_{in}(E)$, $\sigma_c(E)$ = total, elastic, inelastic scattering, and capture cross sections for an element at energy E.

$\sigma^D(E)$ = detector sensitivity at energy E.

$\sigma_{el}(E \rightarrow E')\,dE'$ = cross section at energy E for producing neutrons between energies E′ and E′ + dE′ by elastic scattering.

$\sigma_{in}(E \rightarrow E')\,dE'$ = cross section at energy E for producing neutrons between energies E′ and E′ + dE′ by inelastic scattering.

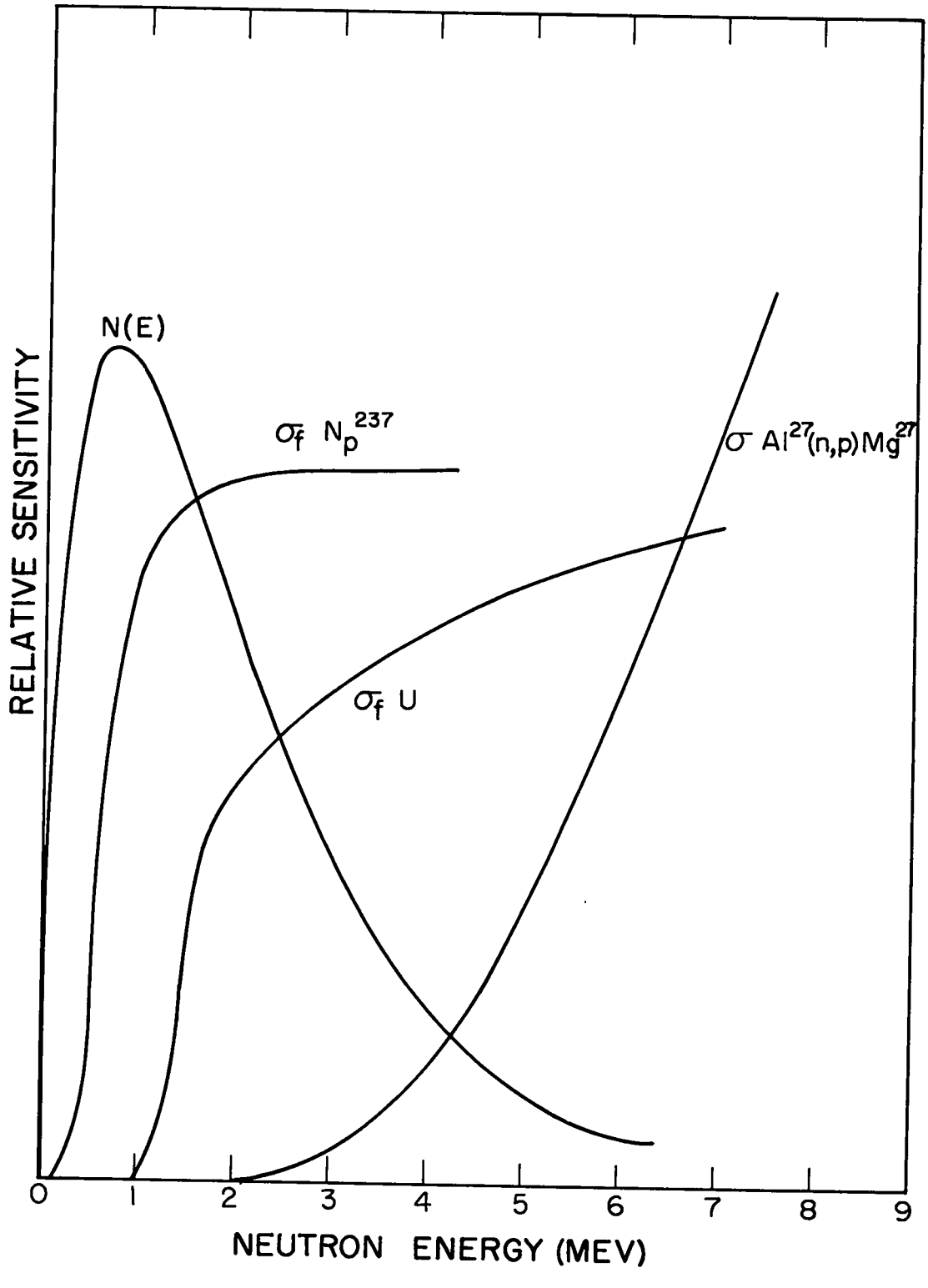

Fig. 7.1 — Relative detection sensitivities for the three threshold detectors used in the sphere transmission experiments. The general shape of the fission neutron spectrum is also shown.

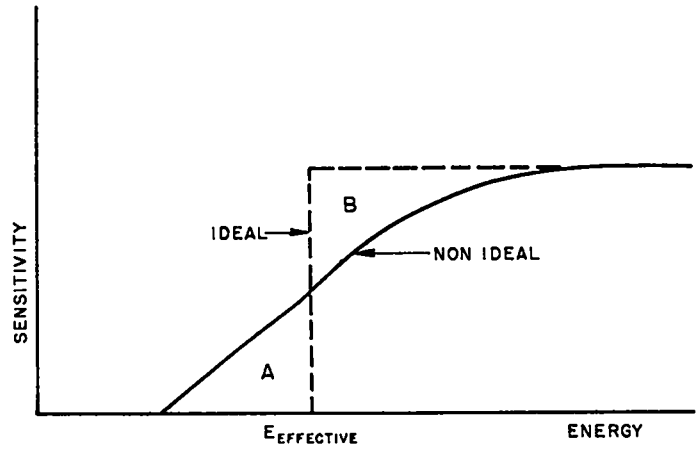

Fig. 7.2

The counting rate in the neutron detector with no sphere present is

$$\int_0^\infty N(E)\, dE\, \sigma^D(E) \tag{7.1}$$

The counting rate in the detector, in this thin shell approximation, due to neutrons that have made no collisions is

$$\int_0^\infty N(E)\, dE\, \sigma^D(E) - X \int_0^\infty N(E)\, dE\, \sigma_t(E)\, \sigma^D(E) \tag{7.2}$$

The detector response to the neutrons that have made one scattering is

$$X \int_0^\infty \int_0^E N(E)\, dE\, [\sigma_{el}(E \to E') + \sigma_{in}(E \to E')]\, dE'\, \sigma^D(E') \tag{7.3}$$

The sphere transmission to order X can be written

$$T = 1 - X(\overline{\overline{\sigma}}_{in} + \Delta\sigma) \tag{7.4}$$

where $\overline{\overline{\sigma}}_{in}$ is defined by the relation

$$\overline{\overline{\sigma}}_{in} = \frac{\int_0^\infty N(E)\, dE[\sigma_{in}(E) + \sigma_c(E)]\sigma^D(E) - \int_0^\infty \int_0^E N(E)\, dE\, \sigma_{in}(E \to E')\, dE'\, \sigma^D(E')}{\int_0^\infty N(E)\, dE\, \sigma^D(E)} \tag{7.5}$$

and

$$\Delta\sigma = \frac{\int_0^\infty N(E) dE\ \sigma_{el}(E)\, \sigma^D(E) - \int_0^\infty \int_0^E N(E)\, dE\ \sigma_{el}(E \to E')\, dE' \sigma^D(E')}{\int_0^\infty N(E)\, dE\, \sigma^D(E)} \tag{7.6}$$

Equation 7.6 is the apparent inelastic cross section due to losses of energy on elastic collisions, and is exactly the same as Eq. 6.37. Equation 7.5 is one of the ways of defining the

average inelastic cross section that we measure experimentally. This integral definition is, of course, approximate since only a thin shell analysis has been used in this discussion.

Another cross section which we use in the numerical analysis is the average total cross section

$$\overline{\overline{\sigma_t}} \equiv \frac{\int_0^\infty N(E)\, \sigma_t(E)\, \sigma^D(E)\, dE}{\int_0^\infty N(E)\, \sigma^D(E)\, dE} \tag{7.7}$$

The average elastic cross section to use then is

$$\hat{\sigma}_{el} = \overline{\sigma}_t - \overline{\sigma}_{in} \tag{7.8}$$

The proper average total cross section to use in the analysis (Eq. 7.7) was obtained either by numerical integration of Eq. 7.7 or by measuring this average directly. E. T. Jurney and C. W. Zabel performed these measurements using a beam from the Los Alamos Fast Reactor.[6,15] Angular distributions for elastic scattering used in our numerical analysis were those for elastic collisions as defined by Eq. 7.8. These angular distributions were also measured by Jurney and Zabel for the Np^{237} and U^{238} threshold detectors.[6,15] Angular distributions used in the aluminum threshold detector analysis are discussed in Chapter 13. A single set of average cross sections was used for all collisions in the shell. No hardening effects or spectrum changes were considered in the analysis, and the results of the analysis have indicated no need for considering these effects.

A method of comparing integral inelastic cross sections given in Chapters 11, 12, and 13 quantitatively with inelastic cross sections obtained with monoenergetic neutron sources, is to evaluate Eq. 7.5 numerically using the differential data. Equation 7.5 indicates that it is not correct to just average the differential data over the fission spectrum, but that the detector energy response must be included. In other words the inelastic cross section depends on an apparent spectrum shape that is given by $N(E)\, \sigma^D(E)$. These so-called spectra are shown in Fig. 7.3 for the three detectors.

Thus, in conclusion, one may think of the inelastic cross sections for fission spectrum neutrons given in this report as defined by (1) the neutron cross section for collisions leading to energies below the effective detection threshold, or (2) the neutron cross section defined by Eq. 7.5.

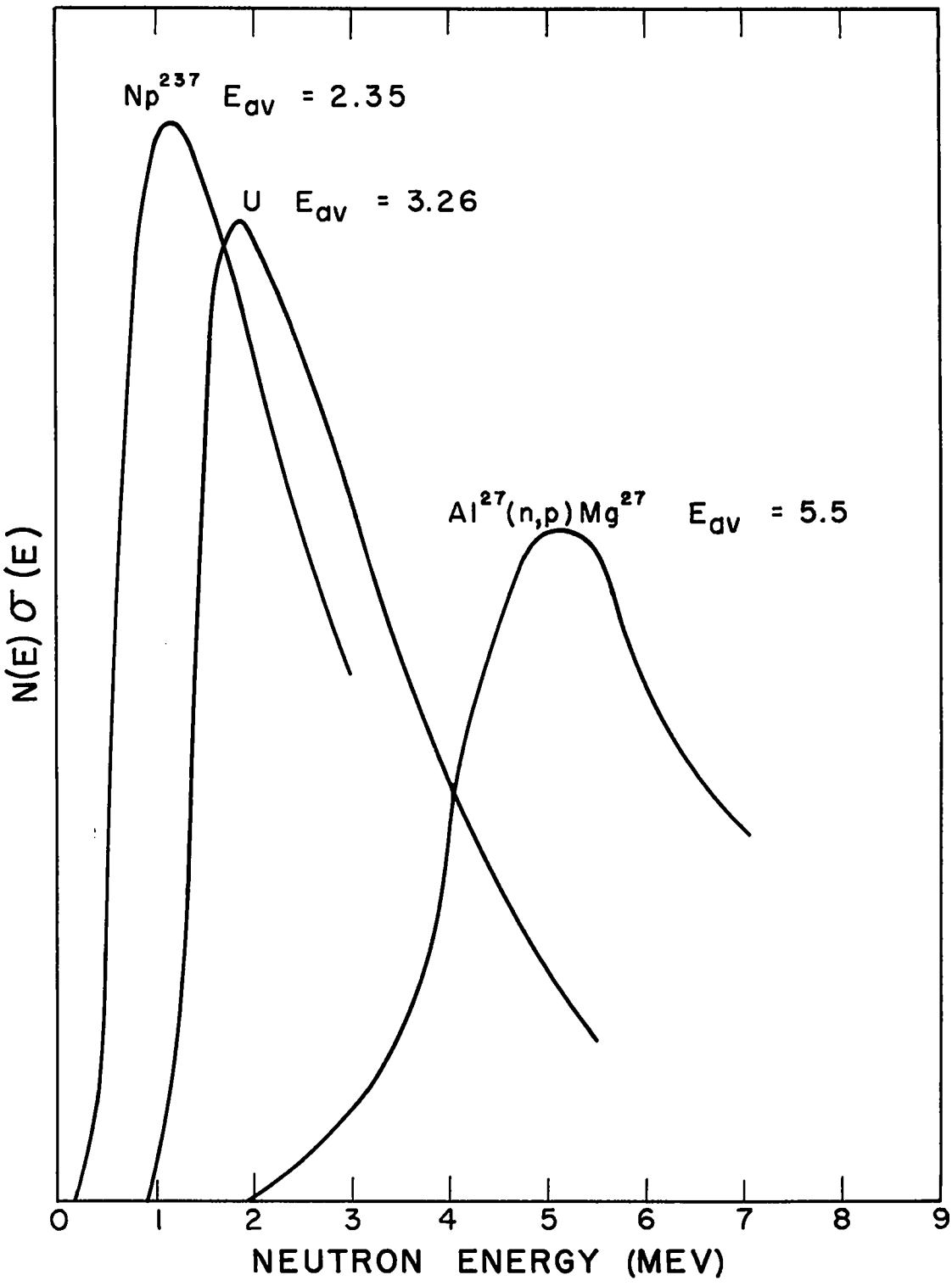

Fig. 7.3 — N(E) σ^{D}(E) curves obtained by combining the sensitivity of each neutron detector with the fission neutron spectrum.

Chapter 8

GENERAL GROUP THEORY

To study the behavior of a continuous spectrum of neutrons realistically in a material, it is very often necessary to divide the spectrum into several energy groups and to assign average cross sections to each energy group. We have until now in this report placed all neutrons in one energy group in deriving sphere transmission and correction formulas. However, the methods developed in previous chapters are adaptable to the description of many group phenomena where transfer of neutrons back and forth between groups by successive scatterings occurs.

We are, of course, interested mainly in spherical geometries with the detector inside the sphere and an external source. However, as before, the transmission equations are most easily derived for a central source and external detector. Therefore it is again necessary to test the validity of the reciprocity theorem. Unfortunately, the reciprocity theorem (source-detector interchange) does not hold unless one makes certain changes in the formulas derived with source inside of the sphere. We will first show what those changes have to be.

8.1 Reciprocity Conditions

As nearly as possible, we will follow the proof of the reciprocity theorem given in LA-1428.[1] However, in that report it was assumed that elastic scattering did not change the energy of the neutron and that inelastic scattering rendered the neutron undetectable. The second assumption is not made in the generalized group treatment in this section. Unfortunately, some of the parameters will be designated by slightly different symbols here to conform with nomenclature in this report. In this report, r_1 and r_2 are the inner and outer radii of the scattering shell and r the radius of an arbitrary point in the shell. σ_i^t is the total cross section measured in cm^{-1} in energy group i. $\sigma_i(\theta)\, d\omega$ is the elastic scattering cross section into solid angle $d\omega$ for neutrons in energy group i. $\sigma_{ij}(\theta)\, d\omega$ is the inelastic scattering cross section into solid angle $d\omega$ for events that remove neutrons from energy group i and furnish these same neutrons to energy group j.

We will consider a neutron source at the center of the sphere with a probability of emission into energy group i of P_i^S and treat two successive inelastic scatterings followed by escape from the shell. The first inelastic collision occurs in arbitrary volume element dV_1 and the second in dV_2 (see Fig. 8.1). On the first inelastic collision the neutron changes from group i to group j, and on the second from group j to group k. After escaping from the sphere, the neutrons in energy group k hit an isotropic detector of area A_d, thickness T_d, and detection sensitivity per unit volume of P_k^D at distance b from the sphere center. P_k^D is, of course, proportional to σ^D, used in Section 6.5 and Chapter 7.

Assuming that the first scattering volume has an area dA_1, and a thickness $dT_1 = dV_1/dA_1$, the number of source neutrons in energy group i hitting it is

$$\frac{P_i^S\, dA_1}{4\pi\, r_{01}^2}\, e^{-\sigma_i^t X_1} \tag{8.1}$$

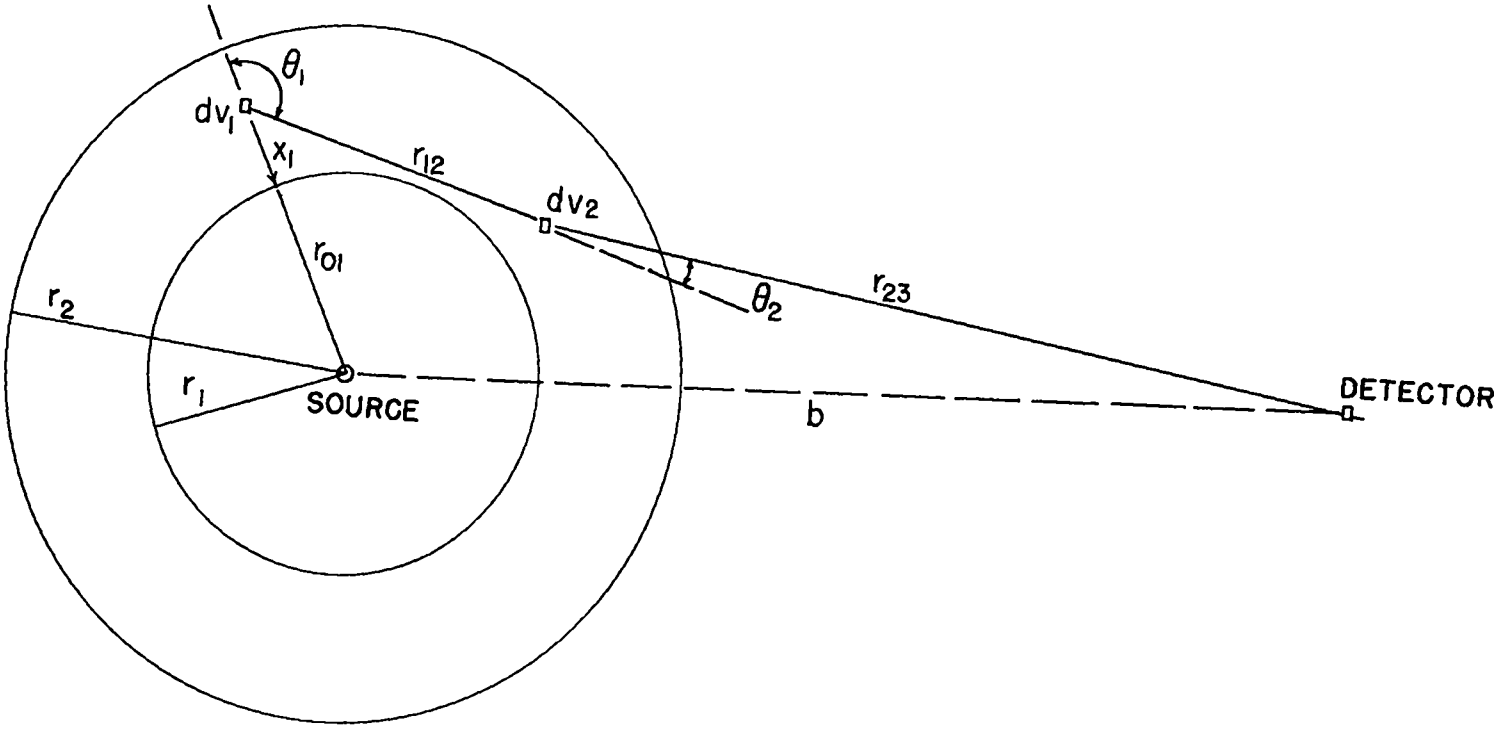

Fig. 8.1—Geometry used for discussion of reciprocity conditions for multi-group analysis.

where r_{01} is the distance of dV_1 from the sphere center, and X_1 is the distance actually traveled through the shell material. The fraction of expression 8.1 which is inelastically scattered at dV_1 from group i to group j through angle θ into solid angle $d\omega_1$ is

$$\sigma_{ij}(\theta)\, dT_1\, d\omega_1$$

Thus the number of neutrons scattered into solid angle $d\omega_1$, at the same time changing energy group from i to j, is

$$\frac{P_i^S\, dV_1\, e^{-\sigma_i^t X_1}\, \sigma_{ij}(\theta)\, d\omega_1}{4\pi\, r_{01}^2} \tag{8.2}$$

The second scattering volume of area dA_2 and thickness dT_2 subtends at dV_1 the solid angle

$$d\omega_1 = \frac{dA_2}{r_{12}^2} \tag{8.3}$$

where r_{12} is the distance between dV_1 and dV_2. The number of neutrons hitting dA_2 is given by Eq. 8.2, using Eq. 8.3, and multiplied by an attenuation factor

$$e^{-\sigma_j^t X_{12}} \tag{8.4}$$

where X_{12} is the distance traveled through material from dV_1 to dV_2. The scattering probability through an angle θ_2 into $d\omega_2$ and from energy group j to group k is $\sigma_{jk}(\theta_2)\, d\omega_2\, dT_2$. The absolute number scattered, as discussed above, is

$$\frac{P_i^S\, dV_1}{4\pi\, r_{01}^2}\, e^{-\sigma_i^t X_1}\, \sigma_{ij}(\theta_1)\, \frac{dV_2}{r_{12}^2}\, e^{-\sigma_j^t X_{12}}\, \sigma_{jk}(\theta_2)\, d\omega_2 \tag{8.5}$$

Now the detector subtends at dV_2 the solid angle

$$d\omega_2 = \frac{A_d}{r_{23}^2} \tag{8.6}$$

where r_{23} is the distance from dV_2 to the detector. The detector will count the fraction $T_d\, P_k^D$ of the neutrons incident upon it. Therefore the number of neutrons detected is

$$D_{12} = \frac{P_i^S\, dV_1}{4\pi\, r_{01}^2}\, e^{-\sigma_i^t X_1}\, \sigma_{ij}(\theta_1)\, \frac{dV_2}{r_{12}^2}\, e^{-\sigma_j^t X_{12}}\, \sigma_{jk}(\theta_2)\, \frac{V_d}{r_{23}^2}\, P_k^D\, e^{-\sigma_k^t X_{23}} \tag{8.7}$$

If the shell is removed, the counts in the detector would be

$$D_0 = \frac{\sum_{i=0}^{n} P_i^S\, P_i^D\, V_d}{4\pi b^2} \tag{8.8}$$

and the contribution to the shell transmission due to D_{12} is D_{12}/D_0.

Now let us consider the inverse problem with the source outside the sphere. We would like to place the source outside the sphere, but subject to the condition that we get the same sphere transmission or that the term D_{12}/D_0 is given by the same expression as above. However, now the problem is more involved, since if we start with group i neutrons outside and retrace the chosen path between source and detector, we do not get the same expression. For example, $\sigma_{ij}(\theta_2)$ occurs instead of $\sigma_{jk}(\theta_2)$ and the exponentials have incorrect total cross sections. In spite of these differences, we shall show that if one postulates three things it will be possible to obtain the desired expression for the term D_{12}/D_0 with an external source:

1. The probability of detection of group i neutrons when the detector is outside is the probability of emission of group i neutrons when the source is outside.

2. The probability of emission of group i neutrons with the source inside is the probability of detection of group i neutrons with the detector inside.

3. If $\sigma_{ij}(\theta)$ is the transfer cross section of neutrons from group i to group j and $\sigma_{ji}(\theta)$ that from group j to i with the source inside the sphere, then $\sigma_{ji}(\theta)$ is the transfer cross section from i to j and $\sigma_{ij}(\theta)$ is that from j to i when the source is outside.*

Using this method, let us retrace the arbitrary path through the shell, starting with group k neutrons outside the sphere. The number of source neutrons hitting dV_2 is now

$$\frac{P_k^D \, dA_2 \, e^{-\sigma_k^t X_{23}}}{4\pi \, r_{23}^2}$$

The number of those scattered at dV_2 from group k to group j which hit dV_1 is

$$\frac{P_k^D \, dV_2}{4\pi \, r_{23}^2} e^{-\sigma_k^t X_{23}} \sigma_{jk}(\theta_2) \frac{dA_1}{r_{12}^2} e^{-\sigma_j^t X_{12}} \tag{8.9}$$

where we have used condition 3 for $\sigma_{jk}(\theta_2)$. The number detected by the central detector is

$$D_{21} = \frac{P_k^D \, dV_2}{4\pi \, r_{23}^2} e^{-\sigma_k^t X_{23}} \sigma_{jk}(\theta_2) \frac{dV_1}{r_{12}^2} e^{-\sigma_j^t X_{12}} \sigma_{ij}(\theta_1) \frac{V_s P_i^S}{r_{01}^2} e^{-\sigma_i^t X_1} \tag{8.10}$$

where V_s is the volume of the original source inside the sphere and P_i^S is the sensitivity per unit volume. The counting rate with the sphere removed is

$$D_0' = \frac{\sum_{k=0}^{n} P_k^D \, P_k^S \, V_s}{4\pi b^2} \tag{8.11}$$

It is clear then that

$$\frac{D_{12}}{D_0} = \frac{D_{21}}{D_0'} \tag{8.12}$$

It is, therefore, possible to do an experiment with the neutron source outside the sphere and to do the group multiple scattering analysis by putting the source inside the sphere, if the source and detector used in the analysis have the characteristics given in conditions 1 and 2 above, and if one also satisfies condition 3 concerning the group transfer cross sections. Of course, there was no mention of these conditions when we were only concerned with elastic scatterings, as in LA-1428.[1] The reciprocity theorem for the elastic scattering case can be proved, either using the three conditions or not using them.

8.2 Group Formulation

The purpose of this section is to derive general formulas for use in determining average transfer cross sections between energy groups. Using a central neutron source, the expression for the number of neutrons escaping from a spherical shell in energy group i, the measurable quantity q_i, will be formulated in terms of average group transfer coefficients and known group cross sections. We will consider i_0 energy group. The highest energy group will be denoted by the highest group number. The fraction of the neutrons from the central source

*The third condition was originally suggested to us by Bengt G. Carlson of LASL.

in energy group i is ϕ_i. Ψ_i^n is the flux of group i neutrons that have suffered n collisions, integrated over the shell volume. σ_i^{tr}, σ_i^{et}, σ_i^f, σ_i^c, and σ_i^{in} are the transport, elastic transport, fission, capture, and inelastic scattering cross sections, respectively, for energy group i. We are assuming, for generality, that the substance of the shell is fissionable, in addition to having inelastic and elastic scattering. ν_i is the number of neutrons for each fission produced by a neutron in group i, and σ_{ji} is the cross section for transferring neutrons from group j to group i by inelastic collisions. The fraction of the fission neutron spectrum in energy group i is f_i. Then the number of n + 1 collisions for neutrons in energy group i is $\Psi_i^n \sigma_i^{tr}$.

The number of neutrons of group i produced in the n + 1 collisions is

$$S_i^{n+1} = \Psi_i^n \sigma_i^{et} + \sum_{j>i}^{i_0} \Psi_j^n \sigma_{ji} + \sum_{j=1}^{i_0} \Psi_j^n \sigma_j^f \nu_j f_i \tag{8.13}$$

We shall rewrite S_i^{n+1} as follows

$$S_i^{n+1} = \sum_{j=1}^{i_0} C_{ji} \Psi_j^n \tag{8.14}$$

where

$$C_{ji} = \sigma_j^{et} \delta_{ji} + \sigma_{ji} + \sigma_j^f \nu_j f_i \tag{8.15}$$

Of course, $\sigma_{ji} = 0$ for $j < i$.

The number of neutrons of group i which stay in the shell after the n + 1 collision is $S_i^{n+1}(1 - P_i)$. This is also the number of n + 2 collisions for group i neutrons. Therefore

$$S_i^{n+1}(1 - P_i) = \Psi_i^{n+1} \sigma_i^{tr} \tag{8.16}$$

The same escape probability will be used in this analysis after every collision for energy group i. This is a highly desirable simplification and introduces very little error, as discussed in Section 5.4. Indeed, this simplification makes it possible to sum Eq. 8.16 over all collisions, which gives the more useful equation

$$\sigma_i^{tr} \sum_{n=0}^{\infty} \Psi_i^{n+1} = (1 - P_i) \sum_{n=0}^{\infty} S_i^{n+1} \tag{8.17}$$

Or, using Eq. 8.14

$$\sigma_i^{tr} \sum_{n=0}^{\infty} \Psi_i^{n+1} = (1 - P_i) \sum_{n=0}^{\infty} \sum_{j=1}^{i_0} C_{ji} \Psi_j^n \tag{8.18}$$

We now introduce a quantity Ψ_i, which is the total flux of neutrons of energy group i in the shell

$$\Psi_i = \sum_{n=0}^{\infty} \Psi_i^n \tag{8.19}$$

Rewriting Eq. 8.18

$$\sigma_i^{tr} (\Psi_i - \Psi_i^0) = (1 - P_i) \sum_{j=1}^{i_0} C_{ji} \Psi_j \tag{8.20}$$

This is essentially the desired equation, relating the total fluxes Ψ_i to each other and to Ψ_i^0. We can find Ψ_i^0 since we know the total number of first collisions, namely

$$\sigma_i^{tr} \Psi_i^0 = \phi_i (1 - e^{-\sigma_i^{tr} X}) \tag{8.21}$$

The purpose of the multi-group analysis is, of course, to find C_{ji}, the transfer cross sections between groups. This can be done from Eq. 8.20 if we know Ψ_i. The directly measurable quantity is q_i, the number of neutrons in energy group i escaping from the shell. Thus we must obtain Ψ_i from q_i. It is easily seen that

$$q_i = \phi_i e^{-\sigma_i^{tr} X} + P_i \sum_{n=0}^{\infty} S_i^{n+1} \tag{8.22}$$

From Eqs. 8.17 and 8.19

$$\sum_{n=0}^{\infty} S_i^{n+1} = \frac{\sigma_i^{tr}(\Psi_i - \Psi_i^0)}{(1 - P_i)} \tag{8.23}$$

Inserting Eq. 8.23 in Eq. 8.22, we obtain

$$\sigma_i^{tr}\Psi_i = \phi_i(1 - e^{-\sigma_i^{tr} X}) + \frac{(1 - P_i)}{P_i}(q_i - \phi_i e^{-\sigma_i^{tr} X}) \tag{8.24}$$

This is the desired equation, giving Ψ_i in terms of the measured quantity q_i and other known quantities.

8.3 A Conservation Theorem

Unfortunately, the Ψ_i do not give us sufficient information to solve Eq. 8.20 for the C_{ji}. In fact, there are only i_0 equations 8.20, one for each i, while there are altogether i_0^2 unknown coefficients C_{ji}. The situation could be changed by doing the measurement not only with one source, but with i_0 different sources having different spectra ϕ_i. If, for instance, each source emitted only neutrons of one group, it is clear that we would have enough information to determine all the C_{ji}. Unfortunately, at least in our experiments, we had only one source available, the fission source.

On the other hand, the C_{ji} are not entirely unknown. Going back to their definition, Eq. 8.15, we may assume that we know the fission cross section σ_j^f, the number of neutrons per fission, ν_j, and the fission spectrum f_i. Furthermore, we may assume that we know the total cross section σ_j^t and $\sigma_j^{et}/\sigma_j^{el}$. Hence, if we know all inelastic cross sections σ_{ji}, we also know σ_j^{el} and therefore σ_j^{et}. This means that the unknowns are really only the inelastic cross sections σ_{ji}, which are $i_0(i_0 - 1)/2$ in number. We shall do all our analyses with three groups, $i_0 = 3$, and in this case the number of σ_{ji} values is also three, so that it seems that we have sufficient information to determine all of the unknowns from the three values of Ψ_i measured with a given source.

However, this is not so because there is a linear relation between the Ψ_i which is always fulfilled. This is most easily seen for a material which has neither capture nor fission. Then the total number of neutrons emerging must be equal to the total number of source neutrons, in other words

$$\sum_{i=1}^{i_0} q_i = \sum_{i=1}^{i_0} \phi_i$$

This means, for example, that q_1 can be predicted once all the other q_i (from $i = 2$ to i_0) have been measured. Thus, the measurement of q_1 does not give any further information, but merely a check on the other measurements. The number of independent pieces of information is $i_0 - 1$, not i_0, and in particular, when we use three groups, we have only two sets of experimental data. One of the three inelastic cross sections σ_{ji} will, therefore, remain undetermined.

Similarly, if the material captures neutrons, then the total number of emitted neutrons Σq_i will determine the average capture cross section σ^c of the sphere material for the neutron spectrum. If the material also undergoes fission, the quantity determined will be the average of $\sigma^f(\nu - 1) - \sigma^c$. To show this explicitly, divide Eq. 8.20 by $1 - P_i$ and sum over i. Then the inelastic cross sections σ_{ji} combine to form $\sum_i \sigma_{ji} = \sigma_j^{in}$. Using Eq. 8.15 and the definition

$$\sigma_j^{tr} = \sigma_j^{et} + \sigma_j^c + \sigma_j^f + \sigma_j^{in} \tag{8.25}$$

We obtain then

$$\sum_{i=1}^{i_0} \frac{\sigma_i^{tr}}{(1-P_i)} (\Psi_i - \Psi_i^0) = \sum_{j=1}^{i_0} [\sigma_j^{tr} + \sigma_j^f(\nu_j - 1) - \sigma_j^c]\Psi_j \tag{8.26}$$

It will be seen that the inelastic scattering has cancelled out. Combining the terms $\sigma_i^{tr}\Psi_i$ on both sides of the equation, we may then use Eq. 8.24 for this quantity and Eq. 8.21 for Ψ_i^0. After some algebra we obtain

$$\sum_{i=1}^{i_0} [\sigma_i^f (\nu_i - 1) - \sigma_i^c]\Psi_i = \sum_{i=1}^{i_0} q_i - \sum_{i=1}^{i_0} \phi_i \tag{8.27}$$

On the right hand side is the difference between the total number of neutrons emerging from the sphere and the total number of source neutrons. On the left is the quantity $\sigma^f(\nu - 1) - \sigma^c$, averaged with the "measured" fluxes Ψ_i (Eq. 8.24) as statistical weights. Equation 8.27 gives a very accurate means of determining the average of $\sigma^f(\nu - 1) - \sigma^c$, or of the capture cross section σ^c alone for non-fissionable materials. The accuracy depends, of course, on one's ability to measure Σq_i precisely; i.e., on the availability of a detector whose response is truly "flat" as a function of energy.

8.4 Determination of Group Constants by Variation of Shell Thickness

The discussion of the preceding section leaves unsolved the problem of determining the three inelastic cross sections σ_{32}, σ_{31}, and σ_{21} (if we decide to use three groups). Of course, if one of these three can be determined from other information, then the remaining two can be found from Eq. 8.20 — in fact from two of the three substitutions in Eq. 8.20 since the third yields Eq. 8.27.

If we have no other such information, and if we have only one primary neutron spectrum available, then the only possibility is to try to moderate that spectrum by using shells of different thickness. As the shell thickness increases, we may expect that the number of neutrons in energy group 3, the highest energy group, will decrease relative to that in the two lower groups. There are two reasons for this: (a) both the lower groups receive neutrons in addition to losing them, and (b) the inelastic cross section is usually largest in the highest energy group (see Chapters 11 to 14).

The increase of the population of group 1 is unimportant since no inelastic scattering starts from this group, but the relative increase of group 2 means that a measurement at large thickness weights σ_2^{in} more than σ_3^{in}. Since the neutron spectrum does not change rapidly with thickness, this method does not permit a very accurate determination of the three inelastic cross sections, but still, if we are satisfied with fairly wide limits, a determination of all three is possible. This method was used to determine the σ_{ji} for some non-fissionable elements; the results are given in Chapter 14.

We shall now derive the necessary formulas for this analysis. The experiments were done with an external fission neutron source, and detector inside the sphere. Since we wish to use our previous calculations of escape probabilities, we must employ the reciprocity theorem of Section 8.1 and the conditions 1, 2, and 3 stated in that section. We shall be interested in the transfer from energy group 3 to 2, σ_{32}. Condition 3 now states that the transfer cross section between groups 3 and 2, σ_{32}, is to be called that between 2 and 3. Condition 2 specifies that the fictitious neutron source inside the sphere must have a group emission probability equal to the actual detector group response.

Two detectors were used for this work. The first ("28" or U^{238} detector) detected only in group 3, and the other ("37" or Np^{237} detector) in both groups 2 and 3, with relative efficiencies of P_2^{37} and P_3^{37} for the two groups. To conform with condition 2, we must, therefore, consider two neutron sources, one emitting only group 3 neutrons and the other both group 2 and group 3 neutrons, with probabilities proportional to P_2^{37} and P_3^{37}.

The sphere transmission measured with the "28" counter, group 3 source, is, of course, the same as Eq. 3.37. With the two-group neutron source, Eq. 8.20 gives

$$\sigma_3^{tr}(\Psi_3 - \Psi_3^0) = (1 - P_3)(\sigma_3^{et}\Psi_3 + \sigma_{32}\Psi_2) \tag{8.28}$$

and

$$\sigma_2^{tr}(\Psi_2 - \Psi_2^0) = (1 - P_2)\,\sigma_2^{et}\Psi_2 \tag{8.29}$$

For the integrated flux in group 2, we obtain from Eq. 8.29

$$\Psi_2 = \frac{\sigma_2^{tr}\Psi_2^0}{(\sigma_2^{in} + \sigma_2^c + \sigma_2^{et}P_2)} \tag{8.30}$$

The number of neutrons escaping in group 2 is given by

$$q_2 = P_2^{37}\, e^{-\sigma_2^n X} + \frac{P_2^{37}P_2\,(1 - e^{-\sigma_2^n X})\sigma_2^{et}}{(\sigma_2^{in} + \sigma_2^c + \sigma_2^{et}P_2)} \tag{8.31}$$

The integrated flux in group 3 is, from Eqs. 8.28 and 8.30

$$\Psi_3 = \frac{\sigma_3^{tr}\Psi_3^0}{(\sigma_3^{in} + \sigma_3^c + \sigma_3^{et}P_3)} + \frac{(1 - P_3)\,\sigma_{32}\sigma_2^{tr}\Psi_2^0}{(\sigma_2^{in} + \sigma_2^c + \sigma_2^{et}P_2)(\sigma_3^{in} + \sigma_3^c + \sigma_3^{et}P_3)} \tag{8.32}$$

The number of neutrons escaping in group 3 is now

$$q_3 = P_3^{37}\, e^{-\sigma_3^n X} + P_3(\Psi_3\sigma_3^{et} + \Psi_2\sigma_{32}) \tag{8.33}$$

Or introducing Eqs. 8.30 and 8.32, we get

$$q_3 = P_3^{37}\left[e^{-\sigma_3^n X} + \frac{(1 - e^{-\sigma_3^n X})\,\sigma_3^{et}P_3}{(\sigma_3^{in} + \sigma_3^c + \sigma_3^{et}P_3)}\right] + \frac{P_2^{37}(1 - e^{-\sigma_2^n X})\,\sigma_{32}\sigma_2^{tr}P_3}{(\sigma_2^{in} + \sigma_2^c + \sigma_2^{et}P_2)(\sigma_3^{in} + \sigma_3^c + \sigma_3^{et}P_3)} \tag{8.34}$$

The transmission with the "37" counter is given by

$$T_{37} = \frac{q_2 f_2 + q_3 f_3}{f_2 P_2^{37} + f_3 P_3^{37}} \tag{8.35}$$

where f_2 and f_3 are the probabilities of fission spectrum neutrons being in groups 2 and 3, respectively, which in the "reciprocal" problem is the detector response in those two groups.

Now that Eq. 8.35 is derived, we may forget the reciprocity theorem and describe how the equation is to be used in analyzing experiments. The experimental information (for a given shell thickness) consists of the transmissions measured with a "28" and a "37" counter. From the "28" transmission, we obtain the group 3 constants, using the analysis of Chapter 3. In Eq. 8.35, we must insert q_2 from Eq. 8.31 and q_3 from Eq. 8.34. The resulting equation contains the known distribution of fission spectrum neutrons f_2 and f_3, the known relative efficiency of the "37" counter for neutrons of groups 2 and 3, P_2^{37} and P_3^{37}, the known group 3 constants σ_3^{tr} and $\sigma_3^{in} + \sigma_3^c$, and finally the two unknowns σ_{32} and $\sigma_2^{in} + \sigma_2^c$ (σ_2^{tr} follows from the measured σ_2^t and $\sigma_2^{et}/\sigma_2^{el}$, once $\sigma_2^{in} + \sigma_2^c$ is known, as given by Section 3.5). From a given measurement, we can therefore obtain only a relation between σ_{32} and $\sigma_2^{in} + \sigma_2^c$.

In practice, we allow σ_{32} to take several values between zero and σ_3^{in} (fixed by the "28" counter analysis) and plot a curve of the resulting $\sigma_2^{in} + \sigma_2^c$ vs σ_{32}.

For each shell thickness we get a different slope for this curve, which is almost a straight line. Thus, if all measurements were infinitely precise, we should obtain an intersection of all the curves of $\sigma_2^{in} + \sigma_2^c$ vs σ_{32} corresponding to different shell thicknesses, and this would represent the correct cross sections. In practice, the various curves are nearly

parallel, and not very precise, so that their intersection cannot be obtained very accurately. This is illustrated in Chapter 14 by the application of these methods to actual measurements.

8.5 An Approximate Relation Between Cross Sections

In Chapter 12 it is shown that it is possible to deduce consistent one-group cross sections from the "37" counter measurements that are independent of shell thickness. This result is rather surprising in view of the fact that group 2 neutrons increase at the expense of group 3 as the shell thickness increases, and the inelastic scattering for the two groups is very different. In fact, we can explain the result only if there is an approximate relation between the various inelastic cross sections. To obtain this relation, we note that the cross section for removal of neutrons from group 2 is $\sigma_2^{in} + \sigma_2^c$. The effective cross section for removing from the "37" counter counts that are due to group 3 neutrons, is

$$\sigma_3^{eff} = \sigma_{31} + \sigma_{32}\left(1 - \frac{\sigma_2^{37}}{\sigma_3^{37}}\right) + \sigma_3^c \tag{8.36}$$

where σ_2^{37} and σ_3^{37} are the detection cross sections of the "37" counter for groups 2 and 3.

Since the experiments tell us that the neutron removal cross section as measured by a "37" counter is apparently independent of the spectrum of neutrons in the shell (i.e., of the fraction of group 2 and group 3 neutrons present), the removal cross sections σ_3^{eff} and $\sigma_2^{in} + \sigma_2^c$ must be approximately equal, i.e.

$$\sigma_2^c + \sigma_2^{in} = \sigma_{31} + \sigma_{32}\left(1 - \frac{\sigma_2^{37}}{\sigma_3^{37}}\right) + \sigma_3^c \tag{8.37}$$

It should be emphasized once more that this equation is only approximate because the fact that the inelastic cross section as measured with a "37" counter is independent of shell thickness, can only be established crudely. The analysis using Eq. 8.35 for various shell thicknesses is more reliable.

Chapter 9

EXPERIMENTAL ARRANGEMENTS

9.1 Reactor Facilities

A schematic diagram and typical photographs of the experimental set-up at the "Water Boiler" reactor[11] are given in Figs. 9.1, 9.2, and 9.3. The large cavity in the graphite thermal column provides an external thermal neutron flux of relatively high intensity and cadmium ratio. The internal tapered paraffin blocks reduce the number of escaping fast neutrons. Both internal and external collimators are made of materials which either produce low-energy capture γ rays, or have low thermal neutron capture cross sections. Cadmium, in particular, was avoided wherever the thermal neutron flux was high. This is because the photo-fission cross sections of the detectors are not zero for the high-energy capture γ rays emitted by cadmium. Experimental checks on this point are described in Section 10.6.

The thermal neutrons irradiated a plate of U^{235}, producing a fission spectrum[12] source of about 2×10^{10} neutrons per second. The uranium was covered on the outside by a thin sandwich of aluminum and boron[10]. This had two functions: (1) to attenuate the thermal neutrons which passed through the uranium plate, and (2) to prevent scattered thermal neutrons from entering the uranium plate from the room and causing fission. It was calculated that less than 2 percent of the fast source neutrons suffered collisions in the uranium and aluminum–boron cover plate before escaping. The last 10 inches of collimator, onto which the source plate was fastened, was a thin aluminum box containing boron[10] (Fig. 9.2). Not more than about 1 percent of the neutrons reaching the detector resulted from single scattering in this collimator. The scattering from the floor and reactor face is discussed in Section 10.2.

The thermal column used for this work is provided with a boron "curtain" which can be lowered easily to decrease the neutron flux by a factor of about 500. This curtain was lowered when personnel entered the reactor room.

The fast neutron detectors were held in position by a system of clamps and stands which were completely independent of the sphere supports. The spheres were held by an aluminum cone, supported on a thin aluminum vertical tube, and braced at right angles by aluminum tubes. A discussion of the scattering by supports is in Section 10.3.

The source-to-counter distance was measured from the midpoint of the uranium plate to the middle of the detector, and was accurate to about $\frac{1}{16}$ inch. The detector was centered in the sphere to about $\frac{1}{32}$ inch.

9.2 Monitor Systems and Reactor Stability

Two independent neutron monitors were inserted into the side of the thermal column (Fig. 9.1). One was a spiral fission counter[13] containing U^{235}. The slope of its counting rate

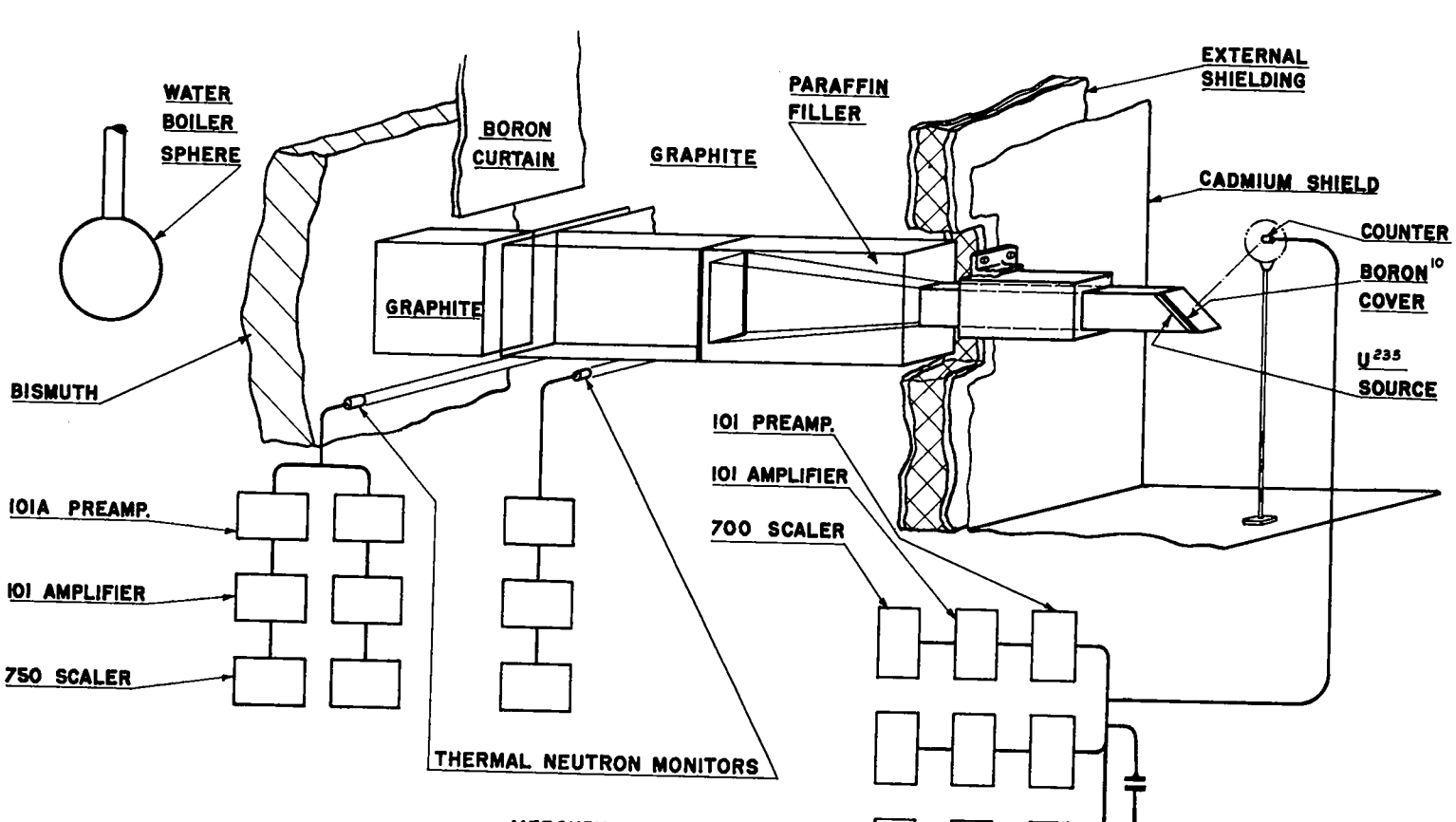

Fig. 9.1—Schematic drawing of "Water Boiler" and the experimental arrangement.

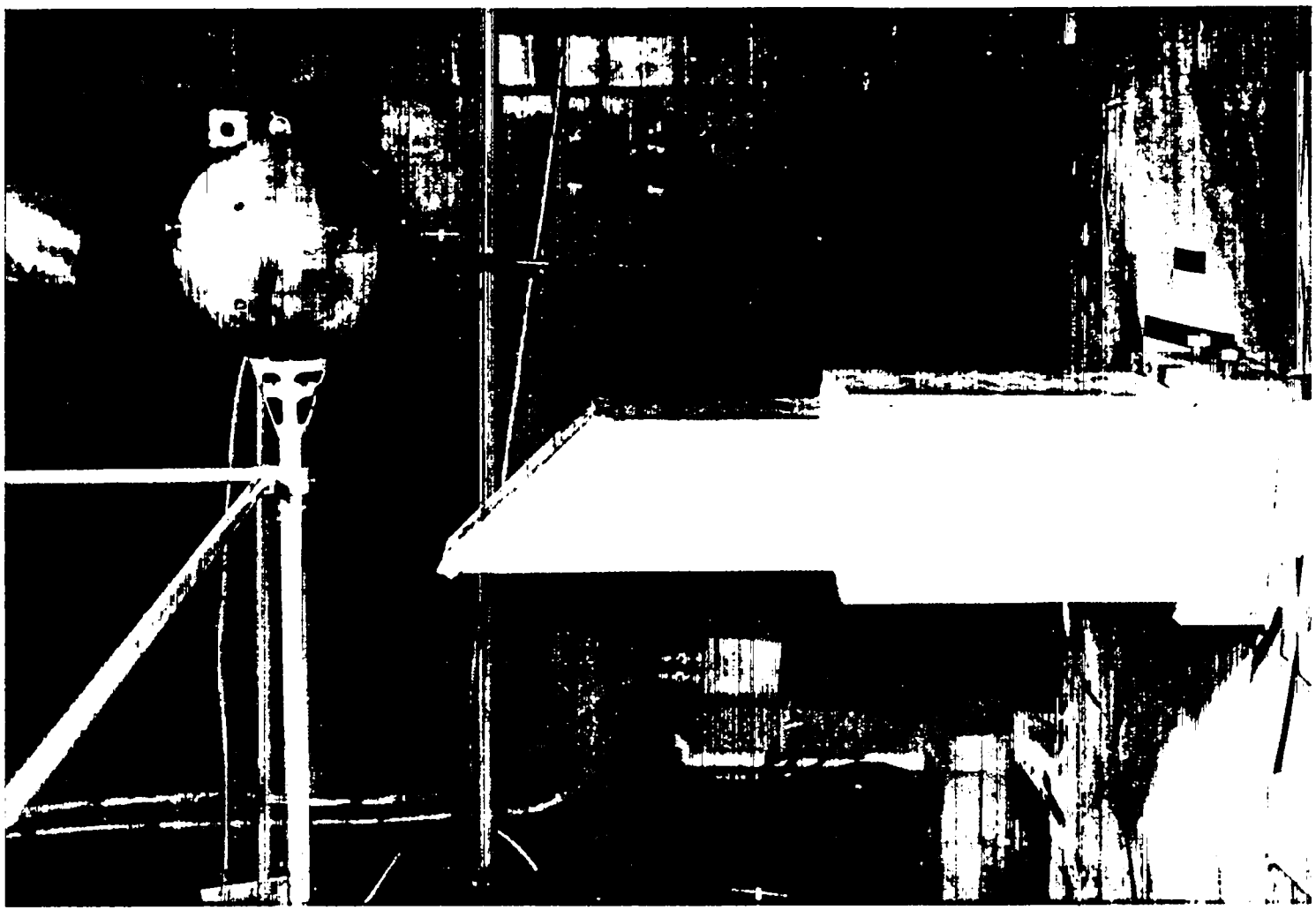

Fig. 9.2—External collimator with source and a typical 8 inch outside diameter sphere on its supporting cone.

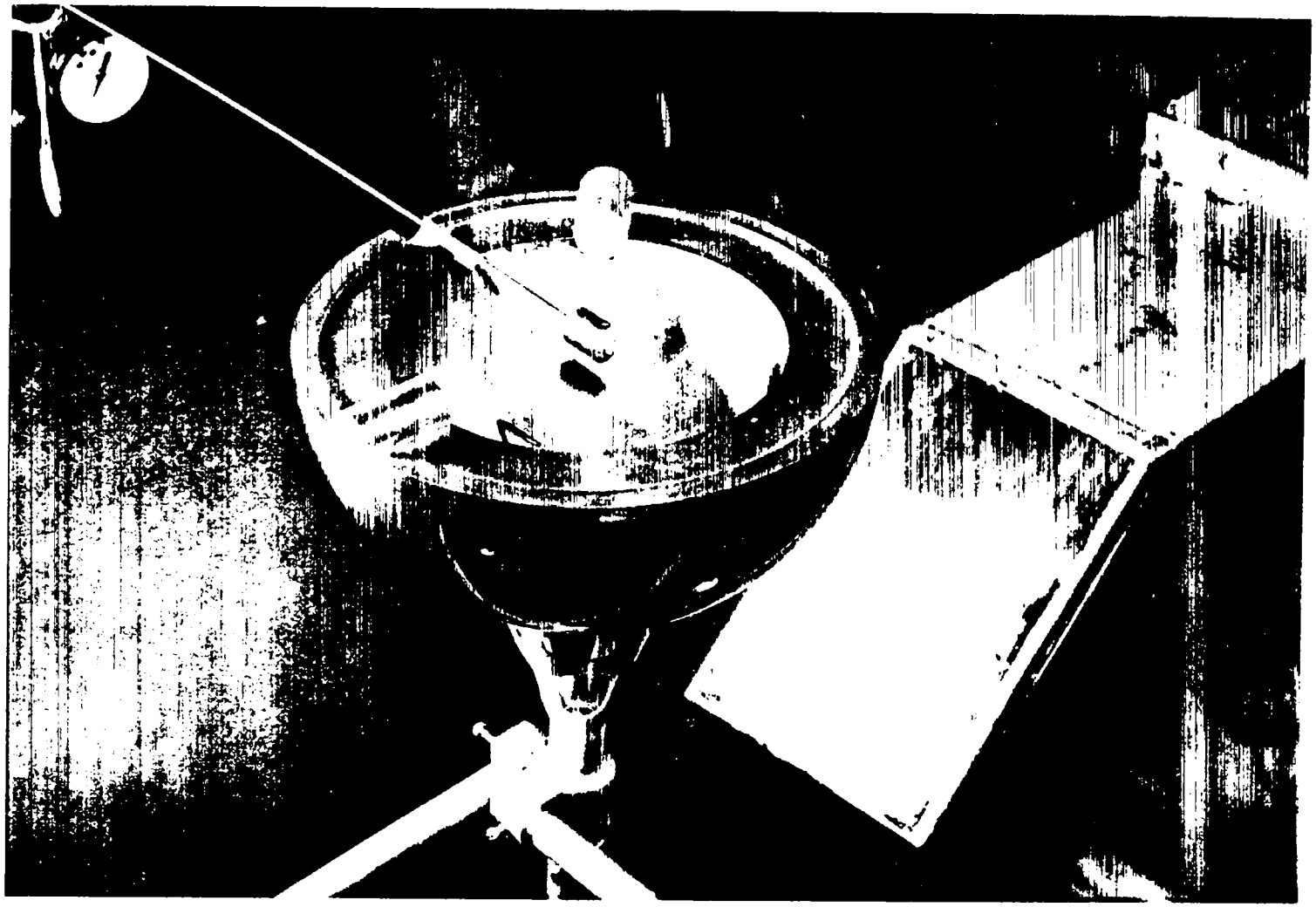

Fig. 9.3—Source plate and a spiral counter in position at the center of a hemisphere.

vs bias curve was about 0.2 percent per volt, for about 25 volts. The electronic circuits for this counter were duplicate systems, housed in a thermostated cabinet.

The second monitor also contained U^{235}, and the slope of its counting rate vs bias curve was about 0.1 percent per volt for about 60 volts. The positions in the column of these two monitors were arranged so that their counting rates were approximately equal, and about 10 to 100 times the counting rates of threshold detectors. The monitor counts were always used to normalize the data.

With these monitors, incidentally, the flux from the "Water Boiler" was found to be constant to about 0.2 percent over periods of the order of an hour or two. These were the lengths of time involved in making a single transmission measurement.

9.3 Spiral Counter System

9.3.1 Counters and Electronics

In order to obtain sufficient sensitivity in the fission threshold detectors, spiral counters were used (Fig. 9.3). If the fissionable material is thicker than a few tenths of a milligram per square centimeter, the counting rate will generally be a rapid function of the discriminator setting. This was the case for the counters used in these experiments, the counting rates changing a few percent per volt change in bias. To obtain accuracies of the order of 0.1 percent, therefore, required electronics stability of the order of a few hundredths of a volt.

Some of the things which were done to the electronic counting systems to promote reliability and convenience are listed below.

1. A special service transformer isolated the electronics circuits from the commercial power line.
2. Line filters and Sorenson voltage regulators were used on all circuits.
3. All circuits were housed in closed cabinets, thermostated to ±2°C.
4. Some questionable components in the circuits were replaced. Principally, the one-turn discriminator potentiometers were replaced by heliopots in the Model 700 and 750 scalers.
5. The electronic circuits on the threshold detector were in triplicate, from preamplifier through scaler.
6. Care was taken to avoid grounding the detector, except through the cable shields connecting to the main amplifier chassis.
7. The sensitivity of the detectors to the collecting voltage was checked at different gain settings.
8. The amplifier noise and preamplifier noise were periodically examined on an oscilloscope.
9. A thermostated Los Alamos Model 500 pulser was used between runs to check overall gains through a 1 $\mu\mu$f capacitor.
10. Most of the vacuum tubes were checked before each running period.
11. The circuits were normally left on, so that temperature equilibrium was established.
12. The counter and preamplifiers were mounted on rubber to minimize microphonics.
13. To minimize radiation hazards, the counts were registered in an adjacent, shielded room.

Checking the gain stability of the electronic components through the small capacitor was done as follows:

The coarse gain of the Model 101 amplifier was reduced, the fine gain left in its running position. The 60 cycle pulser was plugged into the preamplifier distribution box and the discriminators on the three scalers were adjusted to give a counting rate of 30 ± 3 counts per second on each one.

The discriminator heliopot readings could be estimated to 0.02 volt, and changes of about this amount would remove the pulser counting rate from within the above limits. On successive

gain checks, at intervals of approximately 30 minutes, the three systems generally did not change in the same direction. This indicated that the pulser, when used in this way, was stable to about 0.02 volt. The actual changes required in discrimator setting were usually not more than about 0.03 volt.

Estimates of counting rate stability, based on the gain checks and bias curves of the counters were as follows:

(1) U^{238} counter ±0.05 percent
(2) Np^{237} counter ±0.09 percent

These numbers, together with the confidence gained by making independent repeat transmission measurements, indicate that the statistical uncertainties quoted on the transmissions are reliable. The results of the experiments recorded in Chapters 11, 12, and 13 show that the present accuracy was necessary for the following reasons:

1. To obtain meaningful transmissions for very thin shells.
2. To obtain reliable measurements of some of the small effects in order to verify the theory which explains them.
3. To obtain reasonably accurate final inelastic scattering cross sections.

9.3.2 Collection of Data

With the reactor off, the source, counter, and sometimes a sphere were set up. The amplifier gains were checked with the pulser, and the noise patterns were observed with the oscilloscope. The reactor was started. Personnel left the reactor room, the boron curtain was raised, and three to six 10-minute runs were taken. The three sets of counts from the threshold detector, and three sets from the monitors were recorded for each run. All counting rates were examined to insure that all systems indicated the same changes, if any.

The boron curtain was then lowered, the amplifier gains were checked with the pulser, and the sphere was changed, if appropriate. After more data were taken, transmissions were computed for each of the six electronic channels.

If there was not agreement to well within the statistics for at least two of the three systems on the threshold detector, the data were not used, but the counter and electronics were suspected and investigated. When at least two of the systems did agree, which usually occurred, the average of these was computed, and this was divided by the average ratio of counts for the monitors. The resultant transmissions are given in the Tables 11.1, 12.1, 13.1. The statistical uncertainty is that computed from the numbers of counts recorded. The fractional statistical uncertainty in the monitor transmissions was about $\frac{1}{6}$ of that for the threshold detectors.

In many cases, the transmission which is recorded in the tables is the average of two or more independent measurements made on different days. Such repeat runs were seldom outside of the combined statistical accuracies.

9.4 $Al^{27}(n,p)Mg^{27}$ Counting System

9.4.1 Detector and Counting Arrangement

For sensitivity reasons, spirals of aluminum foil were used as detectors. Pure 2-S aluminum foils were cut uniformly to the following dimensions: 0.010 inch thick by 0.50 inch wide by 18 inches long. During irradiation, a foil was rolled into a tight spiral and inserted into a small brass holder which was similar in design to, and supported like, the fission detectors. The foil was then covered by a $\frac{1}{64}$ inch thick cadmium cup.

During counting, the foil was wrapped around a 0.003 inch thick aluminum sleeve which fitted snugly over a cylindrical, aluminum walled, proportional, methane flow β counter. This counter, with a 0.0005 inch diameter central stainless-steel wire operated at about 2.5 kv, had

a flat bias curve, and at the gain and bias settings used, had a voltage plateau of about 1 percent per 100 volts. The effective dead-time of the system was less than 10 microseconds. This was the primary reason for building it. The counts were recorded on either one of two Model 750 scalers which could be alternated instantaneously by a switch.

The uniformity of sensitivity of the counter was checked by sliding a Cs^{137} β source over the surface of the aluminum sleeve. The counting rate over most of the surface was constant to within ±1 percent. The maximum deviation from the average was 2 percent. The effect seems to be caused by variations in the wall-thickness, and is expected to be smaller for the higher energy Mg^{27} β's.

For the aluminum foils used, the self-attenuation of neutrons during irradiation and of β's during counting are both small, and are about the same for both sphere-off and sphere-on runs. Errors of this sort tend to cancel out, particularly if the neutron attenuation is caused principally by elastic scattering. A directional asymmetry in sensitivity of the spiral is an indication that effects caused by attenuations will not cancel in a sphere transmission. The foils which were used in these experiments had been checked in a well-collimated fast neutron beam and re-cut to decrease such asymmetry to not more than 1 percent.

Some incidental observations made during the course of these runs are:

1. The Mg^{27} half-life was checked to about 1 percent, and, though slightly shorter, does not disagree with the previously reported value.[14]

2. The coincidence output unit on Los Alamos Model 750 scalers may be subject to large errors, especially for short-duration pulses whose peaks are close to the bias setting. The condition of the 6J6 tubes is important.

3. A localized decrease in gas amplification of about 20 percent was found after 10^9 counts. This was produced by a collimated β source, and was easily observed by sliding the source along the counter. The effect may have been caused by a deposit on the 0.0005 inch diameter central wire. The measurements of this report were not affected by this change in gain.

9.4.2 Collection of Data

With the reactor off, the foil was inserted into its holder. The reactor was brought up to operating power in about 1 minute, and a 30 minute irradiation was timed by a stop watch and monitored with counters. Shutting off the reactor ended the irradiation. The aluminum foil was unwound, washed in clean acetone, and wrapped around an aluminum sleeve, which was slid over the β counter. With the two scalers and the alternating switch, counts were taken every 30 seconds for about 10 minutes, and then every minute for about 20 minutes more.

Two or three more counts were taken at intervals of a couple of hours to determine the effective background, of which about 60 percent was true counter background and about 40 percent was due to the foil. The half-life of this latter activity was about 14 hours, and presumably was caused by the $Al^{27}(n,\alpha)Na^{24}$ reaction.

The background, long-lived activity, and short-lived $Al^{27}(n,\gamma)Al^{28}$ activity were subtracted graphically from the total counts recorded in 30 minutes. This left only the counts caused by the $Al^{27}(n,p)Mg^{27}$ reaction. Of approximately 10^5 counts recorded for each irradiation, about 90 percent were due to the (n,p) reaction. A systematic method of making the subtractions had been established by studying foils whose activations were much higher than the foils irradiated in the transmission measurements.

9.5 Sphere Design and Dimensions

The spheres were machined as two hemispheres with an overlap in the equatorial plane. There was one hole, centered in this plane, through which the counter stem entered. The area of the hole was, in general, much less than 1 percent of the sphere surface area, and faced normal to the line joining source and detector.

All sphere dimensions were measured with a micrometer to the nearest 0.001 inch, and the spheres were weighed to an accuracy of better than 0.1 percent. Average densities were then computed to about 0.1 percent, and usually agreed with the best handbook values.

The composition or uniformity of some spheres was questionable. Spectroscopic analyses or radiographic measurements were made, and where these indicated a necessity, corrections were made, or the limits of error were increased on the inelastic cross section.

In making repeat transmission measurements, the positions of the hemispheres were sometimes interchanged, with no apparent real change in the observed transmission.

Chapter 10

EXTRANEOUS EFFECTS

In this chapter a more detailed discussion is presented of some of the effects which may cause uncertainties or errors in a sphere transmission experiment. Some are characteristic of the present experiments, in which a reactor was used, and some are characteristic of sphere transmission experiments in general.

10.1 Fast Neutrons Not Produced by the Source

In reactor experiments, some fast neutrons are always present. These constitute a background of uncertain spectrum and geometry. In the present cavity and collimation system the magnitude was less than 1 percent at all source-to-counter distances used, and was nearly the same for both U^{238} and Np^{237} detectors. Since these neutrons were in a broad beam, however, it was not clear how they would affect the measured transmission of a sphere. Sphere transmissions were therefore run without the U^{235} fission source in order to remove this effect. The largest correction, about 1 percent in transmission, was found for the largest spheres at the 5 inch source-to-counter distance.

10.2 Room Scattering of Source Neutrons

The distances of the source and detector from the floor and reactor face were not large, so there was a background at the counter caused by source neutrons scattered from these surfaces. This background was expected to be relatively uniform throughout the region around the source which was used in these experiments. The neutron flux coming directly from the source will fall off approximately as the inverse of the square of the distance. Therefore, if measurements of this background are made at the largest source-to-counter distance, a rough estimate can be made of the background at other positions.

The following measurements were made with the U^{238} counter to evaluate this background, and its effect on a sphere transmission:

(1) The residual counts were determined behind a bulk shadow shield covering the large ($4\frac{1}{2}$ by 6 inches) source plate.

(2) The residual counts were determined behind a good geometry shadow shield of a 1 inch diameter fission source.

(3) An approximate computation of the percentage of scattering was made.

(4) A measurement was made of the counting rate as a function of source-to-counter distance.

(5) Sphere transmissions were run behind the bulk shadow shield.

10.2.1 Large Source with Bulk Shadow Shield

The detector was mounted 20 inches from the large U^{235} source, and the counting rate was determined with various thicknesses of the scattering pieces between the two. The scattering pieces, made of steel, polyethylene, or a B_4C-paraffin mixture were large enough to shield the counter from every point of the source. With a 13 inch thickness of each of these, for which the simply computed transmission is not more than 1 percent, the apparent background was about 6 percent. To eliminate the possibility that much of this apparent background was caused by the poor geometry of the shadow shield, the following experiment was done:

10.2.2 Small Source with Good Geometry Shadow Shield

The large U^{235} plate was replaced by a 1 inch diameter disk of U^{235}, and the counter set up at 20 inches. In this geometry, the computed transmissions of the shadow bars were less than 1 percent, but the same value, approximately 6 percent, was obtained for the background at 20 inches. The counter was moved farther from the source and longer shadow bars inserted. The apparent relative background increased with increasing source to counter distance, as was expected.

10.2.3 Computation of Background

The expected behavior of the relative background as a function of source to counter distance was computed under the following assumptions:

(1) Source neutrons are emitted isotropically from a point.

(2) All neutrons which enter either the floor or reactor face are elastically scattered isotropically at the surface.

(3) Air scattering is neglected, and the roof and other walls are very far away.

This should give an overestimate, because of assumption 2, and because the counter actually has a relatively high threshold. The computed relative background at 20 inches from the source was 9 percent.

10.2.4 Inverse Square Measurement

A measurement was made of the counting rate as a function of the distance between the 1 inch disk source and the counter. The accuracy was not high, but the deviation from an inverse square fall-off indicated about 5 percent relative background at 20 inches from the source.

10.2.5 Small Sphere Transmission Behind Bulk Shadow Shield

Since all measurements were consistent with a relative background of about 6 percent at 20 inches from the source, the effect on a sphere transmission was studied directly. The transmissions of small spheres were measured while the counter and entire sphere were shielded from the large U^{235} source by bulk shadow shields. In the cases tried, the transmission of the background was within 2 percent of that obtained with no shadow shield present. Upon removal of the properly weighted background transmission from the transmission obtained with no shadow shield present, the apparent inelastic cross section changed by only about 1 percent. On transmissions run at 5 inches and 10 inches from the source, the background effect must be several times smaller, but it was not measured. Since this background correction is not large, it has not been applied to the data.

With the Np^{237} counter, the relative background at 20 inches from the source was 8.5 percent. The transmissions of the small spheres were not measured behind the large shadow shield, however. This is because of relatively low counter sensitivity, and the fact that the sphere transmissions would have been very close to unity and consequently difficult to interpret. As in the case of the U^{238} counter, the effect at 5 inches was not measured because of the prohibitively high transmissions of such short "shadow shields".

For the Np^{237} counter, correction for this background might increase the inelastic cross sections by 5 percent at the most. However, since it is probably smaller in most cases and we do not know it accurately, we have not made this correction.

Because of the shape of the fission spectrum and the positions in energy of the thresholds, the background in the $Al^{27}(n,p)Mg^{27}$ detector was expected to be even lower than in the U^{238} counter. A measurement was not made, however, nor a correction.

10.3 Scattering from Supports

In the initial experiments, small steel rods were used for hanging the spheres. When a sphere was removed, it was most convenient to remove the rods also. This procedure removed some scattering material, and caused an error of 2 to 5 percent in cross section. A small aluminum cone system was later used for supporting the spheres. This caused less then 0.2 percent scattering into the counter. The cone was left in place when the sphere was removed and mechanically was much superior to the hanging rods. All of the data in the tables of Chapters 11, 12, 13 and 14 have been obtained with this cone support.

10.4 Check on Neutron Spectrum

Some of the data on total cross sections and angular distribution of elastic scattering which are used in the calculations of σ_{in} (see Chapters 11 and 12) were obtained with a beam of neutrons from the fast reactor (Clementine). In order to determine how similar the spectrum of that beam was to a fission spectrum for neutrons above the U^{238} threshold, the same detector was used to measure the total cross section of hydrogen in both spectra. The measurements in the fast reactor beam were made by E. T. Jurney and C. Zabel.[15] The value obtained in the fast reactor beam was 2.15 ± 0.2 barns.

To determine the average hydrogen cross section at the "Water Boiler," polyethylene and graphite scatterers were interposed midway between the external 1 inch diameter U^{235} source and the U^{238} counter. The scattering cylinders were 1.27 inches in diameter and about 1 inch long. The distance between source and counter was 13 inches. The total cross section for hydrogen which was obtained, with no correction for in-scattering, was 2.18 ± 0.11 barns. The numerical integration of the published hydrogen cross section over the fission spectrum[16] and the U^{238} fission cross section gave 2.45 barns.

10.5 Non-threshold Neutron Detection

Two effects to be considered here may introduce errors into the sphere transmission measurements. First, the fissionable material of the threshold detector may have a finite thermal fission cross section. Second, there might be a contaminant which has a finite fission cross section at all energies. If either of these should occur, some low energy neutrons will be detected.

With cadmium sheets placed on the floor and face of the reactor, cadmium cups on the detector made no observable effect on the counting rate. The fraction of the counts to be expected from the two above causes was determined by further experiments to be less than 10^{-4} for the Np^{237} and U^{238} counters. Any such effects were routinely eliminated by the method of analysis of the $Al^{27}(n,p)Mg^{27}$ data.

10.6 γ Ray Effects

10.6.1 γ Fission in the Threshold Detectors

High energy γ rays can produce photo-fission in the detectors. The two principal γ ray sources are capture of thermal neutrons in the collimator materials and γ rays accompanying

fission or radiative capture in the U^{235} source. The first was minimized, as has been pointed out in Section 9.1. The second could not be avoided. The following two evaluations were made of these effects:

(1) Transmission measurements were made on small spheres behind different types of shadow shields.

(2) Computations were made of the number of γ rays from the fission source.

In the experiments when a low atomic weight shadow shield was inserted (Section 10.2.5), the neutrons were attenuated by a factor of about 20, whereas the high energy γ rays were attenuated by a factor of 2. This increased the relative number of γ rays by a factor of about 10. Sphere transmissions behind the shadow shield thus gave an upper limit of the relative numbers of photo-fissions in the detector.

By replacing the central 2 inches of B_4C-paraffin shadow shield with 2 inches of lead and repeating the sphere transmission measurements, a more accurate value was obtained. The relative number of photo-fissions in the detector with no shadow shield and no sphere was 0.000 ± 0.005.

For the computations, the following assumptions were made:

(1) All γ rays come from the source.

(2) There are 12 γ rays per fission, distributed in energy like the spectrum reported by Motz.[17]

(3) The photo-fission cross section in the region of 6 to 7 Mev is 0.030 barns.

With no sphere around the detector, the number of photo-fissions in the U^{238} detector is computed to be 0.1 percent of the number of neutron fissions.

10.6.2 Photo-Neutron Production in the Sphere

The γ-n cross section of many of the sphere materials is finite at the γ ray energies involved. Some of the neutrons produced are above the counter thresholds. However, the contribution is less than 0.01 percent in transmission.

10.7 Spurious Counter Effects

It was desired that the statistical uncertainties in counting should give reliable estimates of the accuracy of the experiments. Therefore, it was necessary to look for obscure and spurious counter effects which might cause about 0.1 percent error in a transmission. Many effects, such as dead-time counting losses, γ ray pile-up pulses, α pulses, and temperature effects, have been looked for in the spiral counters used. Simple experiments were performed to evaluate some of these effects separately, and sphere transmissions were measured under various conditions to make integral-type studies. All of the differential measurements indicated that there should be no observable effect, but sphere transmissions run at low bias and high counting rate (at the 5 inch source-to-counter distance) deviated by a few tenths of a percent from those run at lower source strength, higher bias, or lower flux (at 10 inch and 20 inch positions).

The conclusion from the experiments is that transmissions measured at biases which are high relative to noise are not subject to peculiar effects. Those measured with low bias seem to be, and none of these have been used in computing σ_{in}.

10.8 Counter Size and Position in Sphere

In Section 6.2 the calculation of counter size corrections is discussed, and formulas are derived. An effect intimately connected with this is the position of the center of the counter inside of the sphere. If the counter size correction is small, then one also expects the counter position to be relatively unimportant, as long as the distance between sphere center and counter center is of the order of the counter dimensions.

Transmissions run with the U^{238} detector about 1 inch off-center in an 8 inch outside diameter, 7 inch inside diameter sphere were within 0.2 percent of the values obtained with the detector centered in the spheres. This is consistent with the computed counter size corrections of about 0.1 percent in transmission.

10.9 Counter Angular Asymmetry

The method of correcting a measured transmission when the detector is not isotropically efficient is discussed in Section 6.4. As was pointed out there, the correction is most sensitive to the quantity Δ, which can also be measured most easily. The following two things were done to evaluate this factor:

(1) Each detector was irradiated in a 1.4 inch wide, well-collimated, fast neutron beam in two positions. The first position was with the axis of the spiral parallel to the beam, and the second position was with this axis perpendicular to the beam, the center of the detector remaining at a fixed point. The ratio of the two sets of counts is the Δ of Section 6.4. A rough measurement of the angle over which Δ was constant indicated that it was a few degrees. The smallest value of Δ, that for the U^{238} counter, was 0.950 ± 0.004; Δ for the Np^{237} counter was 0.976 ± 0.010; and Δ for the aluminum foils was made 1.00 ± 0.01 by proper cutting of the foils.

(2) The second evaluation of Δ for the U^{238} detector was made by running sphere transmissions with the axis of the counter both parallel and perpendicular to the normal to the fission source plate. For two different spheres, one lead and the other iron, analyzed as discussed in Section 6.4, the values of Δ were 0.952 ± 0.01 and 0.966 ± 0.01. These agree with the directly measured Δ of 0.950 ± 0.004.

Chapter 11

ANALYSIS OF EXPERIMENTAL DATA OBTAINED WITH U^{238} THRESHOLD DETECTOR

In this chapter we will give the "28" detector and fission spectrum data used in our analysis for inelastic cross section and will give the final results of this analysis. It is to be understood that inelastic cross sections obtained here are defined as stated in Chapter 7, viz., (1) by Eq. 7.5 or (2) as the average cross sections for collisions leading to energies below the effective detector threshold for the part of the fission spectrum above the effective threshold. For the "28" detector the effective threshold is about 1.4 Mev.

11.1 Table of Cross Sections

Table 11.1 presents the results of our experiments. In column one are listed the 15 elements studied; in column 2, the sphere diameters; column 3, the sphere thickness in total mean free paths; column 4, the average distance between the "28" counter and effective center of the neutron source; column 5, the average total cross section used in the multiple scattering analysis (Eq. 7.7); column 6, the average σ_{et}/σ_{el} used in the multiple scattering analysis (see Section 3.5 and Chapter 7); column 7 the final transport cross section for neutrons above 1.4 Mev in the fission spectrum, using the column 11 final inelastic cross sections; column 8, the measured shell transmissions; column 9, the inelastic cross section, interpreting the transmissions of column 8 with Eq. 1.1; column 10, the inelastic cross sections obtained using Eqs. 3.36 or 4.5 and correcting for all effects except the detector angular asymmetry and the loss of energy on elastic collisions; and column 11, the final average inelastic cross sections with corrections for these latter two effects.

11.2 Accuracy of Final Inelastic Cross Sections

In assigning the final uncertainties to the numbers reported in column 11, we considered the individual uncertainties in the measured shell transmissions, in the computation of the multiple scattering correction, in computing the source to detector distance effect, in the counter size correction, and in the corrections for loss of energy by elastic scattering and for counter asymmetry. In combining these errors to obtain the final error in the measurement, we assumed that we were dealing with independent errors and calculated the square root of the sum of the squares of individual errors to obtain the final rms error.

The rms errors in the transmission measurements are given also in column 8. These uncertainties imply an uncertainty in inelastic cross section given by

$$\frac{\delta\sigma_{in}}{\sigma_{in}} \simeq C \frac{\delta T}{1 - T} \tag{11.1}$$

where C lies between one and two for most of the shells of interest. When more than one shell was measured, the statistical error in σ_{in} was determined by combining the individual errors

TABLE 11.1—RESULTS OF SPHERE TRANSMISSION EXPERIMENTS USING A U^{238} THRESHOLD DETECTOR AND A FISSION SPECTRUM SOURCE

Element	Sphere outside diameter, inches	Thickness, total mean free paths	Distance to source, inches	σ_t, barns	$\frac{\sigma_{el}}{\sigma_{el}}$	σ_{tr}, barns	Transmission	σ_{in} (by Eq. 1.1), barns	σ_{in} (by sphere theory), barns	σ_{in} (with all corrections), barns
1	2	3	4	5	6	7	8	9	10	11
Al	5	0.307	10	2.67	0.579	1.68	0.9493 ± 0.0020	0.453 ± 0.018	0.40	0.519 ± 0.046
	8	0.618	10	2.67	0.579	1.68	0.8953 ± 0.0023	0.478 ± 0.010	0.40	
Ti	4.5	0.547	10	3.79	0.590	2.47	0.8940 ± 0.0022	0.776 ± 0.016	0.635	0.563 ± 0.051
V	2.52	0.340	10	3.57	0.590	2.34	0.9298 ± 0.0026	0.764 ± 0.028	0.636	0.575 ± 0.050
Fe	8	2.465	10	3.17	0.58	2.13	0.4678 ± 0.0040	0.977 ± 0.005	0.724	
	8	1.106	10	3.17	0.58	2.13	0.7120 ± 0.0018	0.974 ± 0.005	0.730	
	8	1.106	20	3.17	0.58	2.13	0.7080 ± 0.003		0.722	
	5	1.021	20	3.17	0.58	2.13	0.7354 ± 0.0030		0.735	
	5	1.021	10	3.17	0.58	2.13	0.7414 ± 0.0018	0.927 ± 0.006	0.724	
	5	1.021	5.25	3.17	0.58	2.13	0.7494 ± 0.0018		0.724	
	5	1.021	5.48	3.17	0.58	2.13	0.7525 ± 0.0021		0.723	
	8	0.551	10	3.17	0.58	2.13	0.856 ± 0.0018	0.893 ± 0.010	0.742	0.686 ± 0.043
	5	0.511	10	3.17	0.58	2.13	0.868 ± 0.0017	0.877 ± 0.011	0.731	
	5	0.511	20	3.17	0.58	2.13	0.8650 ± 0.0030		0.736	
	3½	0.510	10	3.17	0.58	2.13	0.8660 ± 0.0017	0.893 ± 0.011	0.749	
	2	0.5097	5.48	3.17	0.58	2.13	0.8787 ± 0.0022	0.804 ± 0.014	0.710	
	4.95	0.277	10	3.17	0.58	2.13	0.9314 ± 0.0018	0.834 ± 0.021	0.736	
	4.95	0.277	6	3.17	0.58	2.13	0.9345 ± 0.0018		0.738	
	5.24	0.172	10	3.17	0.58	2.13	0.9584 ± 0.0018	0.786 ± 0.033	0.713	
Ni	5.24	0.2076	10	3.24	0.611	2.26	0.9455 ± 0.0020	0.874 ± 0.032	0.771	
	5.24	0.612	10	3.24	0.611	2.26	0.8370 ± 0.0020	0.942 ± 0.011	0.742	0.713 ± 0.048
Cu	8	1.150	10	3.29	0.607	2.35	0.6483 ± 0.0016	1.24 ± 0.005	0.929	
	5.22	0.570	10	3.29	0.607	2.35	0.8175 ± 0.0018	1.16 ± 0.01	0.954	
	5.22	0.1897	10	3.29	0.607	2.35	0.9420 ± 0.0015	1.035 ± 0.026	0.945	0.900 ± 0.053
Zn	8	0.5716	10	3.37	0.566	2.32	0.8175 ± 0.0018	1.19 ± 0.010	0.995	0.955 ± 0.055
Zr	4.5	0.6534	10	4.61	0.574	3.06	0.8429 ± 0.0028	1.205 ± 0.021	1.00	0.960 ± 0.059
Ag	8	0.7316	10	4.80	0.449	3.07	0.7384 ± 0.0018	1.99 ± 0.012	1.685	1.66 ± 0.090
Cd	8	0.6838	10	4.90	0.469	3.11	0.7765 ± 0.0018	1.81 ± 0.014	1.54	
	8	1.367	10	4.90	0.469	3.11	0.5870 ± 0.0020	1.91 ± 0.007	1.54	1.52 ± 0.082
Sn	8	0.6511	10	5.02	0.482	3.00	0.8380 ± 0.0022	1.362 ± 0.017	1.159	
	8	1.303	10	5.02	0.482	3.00	0.6938 ± 0.0020	1.408 ± 0.008	1.141	1.12 ± 0.061
W	4.95	0.4223	10	6.29	0.391	3.82	0.8503 ± 0.0018	2.57 ± 0.030	2.29	
	4.95	0.4223	6	6.29	0.391	3.82	0.8533 ± 0.0014		2.28	2.23 ± 0.13
	5.25	0.2669	10	6.29	0.391	3.82	0.9096 ± 0.0018	2.36 ± 0.045	2.16	
Au	6.99	0.8644	5	6.60	0.414	3.93	0.7303 ± 0.0018		2.05	
	6.99	0.8644	10	6.60	0.414	3.93	0.7211 ± 0.0018		2.052	2.04 ± 0.11
	6.99	0.8644	20	6.60	0.414	3.93	0.7184 ± 0.0035	2.53 ± 0.027	2.053	
Pb	5	0.4172	10	6.65	0.527	3.84	0.9470 ± 0.0017	0.865 ± 0.030	0.746	
	8	0.695	10	6.65	0.527	3.84	0.9106 ± 0.0013	0.895 ± 0.013	0.741	
	8	0.695	20	6.65	0.527	3.84	0.9069 ± 0.0026	0.934 ± 0.026	0.716	0.712 ± 0.043
	8	1.39	10	6.65	0.527	3.84	0.816 ± 0.0018	0.972 ± 0.009	0.738	
	8	1.39	20	6.65	0.527	3.84	0.805 ± 0.0030	1.037 ± 0.015	0.745	
Bi	4.32	0.282	20	6.70	0.556	4.05	0.9608 ± 0.004	0.955 ± 0.098	0.817	
	8	0.663	10	6.70	0.556	4.05	0.9170 ± 0.002	0.876 ± 0.020	0.729	0.728 ± 0.045
	8	1.321	10	6.70	0.556	4.05	0.8229 ± 0.002	0.988 ± 0.011	0.759	

of the runs. Most of the final uncertainties in σ_{in} due to counting statistics on the transmission measurements were between 0.5 and 2 percent.

In using the multiple scattering analysis discussed previously, one introduces two types of uncertainties: uncertainty in the accuracy of the method, and uncertainties in the quantities σ_t and σ_{et}/σ_{el}. To allow for the first uncertainty, we added 1 percent error to the final error, which included all other effects. This seems reasonable in view of the comparisons in Table 4.1 since, except for iron, Eq. 3.36 was used throughout this work. Iron was analyzed using Eq. 4.5. The uncertainty assumed for σ_t was 10 percent which introduced about 3 percent uncertainty into the inelastic cross section determination. An uncertainty of 10 percent was assumed for σ_{et}/σ_{el}, introducing about the same error.

The error in the determination of the finite distance effect was assumed to be about 10 percent. Equation 6.9 was used except in the case of iron, where Eq. 6.10 was used. This uncertainty consists partly of uncertainty in b (source to detector distance) and partly of the uncertainty in the method of analysis (see Section 6.1.2).

Usually the change in the true sphere transmission due to finite counter size was very small (< 0.001). This correction was made (except for iron) using Eq. 6.27. Equation 6.28 was used for iron. It was assumed that no uncertainty was produced in the final cross sections reported because of uncertainties in this correction.

The correction for loss of energy on elastic collisions is discussed in Section 6.5. The apparent inelastic cross section due to this was obtained using Eq. 6.42. As stated there, we assumed the correction was 50 percent uncertain, which is probably very conservative. The magnitude of this correction to the inelastic cross section varies from 20 percent for lightest elements to 1 percent for the heaviest elements. The uncertainty in this correction is responsible for most of the uncertainty in the cross sections reported for the lighter elements in column 11 of Table 11.1.

The counter asymmetry correction was computed using Eq. 6.33 or 6.34. As stated in Chapter 10, Δ for this counter is 0.950 and Ω is 0.10. The magnitude of the correction was between 1 and 3 percent of the inelastic cross section. An uncertainty of 50 percent was assumed in the correction because of approximations made in the analysis of Section 6.4.

11.3 Errors Involved in Use of Equation 1.1

Comparing the inelastic cross sections recorded in column 9 of Table 11.1 with those in columns 10 and 11, it is apparent that one must make an effort to correct for multiple scattering of neutrons in shells even a few tenths of a mean free path thick, if accuracies of a few percent are desired. To show this, in Fig. 11.1 the inelastic cross sections of columns 9 and 10 are both plotted vs shell thickness for various shell outside diameters. It is seen that the sphere theory developed in this paper gives the same inelastic cross section for all sphere thicknesses and sizes, within about 1.5 percent. The cross sections deduced from the exponential, on the other hand, increase rapidly with increasing shell thickness, and are more than 30 percent too high for the thickest shells, compared with the theory of this report. Even for the thinnest shell measured, the exponential gives σ_{in} still about 10 percent too high, and for this shell the transmission is nearly 96 percent. With our good statistical accuracy, the cross section can be determined only to ±5 percent by extrapolating the inelastic cross sections determined from the exponential formula to zero shell thickness.

It should also be clear from Fig. 11.1 that it is no guarantee of a correct result if the transmission is measured for different shell thicknesses, and the cross sections (evaluated by the exponential method) agree within experimental error. For instance, the 5 inch spheres with shell thickness 0.45 and 0.75 inch give $\sigma_{in} = 0.834 \pm 0.021$ and 0.877 ± 0.011, respectively—almost within each other's error—and still their average is 20 percent too high. A linear extrapolation through these results to zero thickness would still give a cross section that is 10 percent too high. These difficulties would be aggravated if the transmission were measured to an accuracy of only 1 percent in each case. Therefore, to establish that multiple scattering corrections are both necessary and valid, it is necessary to measure the transmissions to a few tenths of a percent, and to vary the shell thickness by at least a factor of 4 (actually, in Fig. 11.1, it was varied by a factor of 14!).

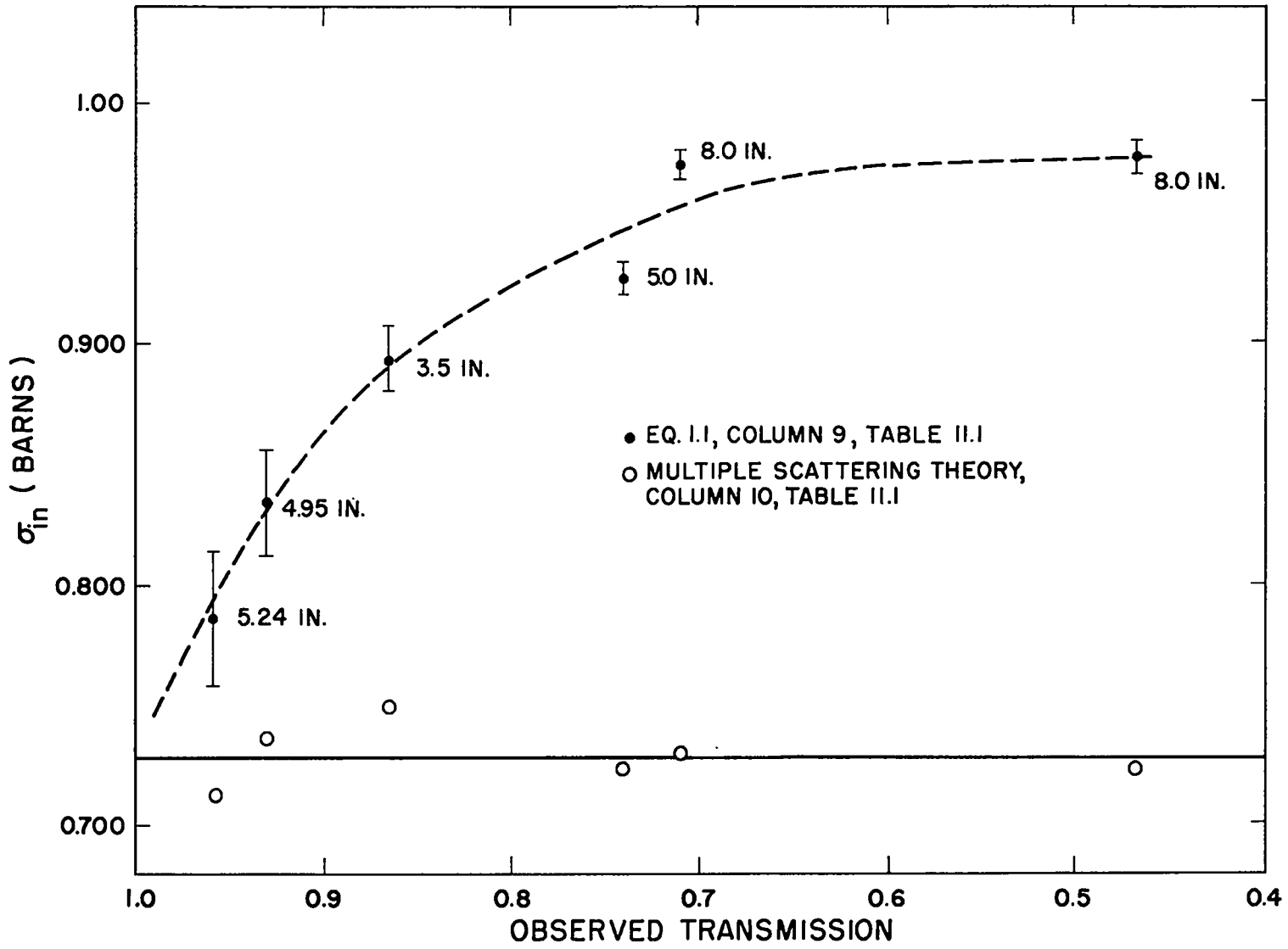

Fig. 11.1 —Inelastic cross sections computed from the exponential formula and from the sphere theory presented in this report. The statistical error is placed on the cross sections determined from the exponential. The sphere outside diameter in inches is also given for each of these cross sections.

If the observed transmission had been corrected by the methods of Chapter 6 for all the geometrical effects of the experiment except multiple scattering, and if the inelastic cross sections were determined from this corrected transmission by the exponential relationship, the values obtained would be, if anything, in worse agreement with those from the sphere theory. Thus, the difference between the two curves in Fig. 11.1 arises because the exponential relationship ignores multiple scatterings, and not because of other geometrical effects of the experiments.

11.4 Interpretation of Corrected σ_{in}

It has been explained in Chapter 7 and in the first paragraph of this chapter that we are measuring an average cross section for going below the effective energy threshold of our detector. However, for many elements considered, there is inelastic scattering without sufficient energy loss to place the resultant neutron below the energy threshold. Furthermore, neutrons in the fission spectrum with the highest inelastic cross section are removed first. Thus, as the shell thickness increases, the spectrum of neutrons detected would be expected to change somewhat. At first it was not known whether these effects would make the average inelastic cross section dependent on shell thickness even after multiple scattering corrections. From column 10, Table 11.1, it is clear that we have observed essentially no changes anywhere attributable to spectrum distortions above the detector threshold, even for very thick shells. Experimentally, then, it has been demonstrated that a set of meaningful average one-group cross sections can be assigned to the neutrons above about 1.4 Mev in the fission spectrum, and that the behavior of these neutrons, even in large amounts of material, can be understood in terms of these cross sections.

11.5 Conclusions

In Fig. 11.2 the inelastic cross sections of column 11, Table 11.1, are plotted vs $A^{2/3}$. This plot shows that in general our observed inelastic cross sections seem to be a linear function of the nuclear area. Exceptions to the above statement occur at the magic number or partially magic number nuclei: Zr, Sn, Pb, Bi. The scarcity of levels in the magic target nuclei may explain why the cross sections are low in these cases.

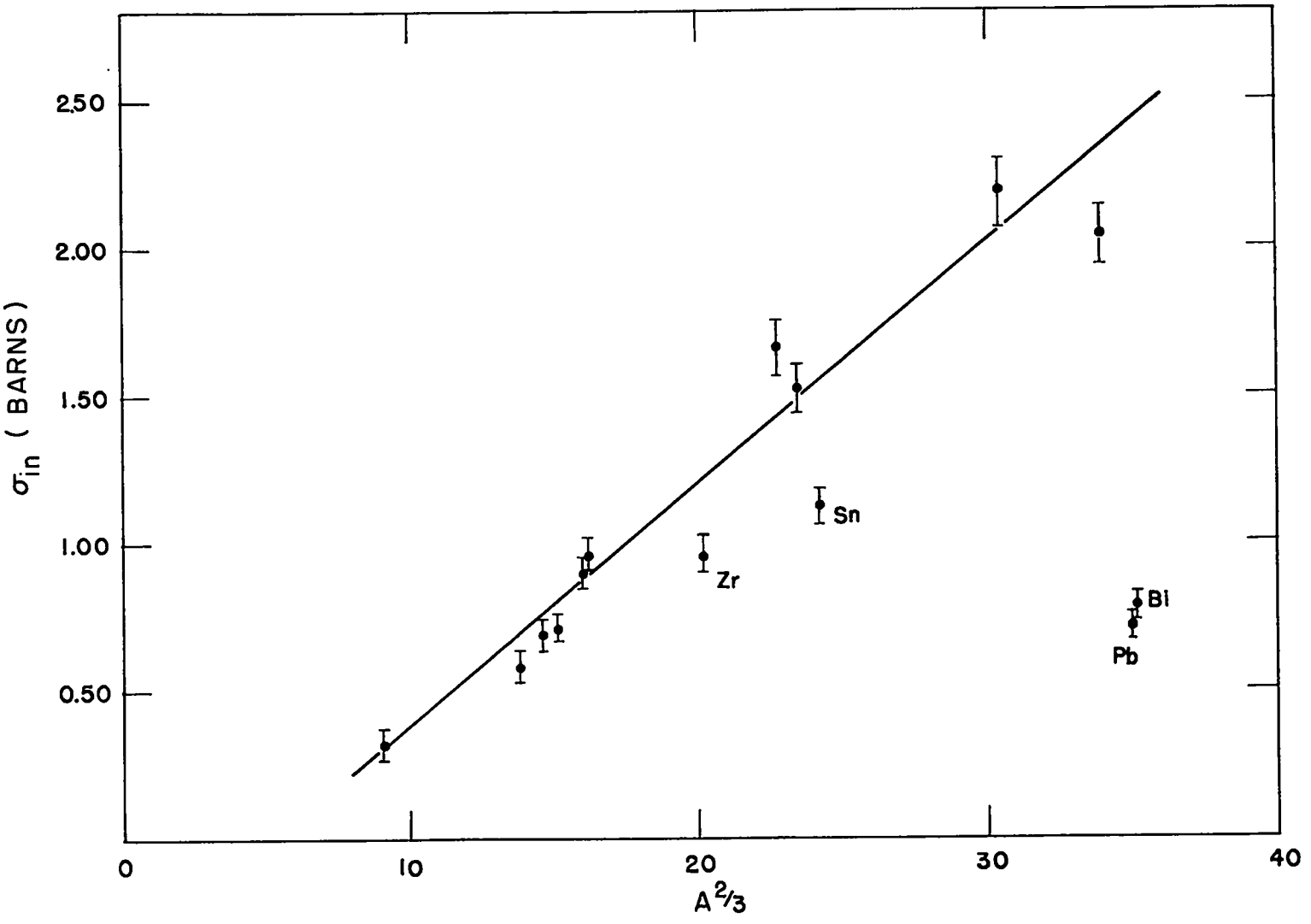

Fig. 11.2—Inelastic cross sections for scattering below the "28" detector threshold as a function of $A^{2/3}$.

Chapter 12

ANALYSIS OF EXPERIMENTAL DATA OBTAINED WITH Np^{237} THRESHOLD DETECTOR

The auxiliary data used in the analysis and the final results of the "37" detector experiments are presented in this chapter. The cross sections which we give here are one-group cross sections and are defined like those determined in the last chapter and as stated in Chapter 7. For the Np^{237} detector, the effective detector threshold is 0.7 Mev.

12.1 Table of Cross Sections

Table 12.1 presents the results of our experimental and analytical investigations. In column 1 are listed the 15 elements investigated; in column 2, sphere outside diameters; column 3, the sphere thickness in total mean free paths; column 4, the average distance between the "37" counter and the effective center of the neutron source; columns 5 and 6, the average total cross sections and σ_{et}/σ_{el}, respectively, used in the multiple scattering analysis (for further information see Section 3.5 and Chapter 7); column 7, the final transport cross section for neutrons above 0.7 Mev in the fission spectrum, using the column 11 inelastic cross sections; column 8, the measured transmissions; column 9, the inelastic cross sections, evaluating column 8 with Eq. 1.1; column 10, the inelastic cross section obtained using Eq. 3.36 and correcting for all effects except detector asymmetry and loss of energy on elastic collisions; and column 11, final average inelastic cross sections with corrections for these latter two effects.

12.2 Accuracy of Final Inelastic Cross Sections

The same effects were considered in assigning the final errors in column 11, Table 12.1, as we considered in Section 11.2. Errors were combined to find the final uncertainty reported, in much the same way. The uncertainties in the quantities σ_t and σ_{et}/σ_{el}, used in the multiple scattering analysis, were assumed to be about 20 percent here, introducing from 7 to 10 percent uncertainty in σ_{in}, due to each of these uncertainties. Corrections were made for the counter asymmetry effect, using Eq. 6.34, with Δ measured as 0.976 and Ω estimated to be 0.1. In general, all corrections made to these data were a larger percentage of the final answer than comparable corrections in Chapter 11.

12.3 Conclusions

As in the previous chapter, it is very apparent from the results (Table 12.1) that one must make the multiple scattering analysis to obtain a reasonably accurate cross section. Column 9 values (evaluation using Eq. 1.1) differ even more percentage-wise from the correct answers for this work than they did for the "28" counter results. As observed in Chapter 11,

TABLE 12.1

RESULTS OF THE SPHERE TRANSMISSION EXPERIMENTS USING THE Np^{237} THRESHOLD DETECTOR AND A FISSION SPECTRUM SOURCE

Element	Sphere outside diameter, inches	Thickness, total mean free paths	Distance to source, inches	σ_t, barns	$\frac{\sigma_{et}}{\sigma_{el}}$	σ_{tr}, barns	Transmission	σ_{in} (Eq. 1.1), barns	σ_{in} (sphere theory), barns	σ_{in} (with all corrections), barns
1	2	3	4	5	6	7	8	9	10	11
Al	8	0.722	10	3.12	0.655	2.07	0.9665 ± 0.0030	0.150 ± 0.013	0.140	0.087 ± 0.032
Ti	4½	0.4562	10	3.16	0.69	2.24	0.9644 ± 0.0040	0.251 ± 0.028	0.209	0.187 ± 0.037
V	2.519	0.3105	10	3.26	0.70	2.35	0.9727 ± 0.0035	0.29 ± 0.037	0.246	0.224 ± 0.046
Fe	5	0.4455	10	2.75	0.701	2.01	0.9450 ± 0.0030	0.350 ± 0.020	0.280	
	8	0.9596	10	2.75	0.701	2.01	0.8616 ± 0.0030	0.427 ± 0.01	0.301	0.276 ± 0.031
	8	2.139	10	2.75	0.701	2.01	0.7237 ± 0.0042	0.416 ± 0.006	0.288	
Ni	5.244	0.588	10	3.11	0.744	2.38	0.9284 ± 0.0030	0.393 ± 0.016	0.293	0.276 ± 0.041
Cu	8	0.6133	10	3.50	0.732	2.64	0.9290 ± 0.0030	0.420 ± 0.017	0.325	
	8	1.23	10	3.50	0.732	2.64	0.8409 ± 0.0031	0.496 ± 0.019	0.316	0.304 ± 0.046
	5.24	0.607	10	3.50	0.732	2.64	0.9256 ± 0.0030	0.447 ± 0.010	0.323	
Zn	8	0.6106	10	3.60	0.691	2.58	0.9348 ± 0.0022	0.398 ± 0.015	0.322	0.305 ± 0.047
Zr	4.5	0.7784	10	5.49	0.71	3.99	0.9409 ± 0.0035	0.430 ± 0.025	0.325	0.302 ± 0.050
Ag	8	0.8385	10	5.50	0.554	3.42	0.8402 ± 0.0030	1.14 ± 0.020	0.855	0.840 ± 0.105
Cd	8	0.7744	10	5.55	0.581	3.50	0.8834 ± 0.0030	0.887 ± 0.027	0.682	0.658 ± 0.079
	8	1.547	10	5.55	0.581	3.50	0.7635 ± 0.0030	0.968 ± 0.011	0.665	
Sn	8	0.7291	10	5.62	0.598	3.51	0.9430 ± 0.0030	0.450 ± 0.024	0.384	0.369 ± 0.050
W	4.95	0.4227	10	6.49	0.484	3.69	0.920 ± 0.0030	1.32 ± 0.05	1.094	1.080 ± 0.145
Au	6.99	0.7989	10	6.10	0.515	3.63	0.8412 ± 0.0032	1.32 ± 0.023	1.01	1.00 ± 0.12
Pb	8	0.6318	10	6.03	0.678	4.16	0.9783 ± 0.004	0.210 ± 0.038	0.223	0.208 ± 0.05
Bi	8	0.6204	10	6.27	0.688	4.38	0.9839 ± 0.0024	0.165 ± 0.025	0.200	0.197 ± 0.035
	8	1.237	10	6.27	0.688	4.38	0.9489 ± 0.005	0.267 ± 0.026	0.225	

the evaluation of the data with the multiple scattering theory gives essentially one cross section independent of shell thickness, while the exponential theory (Eq. 1.1) does not.

If one compares the final cross sections in column 11 of Tables 11.1 and 12.1, it is evident that the Table 12.1 values are considerably less (a factor of 2 or more in most cases). However, 70 percent of the counts in the "37" detector come from the same neutron energy region in which the "28" detector is sensitive. The low "37" cross sections, therefore, clearly imply that most of the inelastic scattering of neutrons above the "28" threshold will lead to energies between the "37" and "28" thresholds.

Let us now denote, as usual, the neutrons above the "28" threshold as group 3, those between the "37" and "28" thresholds as group 2, and those below the "37" threshold as group 1. Then the small "37" inelastic cross section indicates that the number of neutrons in group 2 in the shell must increase at the expense of group 3 neutrons as the thickness of the shell increases. One would, therefore, expect to observe a cross section which depends on shell thickness even after the multiple scattering analysis, but again, as shown in Chapter 11, this does not happen. We have shown in Section 8.5 that this experimental fact forces us to conclude that there is an approximate relation between the various inelastic cross sections, as given by Eq. 8.37.

The significance of the "37" counter measurements may be explored further using the three group method of Chapter 8. The analysis of the "37" data using this theory is given in Chapter 14.

In Fig. 12.1 the final cross section results (column 11, Table 12.1) are plotted vs $A^{2/3}$. Errors indicated are the absolute errors in column 11. Relative errors between cross sections for the various elements are less. Again, the magic number nuclei have cross sections which do not fit with the general cross section trend for the rest of the elements.

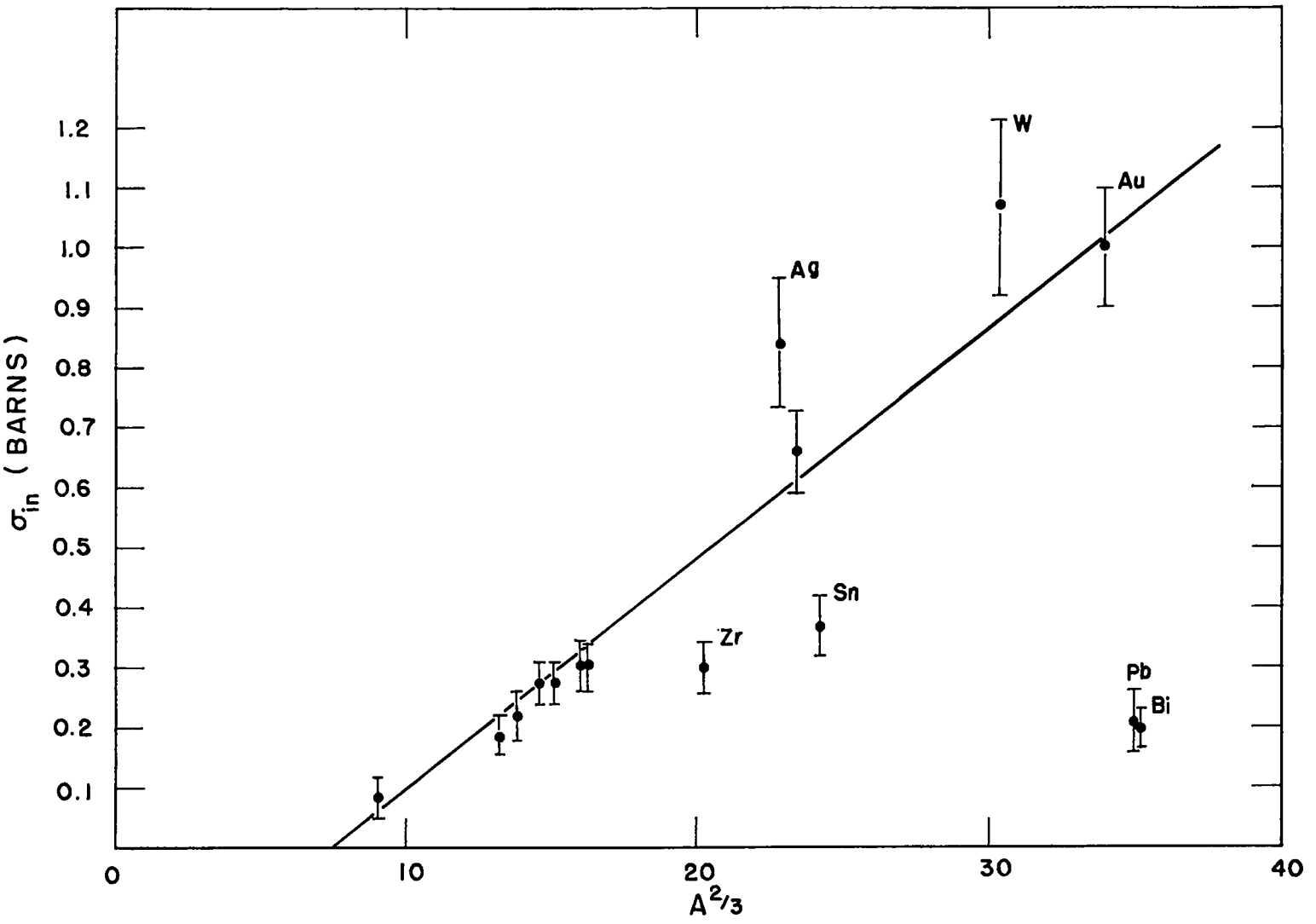

Fig. 12.1—Cross Sections for scattering below the "37" detector threshold as a function of $A^{2/3}$.

Chapter 13

ANALYSIS OF EXPERIMENTAL DATA OBTAINED WITH $Al^{27}(n,p)Mg^{27}$ THRESHOLD DETECTOR

The pertinent data and the cross sections obtained from the work with the $Al^{27}(n,p)Mg^{27}$ detector are presented in this chapter. Again, we point out that the final "inelastic cross sections" are average values for removing fission spectrum neutrons that are above the effective threshold. There are essentially three mechanisms:

(1) Energy loss during elastic scattering.

(2) Capture, such as (n,γ) and (n,p).

(3) True inelastic scattering to some energy below the effective threshold. This process may include some (n,2n) reactions.

The numbers in column 10, Table 13.1 include all three of these processes, and those in column 11 include only the second and third. The average energy of the detected neutrons is about 5.5 Mev, and the effective threshold is about 5 Mev.

13.1 Table of Cross Sections

Table 13.1 for the $Al^{27}(n,p)Mg^{27}$ detector is analogous to Tables 11.1 and 12.1 for the U^{238} and Np^{237} detectors, respectively. The total cross sections, column 5, were obtained from N. Nereson's work.[18]

Values for σ_{et}/σ_{el} were initially computed from the continuum theory of Weisskopf.[8] However, these did not agree very well with experimental data on angular distributions in this energy region. Therefore, the numbers in column 6 were obtained by extrapolation of the data of Jurney and Zabel[6] and of Walt and Beyster,[9] using the continuum theory values as a rough guide.

For further comparisons of inelastic cross sections, we have included in column 12 inelastic collision cross sections for monoenergetic 4.5 Mev neutrons obtained by Beyster, et al.[10]

13.2 Accuracy of Final Inelastic Cross Sections

The assignment of errors and the method of combining them was the same for this chapter as for Chapters 11 and 12. The uncertainty ascribed to σ_t was 10 percent and that to σ_{et}/σ_{el} was 20 percent. Because of the pronounced forward peak in the elastic scattering of these higher energy neutrons, the resultant uncertainties produced in σ_{in} are only about 2 percent and 4 percent, respectively. This is an indication of the decreasing importance of multiple scattering at the higher energies.

A correction was made for energy loss during an elastic collision, and an uncertainty of 50 percent of this correction was included, as in Chapters 11 and 12. Since there was no "observable" angular asymmetry in the aluminum foils (Section 10.9), no correction was made for this type of effect.

TABLE 13.1—RESULTS OF SPHERE TRANSMISSION MEASUREMENTS USING THE $Al^{27}(n,p)Mg^{27}$ THRESHOLD DETECTOR AND THE FISSION SPECTRUM SOURCE

Element	Sphere outside diameter, inches	Thickness, total mean free paths	Distance to source, inches	σ_t, barns	$\frac{\sigma_{et}}{\sigma_{el}}$	σ_{tr}, barns	Transmission	σ_{in} (Eq. 1.1), barns	σ_{in} (sphere theory), barns	σ_{in} (with all corrections), barns	σ_{in} (4.5 Mev), barns
1	2	3	4	5	6	7	8	9	10	11	12
Al	5.0	0.240	10	2.10	0.490	1.40	0.9009 ± 0.007	0.909	0.860	0.760 ± 0.062	0.72 ± 0.04
	8.0	0.4857	10	2.10	0.490	1.42	0.7901 ± 0.0065	1.02	0.900		
Ti											1.18 ± 0.07
Fe	5	0.5831	10	3.60	0.310	1.94	0.7938 ± 0.0071	1.43	1.29	1.20 ± 0.084	1.33 ± 0.05
Ni	5.24	0.2326	10	3.63	0.350	2.10	0.9099 ± 0.007	1.47	1.37	1.31 ± 0.078	1.50 ± 0.06
	5.24	0.6864	10	3.63	0.350	2.13	0.7398 ± 0.006	1.59	1.41		
Cu	8	0.6297	10	3.60	0.350	2.18	0.7460 ± 0.010	1.68	1.49	1.41 ± 0.097	1.60 ± 0.05
Zn											1.84 ± 0.12
Zr	4.5	0.5671	10	4.00	0.370	2.47	0.7736 ± 0.008	1.81	1.66	1.57 ± 0.094	1.59 ± 0.07
Ag	8	0.6217	10	4.08	0.30	2.62	0.7166 ± 0.005	2.19	2.03	1.99 ± 0.10	2.10 ± 0.13
Cd	8	0.5806	10	4.16	0.30	2.75	0.7246 ± 0.006	2.31	2.18	2.14 ± 0.11	2.16 ± 0.12
Sn	8	0.5370	10	4.14	0.320	2.69	0.7524 ± 0.006	2.20	2.05	2.01 ± 0.11	2.18 ± 0.06
W	4.95	0.3679	10	5.50	0.210	3.30	0.8288 ± 0.0066	2.86	2.74	2.72 ± 0.16	2.60 ± 0.20
Au	6.99	0.8055	10	6.15	0.190	3.34	0.6847 ± 0.009	2.89	2.70	2.68 ± 0.16	2.76 ± 0.15
Pb	5.0	0.4142	10	6.60	0.230	3.18	0.8631 ± 0.0073	2.35	2.20	2.21 ± 0.15	2.06 ± 0.14
	8	0.6899	10	6.60	0.230	3.25	0.7727 ± 0.014	2.47	2.29		
Bi	8	0.6527	10	6.60	0.230	3.33	0.7760 ± 0.010	2.56	2.38	2.35 ± 0.16	2.19 ± 0.08

13.3 General Remarks

In comparing columns 9 and 10, one sees that the error in cross section made by using the simple exponential is between 5 and 10 percent. The geometrical corrections included in column 10 are everywhere less than 1 percent, and the rms error in σ_{in} is caused mostly by statistical uncertainties in the measured transmissions. Therefore, the errors in column 9 are mostly real, and result from not treating the multiple scattering correctly.

There are two further points of interest about these data:

(1) Figure 13.1 indicates that most of the magic number effect has disappeared at these neutron energies.

(2) The absolute values of the inelastic cross sections of column 11 have approached a magnitude of about $\frac{1}{2}\ \sigma_t$. In addition, they agree very well in absolute magnitude with the data at 4.5 Mev. This indicates that the inelastic collision cross sections in this energy region are relatively independent of neutron energy and that most of the inelastically scattered neutrons fall well below the threshold.

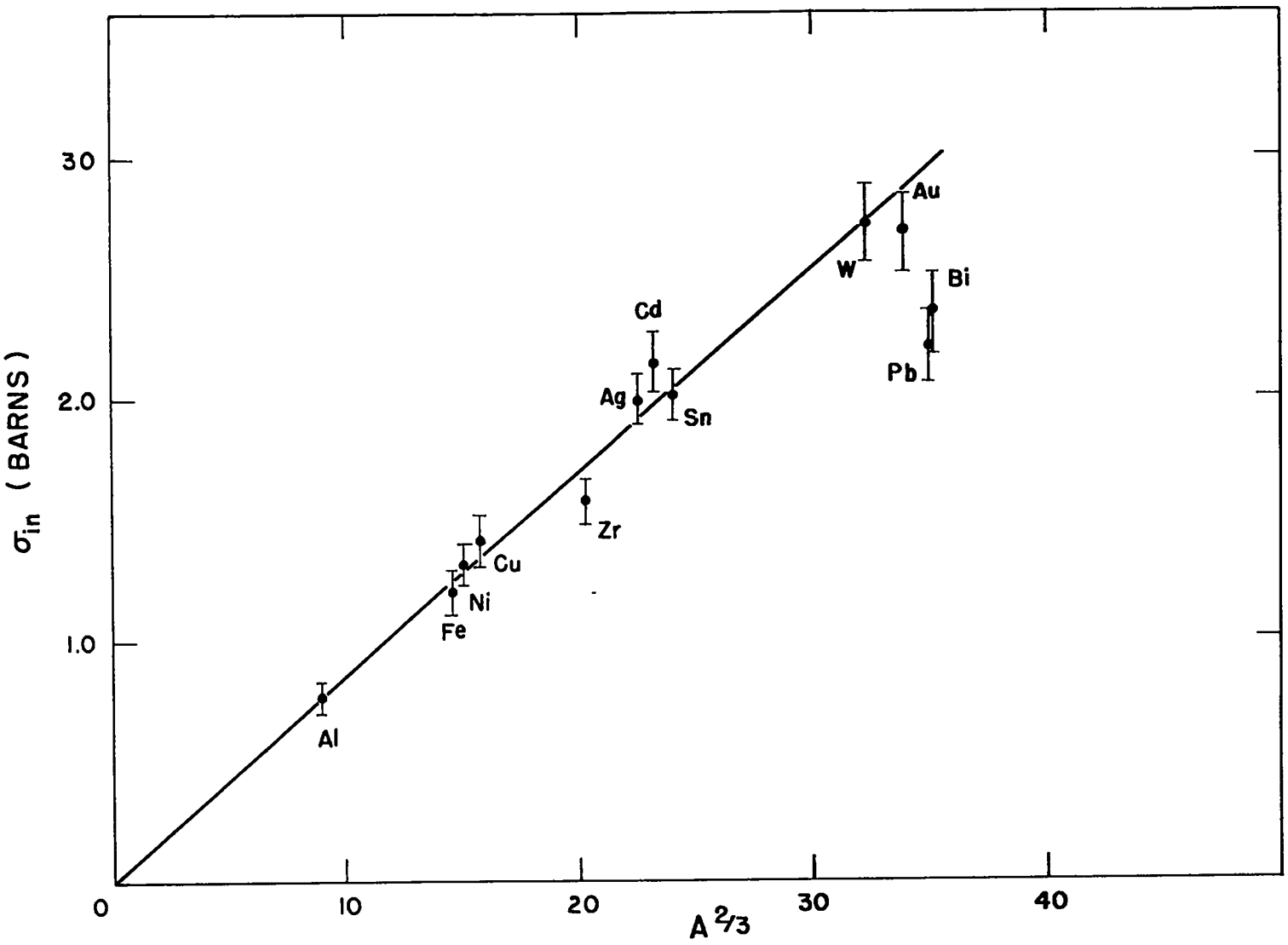

Fig. 13.1—Cross sections for scattering below the $Al^{27}(n,p)Mg^{27}$ threshold as a function of $A^{2/3}$.

Chapter 14

ANALYSIS OF EXPERIMENTAL DATA BY TWO-GROUP METHODS

In this chapter, the group methods of Chapter 8 will be used to determine cross sections for scattering between energy groups. This method will be discussed for the iron and cadmium measurements. A more approximate method will be used to estimate these cross sections in other cases.

14.1 Two-group Analysis of Iron

The energy groups selected for this analysis are 0.4 to 1.4 Mev, called group 2, and 1.4 Mev to infinity, called group 3. The unknowns to be determined are σ_{32} and $(\sigma_2^{in} + \sigma_2^c)$. The total σ_3^{in}, on the other hand, is considered as already determined from the one-group analysis with a "28" counter reported in Chapter 11, and once σ_{32} is determined, σ_{31} follows as $\sigma_3^{in} - \sigma_{32}$. σ_3^c is estimated for this analysis and is quite small. Now Eq. 8.35, together with Eqs. 8.33 and 8.31, gives the transmission observed with a "37" counter in terms of the two unknowns, σ_{32} and $\sigma_2^{in} + \sigma_2^c$, and of many "known" parameters, such as σ_2^{tr} and σ_3^{tr}, the efficiencies of a "37" counter for neutrons of groups 2 and 3, respectively, and the fraction of the fission spectrum in each of these groups. The f_1, f_2 and f_3 values are 0.098, 0.341, and 0.561, respectively, and P_2^{37}/P_3^{37} is 0.70.

Considering all these parameters as known, we may assume values of $\sigma_2^{in} + \sigma_2^c$ and calculate the corresponding value of σ_{32} from the measured "37" counter transmission. This gives a plot of σ_{32} vs $\sigma_2^{in} + \sigma_2^c$ for each transmission measurement (Fig. 14.1). This procedure is then repeated for each shell thickness used in the measurements.

For each shell, a different line in Fig. 14.1 is obtained. Figure 14.1 refers in particular to iron, for which three shell thicknesses were measured. We have plotted for each shell the upper and lower cross section limits allowed by the statistical errors in the transmission experiment. The region of the graph which is permitted by all the shell transmission experiments has been shaded in Fig. 14.1. It is reasonable to assume that the correct values of the unknowns σ_{32} and $\sigma_2^{in} + \sigma_2^c$ fall somewhere within this shaded area. This then places bounds on σ_{32} and $\sigma_2^{in} + \sigma_2^c$.

Auxiliary information is necessary to determine some of the "known" cross sections to put into Eq. 8.35. The neutrons in energy group 3 have the cross sections for iron given in Table 11.1, since they were measured with a "28" detector for which the effective energy threshold is 1.4 Mev. σ_2^t is determined by numerical integration of the iron total cross section between energies 0.4 and 1.4 Mev. The ratio $\sigma_2^{et}/\sigma_2^{el}$ is calculated from the 1 Mev elastic scattering angular distribution of Walt and Barschall.[19] The "37" detector sensitivities in groups 2 and 3 (P_2^{37} and P_3^{37}) are calculated from the fission cross section of Np^{237}. The escape probabilities required for the calculations can be read from Fig. 5.1. The results obtained from the analysis are

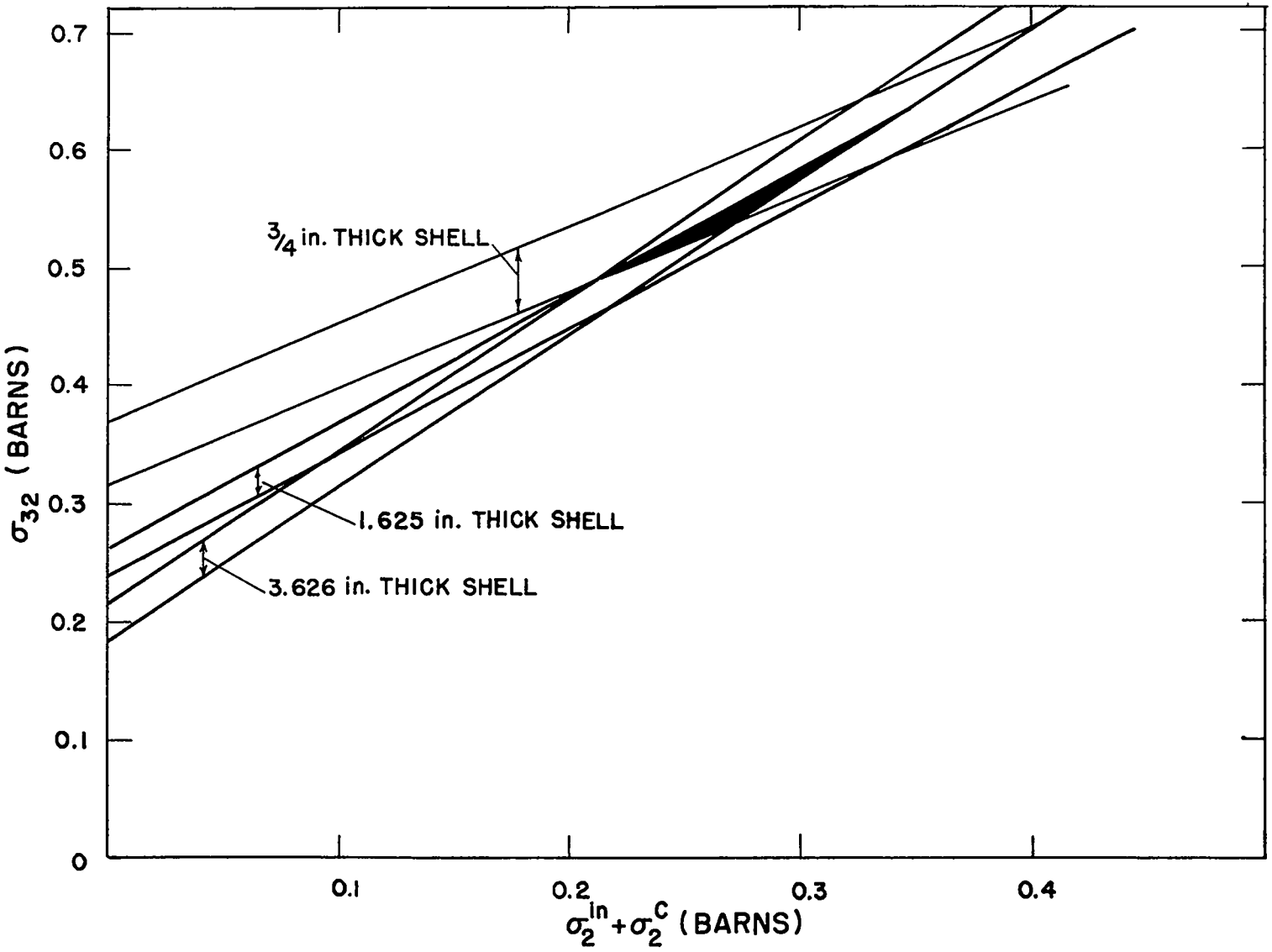

Fig. 14.1 — Plot of σ_{32} (cross section for scattering inelastically between groups 3 and 2) as a function of $\sigma_2^{in} + \sigma_2^{c}$ (inelastic collision cross section in group 2) for three iron shells.

$$\sigma_{32} = 0.56 \pm 0.07$$

$$\sigma_{31} = 0.13 \pm 0.07$$

$$\sigma_2^{in} + \sigma_2^c = 0.28 \pm 0.07 \qquad (14.1)$$

These cross sections are averages of the upper and lower limits permitted in Fig. 14.1, and the errors are such that the cross sections may be anywhere in the shaded region. It should be noted, however, that a much more accurate determination can be made of a certain linear combination between the cross sections than of each individual cross section. For instance, from Fig. 14.1 we see that

$$\sigma_{32} - 1.07(\sigma_2^{in} + \sigma_2^c) = 0.27 \pm 0.01 \qquad (14.2)$$

with a probable error about $1/7$ of those in Eq. 14.1. The reason Eq. 14.2 is so well determined is, of course, that this combination is most closely related to the inelastic cross section measured with a "37" detector.

Since the average neutron energy in group 2 is about 1 Mev, $\sigma_2^{in} + \sigma_2^c$ can be compared with recent monoenergetic work at this energy. The inelastic collision cross section at 1 Mev is $0.40 \pm .03$ barns,[10] which is somewhat above $\sigma_2^{in} + \sigma_2^c$. This is understandable since some of the inelastic collisions of group-2 neutrons do not actually remove neutrons from group 2.

14.2 Two-group Analysis of Cadmium

If one performs the two-group analysis of the "37" counter transmissions of cadmium spheres, the results shown in Fig. 14.2 are obtained. The same pieces of auxiliary information are required here as in the two-group iron analysis and these data are obtained from the same sources. The measured cross sections are

$$\sigma_{32} = 0.92 \pm 0.35$$

$$\sigma_{31} = 0.60 \pm 0.35$$

$$\sigma_2^{in} + \sigma_2^c = 0.56 \pm 0.35 \qquad (14.3)$$

Uncertainties are such that all cross sections in the shaded region of Fig. 14.2 are permissible. The quantity which is accurately determined, in analogy with Eq. 14.2, is

$$\sigma_{32} - 1.06\ (\sigma_2^{in} + \sigma_2^c) = 0.33 \pm 0.03 \qquad (14.4)$$

A recent measurement[10] of the inelastic collision cross section of cadmium at 1.0 Mev gives 1.04 ± 0.08 barns. Any real difference between this value and $\sigma_2^{in} + \sigma_2^c$ given above could again be attributed to inelastic processes which do not remove the neutrons from group 2.

14.3 Two-group Analysis for Other Elements

Estimates of σ_{32}, σ_{31}, and $\sigma_2^{in} + \sigma_2^c$ for elements other than iron and cadmium are determined by a method which is less rigorous than that of Chapter 8. One relationship which we can use is based on the cross sections measured with the "28" detector

$$\sigma_{in}^{28} \equiv \sigma_{32} + \sigma_{31} + \sigma_3^c \qquad (14.5)$$

A similar sort of equation exists for the "37" detector cross section

$$\sigma_{in}^{37} = B_3^{37}\left[\sigma_3^c + \sigma_{31} + \sigma_{32}\left(1 - \frac{\sigma_2^{37}}{\sigma_3^{37}}\right)\right] + B_2^{37}\ (\sigma_2^{in} + \sigma_2^c) \qquad (14.6)$$

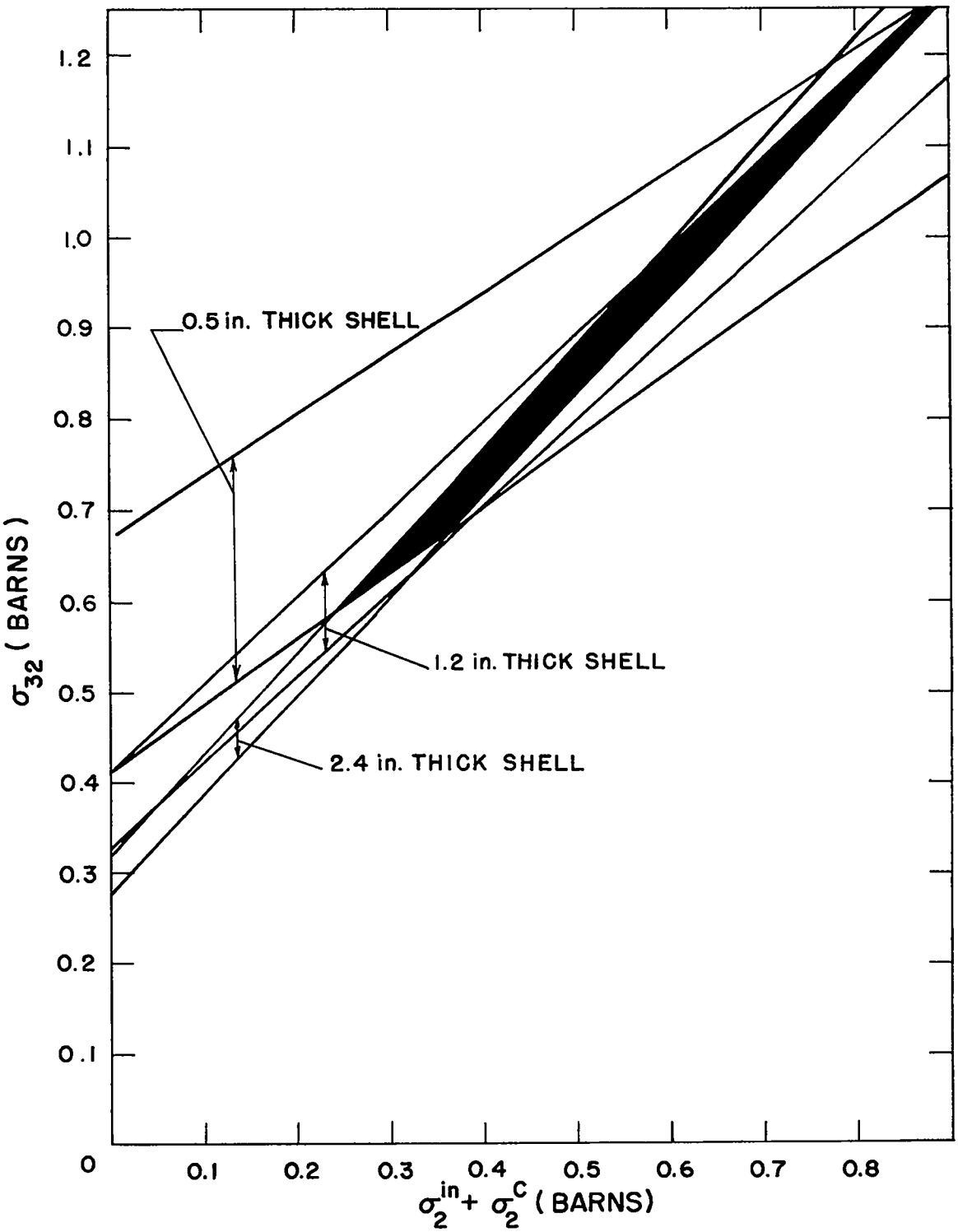

Fig. 14.2— Plot of σ_{32} for cadmium as a function of $\sigma_2^{in} + \sigma_2^{c}$ for three thicknesses of shell.

where B_3^{37} is the probability that a Np^{237} detector count is from a group 3 neutron, B_2^{37} is the probability it is from a group 2 neutron, and σ_2^{37} and σ_3^{37} are the average fission cross sections of the "37" detector for groups 2 and 3, respectively. B_3^{37} and B_2^{37} can be defined in terms of detector quantities used previously in this report.

$$B_3^{37} = \frac{f_3 P_3^{37}}{f_3 P_3^{37} + f_2 P_2^{37}} = \frac{f_3 \sigma_3^{37}}{f_3 \sigma_3^{37} + f_2 \sigma_2^{37}}$$

$$B_2^{37} = \frac{f_2 P_2^{37}}{f_2 P_2^{37} + f_3 P_3^{37}} = \frac{f_2 \sigma_2^{37}}{f_2 \sigma_2^{37} + f_3 \sigma_3^{37}}$$

Equation 8.37 is then used as the third equation. As will be remembered, this equation expresses the fact that σ_{in}^{37} is apparently independent of shell thickness, a fact which cannot be established with great accuracy.

The best estimates of σ_{32}, σ_{31}, and $\sigma_2^{in} + \sigma_2^c$ are given in Table 14.1. It should be understood that the uncertainties for these cross sections are much greater than those in the previous sections. Recent inelastic collision cross section measurements at 1 Mev are given also in Table 14.1 for comparison.[10] The tabulated values of $\sigma_2^{in} + \sigma_2^c$ are consistent with the measured 1 Mev cross sections.

TABLE 14.1—INELASTIC CROSS SECTIONS FOR FISSION SPECTRUM NEUTRONS FOR GROUPS 2 AND 3

Element	σ_{32}, barns	σ_{31}, barns	$\sigma_2^{in} + \sigma_2^c$, barns	σ^{in} at 1 Mev, barns
Al	0.27	0.05	0.07	-0.01
Ti	0.48	0.08	0.17	
V	0.49	0.09	0.22	
Ni	0.61	0.10	0.27	
Cu	0.78	0.12	0.28	0.19
Zn	0.82	0.13	0.27	0.10
Zr	0.80	0.16	0.25	
Ag	1.19	0.47	0.84	1.8
Sn	0.87	0.25	0.30	0.04
W	1.68	0.55	0.90	
Au	1.51	0.53	0.85	1.9
Pb	0.60	0.11	0.17	0.2
Bi	0.61	0.12	0.17	0.12

Chapter 15

CONCLUSIONS

The most striking result of the measurements with "37", "28" and aluminum counters is that the inelastic cross section increases strongly as the threshold is increased. For instance, gold has inelastic cross sections of 1.0, 2.04, and 2.68 barns, respectively, as measured by the three counters, and for iron the corresponding numbers are about 0.28, 0.69, and 1.2 barns. The group analysis of Chapter 14 shows further that the inelastic scattering cross section for group 2 neutrons is not substantially different from that measured with a "37" counter.

This increase of σ_{in} with neutron energy is entirely reasonable: At low energies, only a few levels are available for inelastic scattering, while for high energies there are many. In addition, our threshold detectors indicate only part of the inelastic scattering. For instance, the "28" detector measures effectively all neutrons above 1.4 Mev. Some of these, when they suffer an inelastic collision, will still be detectable by the "28" detector. Thus, the measured cross section gives only a lower limit to the total average inelastic cross section.

The importance of this effect is shown by the comparison of $\sigma_2^{in} + \sigma_2^{c}$, as measured by the "37" detector, with the inelastic cross section for 1 Mev neutrons, as shown in Table 14.1: The 1 Mev collision cross sections for silver, cadmium and gold are roughly twice $\sigma_2^{in} + \sigma_2^{c}$ (the other measurements are less accurate because the cross sections are small). Taking this effect into account, it is likely that the actual inelastic cross section of a neutron around 2 to 3 Mev is considerably higher than the measured "28" cross section and may be as high as the measured aluminum cross section.

This effect is probably not important for the aluminum measurements. For, according to the statistical theory, the energy of neutrons after inelastic scattering is given by a Maxwell distribution, and experimentally, the nuclear temperatures are of the order of 1 Mev or less. Therefore, very few inelastically scattered neutrons will remain detectable by aluminum. Thus, we expect that the aluminum counter indicates essentially the total inelastic scattering for neutrons which have predominantly energies between 4 and 8 Mev.

The inelastic cross sections measured with the aluminum counter represent a rather smooth function of atomic weight, with only slight dips for magic elements (page 126). Moreover, the cross section is nearly proportional to $A^{2/3}$ (Fig. 13.1). These results make it likely that in this energy range the inelastic cross section is very nearly the geometric cross section of the nucleus.

The "28" measurements, as we have mentioned, represent lower limits to the inelastic cross section in the range from about 1.4 to about 4 Mev. The total inelastic cross section for neutrons in this range may well be as high as the geometric cross section, for heavy and non-magic nuclei. The lower limits given by the "28" measurements themselves are about 75 percent of the aluminum results for these nuclei. This sets severe limitations on the transparency of a nucleus which can be admitted in a theory like that of Feshbach, Porter, and Weisskopf (the "clouded crystal ball").[20] It should be remembered, however, that the inelastic scattering is far less sensitive to transparency than the elastic, so that interesting interference effects in the elastic scattering are by no means excluded by our result that the inelastic scattering has "nearly" the geometric cross section.

At lower energy, the inelastic cross section is decidely lower than geometric. This is best shown by the measurements with 1 Mev neutrons reported in Table 14.1, which indicate a cross section of about 1.9 barns for gold, about 70 percent of the "geometric" cross section measured with the aluminum counter. The main cause for this is presumably that few excited states exist for gold below 1 Mev. However, it may indicate in addition some transparency of the nucleus, as required by the "clouded crystal ball" theory.

The magic nuclei have smaller cross sections than the neighboring, non-magic ones at all energies. The effect is most marked at low energy. For example, at about 1 Mev, lead and bismuth have σ_{in} about 10 percent of that of gold. For the aluminum counter, the cross sections of lead and bismuth have increased to about 85 percent of that of gold, while for the "28" counter the ratio has the intermediate value of about 35 percent. This behavior makes it almost certain that the small cross section is due to the absence (or scarcity) of low-lying excited levels in magic nuclei. At high energy, the inelastic cross section for these nuclei will be more nearly that of their "normal" neighbors. An effect may persist, however, because the magic nuclei may be somewhat more tightly packed than the other nuclei, and thus have a smaller geometric cross section.

Tin shows the magic effect somewhat less than the doubly-magic lead and bismuth. Iron has a rather low inelastic cross section at 1 Mev, but already for the "28" detector the effect has almost disappeared. This nucleus is known to have a rather high first excited level.

Information on the energy distribution of the inelastically scattered neutrons is given by the group analysis of Chapter 14, especially Table 14.1. Of the neutrons of group 3, the vast majority are scattered into group 2, and only a small fraction (about 25 percent on the average) are degraded into group 1, i.e., below 0.4 Mev.

To get similar information at higher energy, we may divide the neutrons above 1.4 Mev into two groups: group 3 from 1.4 to 5 Mev, and group 4, 5 Mev and above. Then the fact that the apparent inelastic cross section measured by the "28" detector is independent of shell thickness gives rise to a relation similar to Eq. 8.37, viz.

$$\sigma_3^{in} \cong (\sigma_{42} + \sigma_{41}) + \sigma_{43}\left(1 - \frac{\sigma_3^{28}}{\sigma_4^{28}}\right) \tag{15.1}$$

If we now assume that the efficiency of the "28" detector is the same for groups 3 and 4, we obtain

$$\sigma_3^{in} \cong \sigma_{32} + \sigma_{31} \cong \sigma_{42} + \sigma_{41} \tag{15.2}$$

The cross section measured by the "28" detector is then σ_3^{in}, regardless of the neutron spectrum. The difference between the cross sections measured with a "28" and an aluminum detector is σ_{43}. The experiments then indicate that about 25 percent of the neutrons of group 4 go into group 3.

REFERENCES

1. H. A. Bethe, Los Alamos Scientific Laboratory Report LA-1428, 1952.
2. D. D. Phillips, R. W. Davis, and E. R. Graves, Phys. Rev., 88, 600 (1952); D. D. Phillips, LA-740, 1949.
3. H. H. Barschall, Revs. Modern Phys., 24, 120 (1952).
4. E. Amaldi, D. Bocciarelli, B. Cacciapuoti, and G. Trabacchi, Nuovo cimento, 3, 203 (1946).
5. L. Szilard, S. Bernstein, B. Feld, and J. Ashkin, Phys. Rev., 73, 1307 (1948).
6. E. T. Jurney, Los Alamos Scientific Laboratory Report LA-1339, 1951; E. T. Jurney and C. W. Zabel, Phys. Rev., 86, 594A (1952).
7. E. D. Cashwell, C. J. Everett, O. W. Rechard, Los Alamos Scientific Laboratory Report LA-1583, 1953.
8. Feld, Feshbach, Goldberger, Goldstein, and Weisskopf, Final Report of the Fast Neutron Data Project, NYO-636.
9. M. Walt and J. R. Beyster, Phys. Rev., 98, 677 (1955).
10. J. R. Beyster, R. L. Henkel, R. A. Nobles, Phys. Rev., 98, 1216 (1955).
11. Rev. Sci. Instr., 22, 489 (1951).
12. Norris Nereson, Phys. Rev., 85, 600 (1952); T. W. Bonner, R. A. Ferrell, and M. C. Rinehart, Phys. Rev., 87, 1032 (1952); David L. Hill, Phys. Rev., 87, 1034 (1952); B. E. Watt, Phys. Rev., 87, 1037 (1952).
13. Bruno B. Rossi and Hans H. Staub, Ionization Chambers and Counters, Div. V, Vol. 2, National Nuclear Energy Series, McGraw-Hill Book Company, Inc., New York, 1949.
14. Eklund and Hole, Arkiv Mat., Astron. Fysik, 29A, No. 26, 1 (1943).
15. E. T. Jurney (private communication).
16. Neutron Cross Sections Compilation, AECU-2040, 1952.
17. J. W. Motz, Phys. Rev., 86, 753 (1952).
18. N. Nereson and S. Darden, Phys. Rev., 89, 775 (1953); N. Nereson and S. Darden, Phys. Rev., 94, 1678 (1954).
19. M. Walt and H. H. Barschall, Phys. Rev., 93, 1062 (1954).
20. Feshbach, Porter, and Weisskopf, Phys. Rev., 96, 448 (1954).